Lakehead University

Development of a Consistent Cubic Equation of State for the Calculation of the Phase Behaviour and Thermodynamic Properties of Pure Components

by

Twaha Mohamed

Thesis submitted in partial fulfillment of the requirements.

for the Master of Science in

Chemical Engineering

Supervisor

Dr. Francisco Ramos-Pallares

Co-*Supervisor*

Janusz Kozinski

Thunder Bay, Ontario

September 2023

i. Abstract

This study analyzes two cubic equations of state (CEoS), the Redlich-Kwong (RK) and Peng-Robinson (PR) CEoS, to calculate the properties of 151 pure components. The components were grouped by their intermolecular interactions (polar, non-polar, hydrogen bonding) and their saturation pressure (P^{sat}), enthalpy of vaporization (ΔH_v), and saturated liquid heat capacity (C_p^{sat}) were calculated using a unique combination of the PR and RK CEoS paired with either the Twu or Soave α-functions. Outliers were eliminated using a quantile regression algorithm; additionally, a set of constraints proposed by Le Guennec *et al.*(Le Guennec *et al.* 2016) was applied to ensure that thermodynamic consistency was enforced during optimization. The four models tested were named PR-Twu, PR-Soave, RK-Twu, and RK-Soave, based on the equation of state and alpha function used. The PR-Twu and RK-Twu models predict P^{sat}, ΔH_v, and C_p^{sat} more accurately than the PR-Soave and RK-Soave models. The Twu α-function is more flexible and produces better results but is unsuitable for highly associating components such as carboxylic acids. The PR-Twu model had overall absolute average relative deviation (AARD) values of 9.7, 3.2, and 2.1% for the P^{sat}, ΔH_v, and $C_p^{sat,}$ respectively. In the case of the RK-Twu model, AARD values of 8.7, 3.1, and 2.0 were obtained for the P^{sa}t, ΔH_v, and $C_p^{sat,}$ respectively. The PR-Soave model had, in comparison, overall AARD values of 22.5, 5.8, and 9.1%, while the RK-Soave model had AARD values of 21.0, 5.9, and 8.5% for the P^{sat}, ΔH_v, and C_p^{sat} respectively. The Twu and Soave α-function were evaluated for thermodynamic consistency by calculating derivative properties. The Waring Number (Waring 1954) was used to test the thermodynamic consistency of the P^{sat} curve, and the saturated liquid speed of sound was calculated as a rigorous consistency test.

The Soave α-function was unsuitable for calculating the thermodynamic properties of alcohols due to inconsistencies and high AARD values. For similar reasons, the Soave α-function also can not accurately predict the properties of highly polar and hydrogen-bonding compounds. However, it was found that the Twu α-function is suitable for predicting P^{sat}, ΔH_v, and C_p^{sat} for non-polar and polar compounds. The Twu α-function was found to correctly predict the properties of hydrogen bonding components when that component is predominately defined by one type of interaction.

Acknowledgments

I want to express my sincere gratitude to those who have supported me throughout this dissertation journey. Without the help and encouragement, this project would not have been possible.

First and foremost, I am immensely thankful to my supervisor, Dr. Francisco Ramos-Pallares, for his constant guidance, insightful feedback, and unwavering support during the entire research process. He has been a great mentor and a source of inspiration for me. His expertise and knowledge have been invaluable for the completion of this study.

I am also profoundly grateful to my family, who have always been there for me with their love, care, and understanding. They have motivated me to pursue my goals and overcome any challenges along the way. I dedicate this dissertation to them.

Furthermore, I appreciate the assistance and collaboration of my colleague, Saeed Ataee-Ataabadi, who has been an excellent partner in this research.

Lastly, I would like to acknowledge the participation and cooperation of my committee members. Dr. Thamara Laredo and Dr. Lionel Catalan generously shared their time, expertise, and opinions. Their constructive feedback and suggestions have greatly improved the quality and rigour of this research. I am honoured to have them as part of this dissertation committee. I would also like to acknowledge my co-supervisor, Janusz Kozinski.

Table of Contents

List of Figures

List of Tables

List of Symbols and Abbreviations

ρ	Density
H	Enthalpy
$H^{\text{ideal gas}}$	Enthalpy ideal gas
C_p	Heat Capacity
$C_p^{\text{ideal gas}}$	Heat Capacity deal gas
EoS	Equation of State
CEoS	Cubic Equation of State
EoS's	Equations of State
α-functions	Alpha Functions
SAFT	Statistical Associating Fluid Thermodynamics
i, j, k	Arbitrary Component Indexing
T	Temperature
P	Pressure
PT	Pressure-temperature
V	Volume
P_{total}	Total Pressure
f	Fugacity
ϕ	Fugacity Coefficient
x	Mole Fraction
R	Gas Constant
v	Molar volume
n	Mole Number

A, B, C, D	1st, 2nd, 3rd, and 4th virial coefficients
A_{cp}, B_{cp}, C_{cp}, D_{cp}	fluid-specific parameters reported by Yaws for ideal Cp calculation
vdW	van der Waals.
b	co-volume for CEoS's
a_c	attractive parameter for CEoS's
T_c	Critical temperature
P_c	Critical pressure
v_c	Critical molar volume
δ_1, δ_2	empirical constant for CEoS
T_r	Reduced temperature.
m	fluid-specific parameter for Soave α-function
ω	Acentric factor
NIST	National Institute of Standards and Technology
DIPPR	Design Institute for Physical Properties Research
PR	Peng-Robinson
RK	Redlich-Kwong
Z_c	Critical compressibility factor
Z	Compressibility factor
vdW1f	Van Der Waals one fluid
C_1, C_2, and C_3	Fluid-specific adjustable parameters Mathias−Copeman α-function
k_o, and k_1	Fluid-specific adjustable parameters for the Stryjek−Vera α-function
N, M, and L	Fluid-specific adjustable parameters for the Twu α-function
m_{PR}	Updated m correlation for PR CEoS with Soave α-function Pina *et al.*

m_{RK}	Updated m correlation for RK CEoS with Soave α-function Pina *et al.*
VLE	Vapour-liquid equilibrium
LLE	Liquid-liquid equilibrium
SQP	Sequential Quadratic Programming
ΔH_v	Vaporization enthalpy, kJ/mol
P^{sat}	Saturated liquid vapour pressure, kPa
$C_P{}^{sat}$	Saturated liquid heat capacity, J/ (mol K)
OF	Objective Function
W_f	weighting factor
TDE	Thermo Data Engine
ANN	Artificial Neural Networks
QSPR	Quantitative Structure-Property Relationship

1 Introduction

Predicting fluids' thermodynamic and thermophysical behaviour is paramount in industrial chemical process design, simulation, and optimization. For instance, predicting phase boundaries and phase compositions is required to design separation operations such as distillation and liquid-liquid extraction (Prausnitz *et al.*, 1998). Phase properties such as density (ρ), enthalpy (H) and heat capacity (C_p) are needed for the design and sizing of heat transfer equipment (Valderrama, 2003). Equations of state (EoS) are widely used in engineering calculations to predict fluids' phase behaviour and thermodynamic properties. These equations are mathematical expressions that relate the three variables that define the thermodynamic behaviour of fluids across the phase diagram: pressure (P), molar volume (v) and temperature (T). Numerous EoS have been developed for engineering calculations; some of these equations are based on theoretical considerations, and others are semi-empirical. Theoretical EoS are based on statistical thermodynamics and relate the macroscopic pressure volume temperature (PVT) behaviour of fluids to interactions at the molecular level. Examples of theoretical EoS are those based on the Virial (Thiesen, 1885a) and the statistical associating fluid theory (SAFT) (Chapman *et al.*, 1989). Despite all the recent developments in molecular simulation that have allowed the calculation of theoretical EoS parameters, the application of these EoS in engineering calculations is limited because of their complexity. Semi-theoretical EoS are preferred in engineering calculations because of their simplicity, which arises from the simplifying assumptions taken in their derivation. A Cubic EoS (CEoS) is semi-empirical because it assumes that a system's total pressure arises only from weak, repulsive and attractive intermolecular interactions; however, this assumption is not satisfactory for systems interacting strongly via hydrogen bonding. The assumption regarding weak repulsive and attractive interactions produces a simple EoS with only two fluid-specific parameters that are

calculated as a function of the critical properties of the fluid (Prausnitz *et al.*, 1998). The Van Der Waals one fluid (vdW1f) mixing rules, commonly used in engineering calculations, use a simplifying approach that assumes that the mixture is composed of a single pseudo-pure component. The assumed pseudo-pure component has properties calculated from the pure components that make up this mixture using a set of aptly named mixing rules. The general expression of a CEoS and the vdW1f mixing rules is given by:

$$P = \frac{RT}{v-b} - \frac{\alpha(T)\, a_c}{(v+\delta_1 b)(v+\delta_2 b)} \tag{1.1}$$

$$a_{mix} = \sum_{i=1}^{n}\sum_{j=1}^{n} x_i x_j \left[\left(a_{c,i}\alpha(T)_i\right)\left(a_{c,j}\alpha(T)_j\right)\right]^{0.5}\left(1-k_{ij}\right) \tag{1.2}$$

$$b_{mix} = \sum_{i=1}^{n}\sum_{j=1}^{n} x_i x_j \left(\frac{b_i+b_j}{2}\right)\left(1-l_{ij}\right) \tag{1.3}$$

where a_c and b are fluid-specific parameters calculated using the critical temperature and critical pressure of the pure component; α (or $\alpha(T)$) is a fluid-specific parameter adjusted to fit pure component experimental data; δ_1 and δ_2 are CEoS-specific constants (Table 2.2); x is the mole fraction of component i in a mixture. Both l_{ij} and k_{ij} are binary interaction parameters (BIP) typically fitted to experimental data. However, it is common practice to only fit k_{ij} from most applications, leaving the l_{ij} parameter set to 0, indicating no correction for the calculation of b_{mix}.

Two CEoS that represent the most widely used CEoS in the industry are the models proposed by Redlich and Kwong (RK) (Redlich and Kwong, 1949) and Peng and Robinson (PR) (Peng and Robinson, 1976). The difference between these two CEoS is the expression proposed for the calculation of the volume function found in the denominator of the attractive term (second term on the right-hand side of Eq. 1.1), *i.e.,* the values for the constants δ_1 and δ_2 in Eq. 1.1. Despite the

differences in the attractive terms, the RK and PR CEoS produce results with similar accuracy (Peng and Robinson, 1976; Valderrama, 2003).

RK and PR CEoS are widely used in engineering calculations because of their (Valderrama, 2003):

- Mathematical simplicity,
- Fast convergence and numerical efficiency in computer calculations,
- Accuracy in calculating vapor-liquid phase boundaries,
- Continuity across the phase diagram, including the critical region,
- Easy application to multicomponent mixtures through the Van Der Waals one fluid mixing rule (Eq. 1.2 and 1.3).

However, despite these advantages, CEoS can still produce thermodynamically inconsistent results. A result is thermodynamically inconsistent when it does not agree with the actual physical behaviour of the fluid. For instance, a CEoS could predict the existence of a phase that does not exist. Another typical example of inconsistent behaviour is seen when a CEoS is unable to produce phase boundaries that are sufficiently accurate for engineering calculations. These inconsistencies found in CEoS are further elaborated in section 1.1.

1.1 Inconsistent Thermodynamic Behaviour from Cubic Equations of State

The most widely reported inconsistencies in engineering calculations when using CEoS are the inaccurate prediction of vapour-liquid equilibrium (VLE) for multi-component mixtures and false phase splits (i.e., false VLE) prediction for polar components.

1.1.1 Inaccurate Vapor-Liquid Equilibrium Predictions for Multicomponent Mixtures

Figure 1.1 shows the pressure-temperature (PT) phase diagrams and compositions of a 4-component (Figure 1.1a) and 12-component (Figure 1.1b) synthetic natural gas mixture. The

symbols in Figure 1.1 correspond to experimental data, and the solid and dashed lines are predictions from the GERG and the PR EoS, respectively. The GERG EoS is a complex multiparametric EoS used to predict the highly accurate phase behaviour for mixtures. Still, it is not used in engineering calculations due to its numerical complexity and high number of parameters (Varzandeh *et al.*, 2016). Interestingly, although the mixtures shown in Figure 1.1 are made up of non-polar components, for which the PR CEoS is expected to produce accurate results, there are significant deviations between the experimental phase boundaries and phase boundaries predicted by the PR CEoS. These high deviations may arise from an improper tuning of the PR EoS to match pure component data, or the applied set of BIP cannot capture intermolecular interactions in multicomponent mixtures. BIP (such as k_{ij} and l_{ij} in Eq.1.2 and 1.3) are adjustable coefficients calculated by fitting the PR CEoS to match binary mixture data. When using BIP, we assume that deviations from ideality arise from two-body interactions only. However, this contradicts experimental evidence suggesting multi-body interactions in multicomponent mixtures (Cai *et al.*, 2006). To properly assess the nature of the reported high deviations between data and predictions from a CEoS, we hypothesize it is first necessary to properly tune the CEoS to pure component data and re-calculate the set of BIP. The incorrect representation of pure component thermodynamic behaviour produces the incorrect representation of a mixture's phase behaviour (Le Guennec *et al.* 2016; Twu *et al.* 1991a); therefore, before fitting the CEoS to mixture data, the equation must be accurate for pure components.

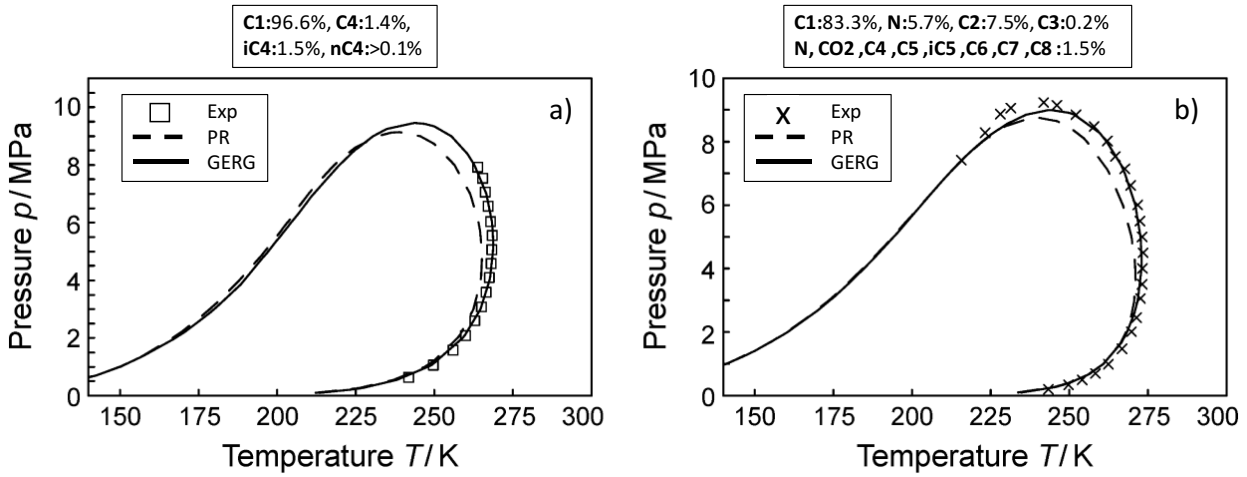

Figure 1.1: Vapor−liquid phase boundary of a four-component hydrocarbon mixture (a); and a 12-component synthetic natural gas (b). Dash lines for Peng-Robinson (PR) equation, solid lines for GERG equation, and symbols for data. Adapted from Kunz and Wagner (Kunz and Wagner, 2012).

1.1.2 False Phase Splits Predictions for Mixtures Containing Polar Components

It is well known that CEoS do not produce very accurate results for mixtures containing polar components because they cannot capture the effect of strong polar interactions in the phase behaviour of the mixture (Kontogeorgis and Folas, 2009; Valderrama, 2003). Despite this severe limitation, CEoS are still widely used in the industry to model the vapour-liquid phase behaviour of mixtures containing polar components; however, the results must always be carefully examined. Figure 1.2 shows the vapor-liquid phase behaviour of the 1-propanol/water binary mixture at 100 kPa. The solid line in Figure 1.2 corresponds to the RK CEoS fitted to the data. This EoS falsely predicts a vapor-liquid-liquid region, as shown in Figure 1.2. This false phase splits prediction is one of the most common inconsistencies when using a CEoS to model the thermodynamic behaviour of mixtures containing polar components. This inconsistency results from using high numerical values for the BIP (Economou and Donohue, 1992; Ghosh, 1999).

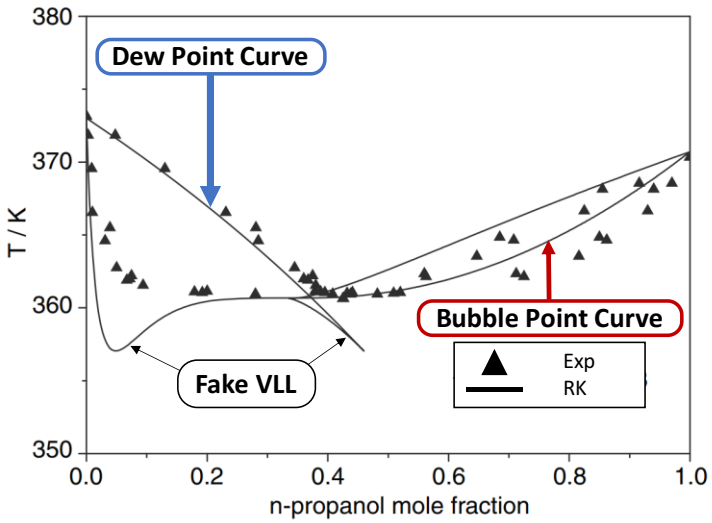

Figure 1.2: Vapour-liquid equilibrium correlation at 1 bar for propanol–water system with Redlich-Kwong (RK) equation using Van Der Waals mixing rules; k_{ij} = 0.0883. Adapted from Kontogeorgis and Folas (Kontogeorgis and Folas, 2009)

1.2 Development of a Consistent Cubic Equation of State

The attempts to produce a consistent CEoS can be classified into two groups: Group 1 involves predicting theoretically correct BIP, and Group 2 is concerned with predicting theoretically correct pure component parameters. Both groups are briefly reviewed in the following subsections.

1.2.1 Group 1: Predicting Theoretically Correct Binary Interaction Parameters

Several authors have suggested that using theoretically correct BIP in CEoS may produce consistent results. When tuned to fit experimental data, calculated sets of BIP are not constrained to satisfy any thermodynamic requirements. Consequently, there is a high chance of producing inconsistent results as those discussed in section 1.1. Peneloux *et al.* (Peneloux *et al.*, 1989) found a theoretical expression for BIP departing from the zeroth approximation of Guggenheim's Quasi-reticular theory (Guggenheim, 1952). The results showed a relationship between the BIP in a CEoS and the energy parameters in an activity coefficient model. This result led Jaubert *et al.*

(Jaubert and Mutelet, 2004; Jaubert and Privat, 2010) to develop a group contribution approach for predicting theoretically correct PR and RK CEoS BIP. Jaubert *et al.* tested this approach on predicting the VLE of binary and multicomponent mixtures containing alkanes with good agreement between data and predictions. However, this approach has some limitations because it requires a tremendous amount of data for fitting model parameters, and the expression for the calculation of the BIP is rather complex. Additionally, this approach has not been widely tested on mixtures containing polar components.

Researchers have also attempted to develop generalized approaches for calculating theoretically correct BIP. Graboski and Daubert (Graboski and Daubert, 1978) correlated BIP for the RK CEoS to solubility parameters for hydrocarbon and non-hydrocarbon components. Arai and Nishiumi (Nishiumi *et al.*, 1988) developed a semi-empirical equation for the BIP in PR CEoS by correlating pure elements' critical volumes and acentric factors (ω). Furthermore, Gao *et al.* (Gao *et al.*, 1992) sought to relate the interaction parameters in the PR CEoS to the critical temperature (T_c) and compressibility factor (Z) of pure components. A different approach was used by Abudour *et al.* (Abudour *et al.*, 2014), who applied artificial neural networks (ANN) and quantitative structure-property relationship (QSPR) modelling to predict interaction parameters for both the RK and PR CEoS. The ANN approach entailed constructing a model based on 30 molecular structural descriptors to forecast the interaction parameters of mixtures. However, despite the proposed approaches, none have provided a universally applicable method. An accurate predictive or correlating method for evaluating interaction parameters remains lacking. The existing correlations and estimation methods often struggle when extrapolated to higher T and P and are usually only suitable for particular mixtures.

1.2.2 Group 2: Predicting Theoretically Correct Pure Component Parameters

The main drawback of the approach described in Group 1 (section 1.2.1) is that if pure component parameters in the CEoS are not theoretically correct, then when the CEoS is used for mixtures, the results may be inconsistent despite the use of theoretically correct BIP. For pure components, the value of parameters α_c and b in Eq. 1.1 are fixed because they are theoretically calculated from the component's critical properties. At the same time, the parameter α is adjustable and fitted to match pure component saturation pressure (P^{sat}), enthalpy of vaporization (ΔH_v) and saturated liquid heat capacities (C_p^{sat}) (Pina-Martinez *et al.*, 2018). Hence, if the parameter α is not correctly adjusted, the CEoS may produce inconsistent results. Le Guennec *et al.* (Le Guennec *et al.*, 2016) reported a set of constraints that, when satisfied, produce a consistent value of α:

$$\alpha \geq 0 \; and \; \alpha(T) \; is \; continuous \tag{1.4}$$

$$\frac{d\alpha}{dT_r} \leq 0 \; and \; \frac{d\alpha}{dT_r} \; is \; continuous \tag{1.5}$$

$$\frac{d^2\alpha}{dT_r^2} \geq 0 \; and \; \frac{d^2\alpha}{dT_r^2} \; is \; continuous \tag{1.6}$$

$$\frac{d^3\alpha}{dT_r^3} \leq 0 \tag{1.7}$$

The physical meaning behind the constraints applied in Eq. 1.4 to 1.7 is presented in section 2.6. It has been hypothesized that using α values that are theoretically correct could subsequently result in producing consistent BIP, thus reducing the potential for predicting inconsistent phase behaviour for mixtures. Several authors have calculated consistent α-values that satisfy Eq. 1.4 to 1.7 (Bell *et al.*, 2018; Ghanbari *et al.*, 2017; Le Guennec *et al.*, 2017; Piña-Martinez *et al.*, 2022). However, they have reported fitted α values without presenting results on the performance of the CEoS in calculating important thermodynamic properties required for process design and simulation, such as enthalpies (H), heat capacities (C_p) and speeds of sound (u). H and C_p are necessary to design heat transfer and mass transfer equipment such as heat exchangers and distillation columns. On

the other hand, u is needed to identify a fluid flow regime (subsonic, supersonic, or hypersonic) for fluid dynamic calculations.

1.1 Knowledge Gaps and Objectives

Despite the research that has been conducted and aimed at developing a consistent CEoS, a consistent CEoS applicable to non-polar and polar components and their mixtures has yet to be developed. Therefore, this research's overall goal is to develop such consistent CEoS. This goal has been divided into two steps: 1) developing a consistent CEoS for pure components and 2) proposing a consistent approach for calculating BIP for the CEoS produced in Step 1. This study focuses only on step 1. The following knowledge gaps related to Step 1 have been detected:

- Most reported α parameters were fitted to pseudo-experimental rather than experimental data. Pseudo-experimental data is produced by molecular simulation or data extrapolation and, therefore, is subjected to uncertainties.
- There has not been an investigation on the performance of reported fitted α parameters in calculating derivative properties such as H, $C_{p,}$ and u.

Based on these knowledge gaps, the main objective of this study was developing and testing a consistent CEoS for pure components applicable across the entire phase diagram. Consequently, the following methodological steps were followed:

1) Collect a database containing pure component experimental saturation pressure, enthalpy of vaporization and heat capacities from the NIST Database (NIST, 2017). One hundred fifty-one components from fifteen different chemical families were included, such as alcohols, aldehydes, alkanes, amines, aromatics, and carboxylic acids.
2) Use a statistical method in combination with manual screening to screen the database and eliminate any outliers that can affect the fitting of the CEoS.
3) Develop a computer optimization algorithm to fit the CEoS simultaneously to pure component P^{sat}, ΔH_v and C_p^{sat} by adjusting the α-parameter in Eq. 1.1 to match the data.

4) Test the fitted α parameters by calculating ΔH_v, C_p^{sat}, Waring numbers (W) and saturated liquid speed of sound (u). The W is a parameter used to assess if the slope of the P^{sat} curve calculated from the CEoS is consistent with the Clapeyron equation.

The α-function chosen in this study was that proposed by Twu (Twu *et al.*, 1995a, 1995b):

$$\alpha(T) = T_r^{\alpha_1} \, exp\left(\alpha_2\left(1 - T_r^{\alpha_3}\right)\right) \qquad (1.8)$$

where α_1, α_2 and α_3 are parameters fitted to data and T_r is the reduced temperature. Equation 1.8 was chosen in this study because the values of its three parameters can be easily constrained to satisfy the criteria shown by Eq. 1.4 to 1.7 (Le Guennec *et al.*, 2016). In addition, Eq. 1.8 has been widely used to model the properties of polar components (Harandi and Haghtalab, 2021; Young *et al.*, 2016; Zhao *et al.*, 2019).

1.3 Thesis Structure

This thesis is divided into five chapters, not including the introduction:

- Chapter 2 provides a review of the literature relevant to the modelling of thermophysical properties using EoS and the analysis of their performance, with a focus on CEoS and α-functions.
- Chapter 3 covers modelling and screening techniques used in this study for data collection. Additionally, methods for validating the thermodynamic consistency of EoS are presented.
- Chapter 4 focuses on discussing modelling results and evaluations of thermodynamic consistency.
- Chapter 5 provides conclusions and recommendations for future work.

2 Literature Review

This chapter reviews the concepts and developments relevant to the application of CEoS for predicting the phase behaviour and thermodynamic properties of pure components and mixtures. It begins with a brief introduction of the phase equilibrium phenomenon, with particular attention to the equal fugacity criteria of equilibrium; then, it presents a review of EoS with emphasis on CEoS: their inputs, capabilities, and limitations. This chapter also examines other EoS, such as the viral, and those based on the statistical associated fluid theory (SAFT). A critical aspect of this study is the tuning and selection of α-function for a CEoS. Therefore, a brief discussion on different α-functions is presented with particular emphasis on their capabilities and limitations.

2.1 The phase Equilibrium Phenomenon

Figure 2.1 represents a closed, two-phase system at thermodynamic equilibrium at a given T and P (Prausnitz *et al.*, 1998). The molar composition of phases ε and β given by the vectors x_i^{ε} and x_i^{β} (mixture compositions), respectively, are typically unknown; however, their calculation is needed because they are used as inputs for chemical engineering calculations in process design, simulation, and optimization. There are two options for determining phase compositions: 1) experimental data collection or 2) calculation based on thermodynamics of fluid phase equilibrium. Option 1 is time-consuming and expensive, requiring sophisticated experimental techniques and equipment. Option 2 is more convenient and efficient because calculations are carried out on a computer by solving the expressions of thermodynamic equilibrium.

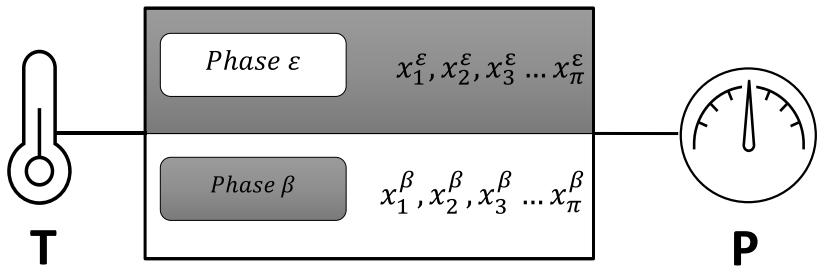

Figure 2.1: Schematic of a closed, two-phase system at equilibrium

For the system shown in Figure 2.1, and for any other system, all the following expressions must be satisfied at thermodynamic equilibrium:

$$T^\varepsilon = T^\beta \tag{2.1}$$

$$P^\varepsilon = P^\beta \tag{2.2}$$

$$f_i^\varepsilon = f_i^\beta \tag{2.3}$$

Equation 2.1 and Eq. 2.2 represents the thermal and mechanical equilibrium between phases ε and β, respectively; and Eq. 2.3 is required to ensure no net mass transfer between the two phases at equilibrium. The parameter f in Eq. 2.3 represents the fugacity of component i. Fugacity is a thermodynamic property dependent on T, P, and mixture composition (x) (Prausnitz *et al.*, 1998). For engineering calculations, it is mathematically convenient to define the following ratio:

$$\phi_i = \frac{f_i}{x_i P} \tag{2.4}$$

where ϕ_i is the fugacity coefficient of component i, and x_i is the molar composition of the component in the phase under analysis. The numerator in Eq. 2.4 represents the fugacity of component i at the system's T and P. The denominator represents the fugacity of the same

component in an ideal gas mixture at the system's T and P. Combining Eq. 2.4 and Eq. 2.3, the following expression is obtained:

$$\phi_i^{\varepsilon} x_i^{\varepsilon} = \phi_i^{\beta} x_i^{\beta} \tag{2.5}$$

Equation 2.5 expresses the equal fugacity criteria of equilibrium (Eq. 2.3) as a function of the ϕ_i. Equation 2.5 is mathematically convenient for engineering calculations as the ϕ_i can be explicitly calculated as:

$$\phi_i = Exp\left[\frac{1}{RT}\left[\int_0^P \left(\frac{\partial V}{\partial n_i}\right)_{T,P,n_j} - \frac{RT}{P}\right] dP\right] \tag{2.6}$$

where *V, n,* and *R* are the molar volume, the mole number, and the gas constant, respectively. The partial derivative $\partial V/\partial n_i$ is required as an input in Eq. 2.6. This partial derivative can be calculated numerically from experimental data or, as typical in engineering calculations, from an EoS.

2.2 Equations of State

An EoS is a mathematical expression that relates the three thermodynamic variables that define the phase behaviour of a fluid: *T, P,* and *V*. An EoS is most commonly used in engineering for the prediction of the number and composition of the phases coexisting at equilibrium at a given *T* and *P*. These calculations are vital for the design, simulation and optimization of reactors, separation operations, enhanced oil recovery operations, carbon capture and storage, etc. (Castier, 2011; Valderrama, 2003; Velasco *et al.*, 2012). To be applicable in engineering calculations, an EoS must satisfy the following requirements (Kontogeorgis and Folas, 2009; Michelsen and Møllerup, 2007):

- Be continuous across the entire phase diagram, including the critical region.
- Applicable to all possible phases: solid, liquid, vapour, supercritical, etc.
- Capable of predicting the existence of the vapour-liquid critical point.
- Able to predict physically correct trends for thermodynamic properties.
- Numerically and computationally efficient to ensure fast convergence.

To satisfy all these requirements, an EoS must be formulated based on the fundamental principles of molecular theory. However, the resulting EoS is usually highly complex, primarily applicable to gases and unsuitable for engineering calculations. One of the principles of molecular theory is that the macroscopic properties of a system are the result of contributions arising from different intermolecular interactions (Brush and Hall, 2003; Van Der Waals and Rowlinson, 1988). This idea has been conveniently used to formulate the following expression for the calculation of the total pressure of a system (Prausnitz *et al.*, 1998):

$$P_{total} = P_{repulsion} + P_{attraction} + P_{association} + P_{electrostatic} \qquad (2.7)$$

The total pressure, P_{total}, is the summation of different contributions arising from molecular, microscopic interaction (between individual molecules) of repulsion attraction and much stronger electrostatic interactions in the case of electrolyte systems, as well as molecular macroscopic (between groups of molecules) interaction such as association. The advantage of using Eq. 2.7 is that P_{total} is a macroscopic variable that can be easily measured. The different contributions in Eq. 2.7 can be either calculated theoretically or semi-theoretically. The following section presents a discussion of theoretical and semi-theoretical EoS.

2.3 Classification of Equations of State

All EoS fall into two distinct groups: theoretical and semi-theoretical. Statistical thermodynamics forms the fundamental groundwork of theoretical EoS, allowing for calculating thermodynamic properties from sound theoretical principles. In contrast, a semi-theoretical EoS uses empirical arguments to simplify theoretical principles and arrive at relatively simple expressions. In this sense, a semi-theoretical EoS is less complex than a purely theoretical EoS and, consequently, preferred for engineering calculations. Figure 2.2 shows some of the different EoS commonly used in engineering applications classified as theoretical and semi-theoretical. A brief discussion of some theoretical EoS is presented first. Then, a comprehensive review of a few semi-theoretical EoS is presented.

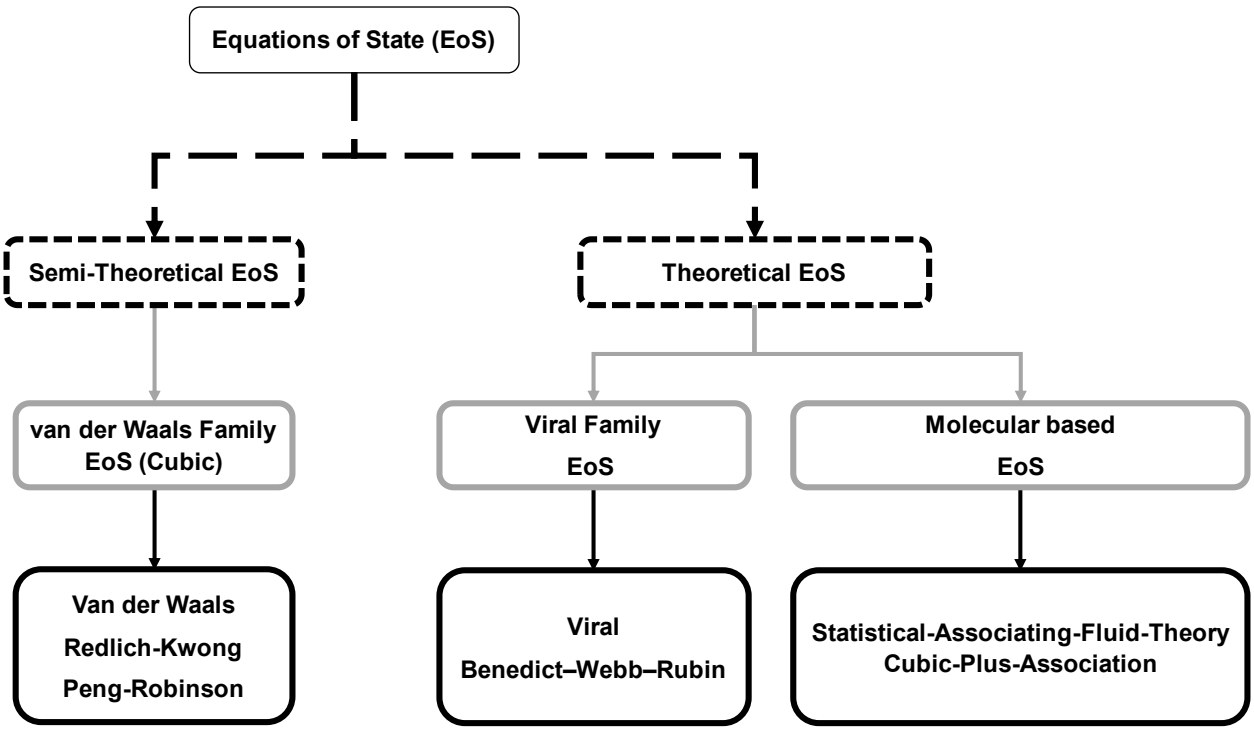

Figure 2.2: Classification of various types of equations of state

2.3.1 Theoretical Equations of State

2.3.1.1 The Viral Equation of State

The viral EoS (Thiesen, 1885a) calculates the pressure of a fluid as a departure from that of the ideal gas:

$$P = \frac{RT}{v}\left[1 + \frac{B}{v} + \frac{C}{v^2} + \frac{D}{v^3} + \cdots\right] \qquad (2.8)$$

where v is the molar volume, the parameters B, C, D, etc., are all volume-independent, temperature-dependent parameters known as the virial coefficients (Bourne, 2016; Sokovnin *et al.*, 2022; Thiesen, 1885b; Trusler, 2000a). What distinguishes the Viral EoS from other EoS is that the viral EoS has a rigorous theoretical foundation in statistical thermodynamics. From statistical thermodynamics, one can find analytical relations between the virial coefficients and the interactions between molecules in isolated clusters (Trusler, 2000b). The second viral coefficient, B, represents the interactions between pairs of molecules. The third viral coefficient, C, represents interactions between groups of three molecules; the fourth, D, represents interactions between clusters of four molecules, and so on (Prausnitz *et al.*, 1998; Sokovnin *et al.*, 2022; Thiesen, 1885b). Note, all virial coefficients, except for the first one, are equal to zero in the case of ideal gases as there are no intermolecular interactions in these fluids; therefore, Eq. 2.8 reduces to the ideal gas equation.

The viral EoS has not seen widespread use in engineering calculations as it requires too many virial coefficients to accurately describe the phase behaviour of fluids across the entire phase diagram. Benjamin *et al.* (Benjamin *et al.*, 2007) reported that at least 7 viral coefficients are needed to reproduce the PVT behaviour along the P^{sat} line. However, calculating high-order viral coefficients is very challenging as it requires complex molecular simulations that are

computationally intensive and expensive (Barker *et al.*, 1966; Benjamin *et al.*, 2006, 2007; Feng *et al.*, 2015; Xu *et al.*, 2022). Due to the complexity of calculating high-order virial coefficients, it is common practice to truncate the Virial EoS at two or three terms for practical applications. Such truncations limit the use of the Virial EoS to gases at or below a reduced density (ρ/ρ_c) of 0.6 (Bourne, 2016), representing only a portion of the entire phase diagram.

Several predictive correlations have been proposed for the second viral coefficient, *B* (Meng *et al.*, 2004; Nothnagel *et al.*, 1973; Xu *et al.*, 2021). These correlations are usually based on corresponding states (F. Ely and Marrucho, 2000; Hayden and O'Connell, 1975) or chemical theory (Nothnagel *et al.*, 1973). The principle of corresponding states proposes that all fluids exhibit similar behaviour when compared at the same reduced temperature (Tr) and reduced pressure (Pr). Those based on corresponding states are preferred for engineering calculations because of their relative simplicity; among them, the method of Hayden and O'Connell (Hayden and O'Connell, 1975) has been used to calculate *B* for polar, non-polar and hydrogen-bonding interacting components. The Virial EoS truncated after two terms is highly accurate for fluids that associate in the vapour phase, such as acids (Anderson and Prausnitz, 1978). However, the Virial EoS truncated after two terms only applies to gases at low to moderate pressures.

2.3.1.2 2.4.2 Statistical Associating Fluid Theory Equation of State

The SAFT EoS was developed from a versatile molecular theory that allows for calculating the phase behaviour and thermodynamic properties of fluids from the total Helmholtz energy of the system. The total Helmholtz energy is calculated from contributions from vdW London dispersion forces (fluctuating dipole moment, induction of dipole moments), polar interactions (permanent dipoles), molecular self and cross association. SAFT was developed by Chapman (Chapman *et al.*,

1989) based on Wertheim's theory for associating fluids (Wertheim, 1986). In SAFT, a fluid is assumed to be composed of equal-sized hard spheres, or segments, with two or more "sticky" spots (Sarkoohaki *et al.*, 2019). Hard spheres are used because there are physically sound expressions for calculating their thermodynamic properties derived from statistical thermodynamics. The hard sphere system is known in SAFT as the reference system. The "sticky" spots in each hard sphere allow the formation of chains that resemble the actual geometry and shape of the molecules. Finally, interaction sites are introduced at specific positions in the chain, enabling the chains to associate through hydrogen bonding or other polar interactions. A fluid's total Helmholtz free energy is calculated by adding the contributions from the segments, chain formation and association, Fig 2.3. An expression in terms of the system pressure, similar to that defined in Eq. 2.7, can be obtained by calculating the partial derivative of the Helmholtz free energy of each contribution with respect to volume at constant temperature as described by Michelsen and Møllerup (Møllerup and Michelsen, 2007).

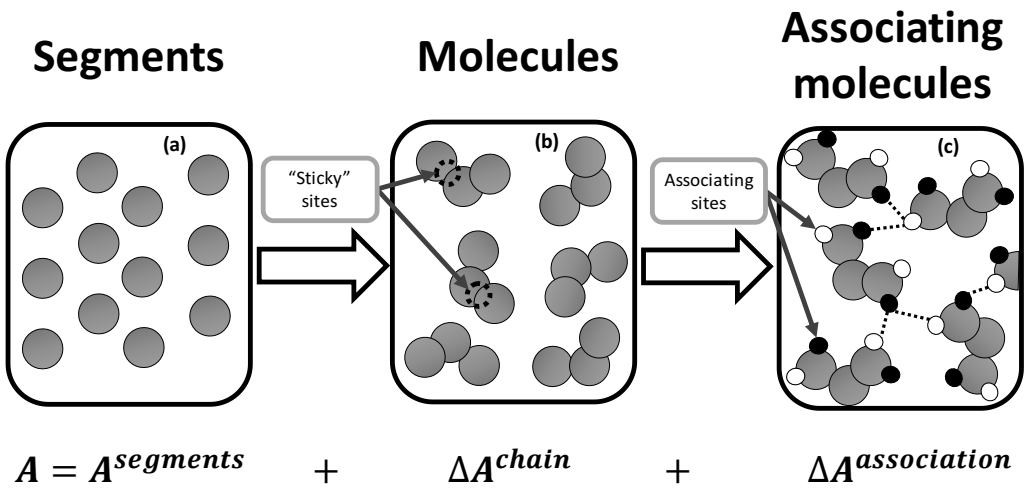

Figure 2.3: Schematic of contributions of the total Helmholtz free energy for Statistical Associating Fluid Theory based Equation of State.

For use in engineering calculations, the SAFT EoS requires the following inputs for non-associating components: the diameter of each molecular segment, the number of segments in the molecule and the interaction energy between molecular segments (Chapman *et al.*, 1989; Gross and Sadowski, 2001; Michelsen and Møllerup, 2007). These parameters are determined by fitting the SAFT EoS to experimental data or correlations (Chapman *et al.*, 1989; Gross and Sadowski, 2001; Kontogeorgis and Folas, 2009). SAFT requires additional inputs for associating components: the number of associating sites per molecule and the type of associating site (Møllerup and Michelsen, 2007). Huang and Radosz (Huang and Radosz, 1991) have reported the number and type of associating sites for different chemical groups such as acids, alcohols, water, amines, and ammonia.

Since its introduction, the SAFT EoS has attracted the interest of many researchers and engineers who have used it to model the thermodynamic behaviour of mixtures containing polar associating components such as water, alcohols, amines, and acids. The success of the SAFT EoS relies on accounting for molecular associations that control the phase behaviour of mixtures containing components interacting through hydrogen bonding and strong polar interactions. For instance, the SAFT EoS has produced accurate phase behaviour results for highly non-ideal systems such as water/hydrocarbon, alcohol/water, alcohol/hydrocarbon, amines/alcohol, amines/water/CO_2 mixtures (Aghaie *et al.*, 2019; Anderson and Prausnitz, 1978; Gokul *et al.*, 2021; Marshall, 2019, 2020; Tsochantaris *et al.*, 2020). These mixtures are essential for designing enhanced oil recovery processes, separation operations in biorefineries, and carbon capture and storage processes. However, despite its accuracy, the SAFT EoS is not widely used in engineering calculations because of its mathematical complexity (Kontogeorgis and Folas, 2009).

2.4 Semi-Theoretical Equations of State

2.4.1 Cubic Equations of State

A CEoS assumes that the total pressure of a fluid arises only from the contributions due to attractive and repulsive forces between pairs of molecules (Prausnitz *et al.*, 1998). Then, for a CEoS, the general expression seen in Eq. 2.7 reduces to:

$$P_{total} = P_{repulsion} + P_{attraction} \tag{2.9}$$

2.4.2 Van Der Waals Type Cubic Equations of State

CEoS are widely used in designing, simulating, and optimizing industrial processes. They have become prevalent due to their simplicity, versatility, and computational efficiency. The first CEoS was proposed by Van Der Waals in 1873 (Van Der Waals, 1873) and is defined below:

$$P = \frac{RT}{v-b} - \frac{a_c}{v^2} \tag{2.10}$$

The first term on the right-hand side of Eq. 2.10 is the repulsive pressure term, and the second on Eq. 2.10 is the attractive pressure term. The repulsive term in the vdW CEoS was derived from the kinetic theory of hard spheres (Cohen, 1993; van Beijeren and Ernst, 1979; Van Der Waals and Rowlinson, 1988), and the attractive term is empirical (Van Der Waals and Rowlinson, 1988). The Van Der Waals equation is called a "cubic" EoS because it can be written as a cubic polynomial of the molar volume.

The parameters b (m^3/kmol) and a_c $\left(\frac{m^3\ kJ\ T^{0.5}}{1000\ kmol^2}\right)$ In Eq. 2.10 are the co-volume and the attractive parameter, respectively. For pure components, these two parameters are calculated by constraining

the first and second derivatives of the CEoS to satisfy the following thermodynamic requirement at the critical point (Whitson and Brulé, 2000):

$$\left(\frac{\partial P}{\partial v}\right)_{P_c,T_c,v_c} = \left(\frac{\partial^2 P}{\partial v^2}\right)_{P_c,T_c,v_c} = 0 \qquad (2.11)$$

T_c, P_c, and v_c are the critical temperature, pressure, and molar volume. The vdW CEoS is continuous across the entire phase diagram by satisfying this requirement at the critical point. Although vdW CEoS provides qualitatively correct phase boundaries, these predictions of vapour liquid phase boundaries are not sufficiently accurate for most engineering calculations, especially at low to moderate temperatures (Valderrama, 2003). This poor accuracy at low to moderate temperatures arises from deficiencies in the mathematical expression for calculating the attractive term, which is too simple to capture the actual repulsion between molecules (Clausius, 1880). These shortcomings motivated the development of the RK and the PR CEoS.

For simplicity, the following generalized expression of a CEoS will be used for the RK and the PR CEoS (Valderrama, 1990).

$$P = \frac{RT}{v-b} - \frac{\alpha(T)\, a_c}{(v+\delta_1 b)(v+\delta_2 b)} \qquad (2.12)$$

The main difference between Eq. 2.12 and the VdW CEoS (Eq. 2.10) is that the attractive term has been empirically modified to improve the flexibility of the CEoS for accurate engineering calculations. Parameters δ_1 and δ_2 in Eq. 2.12 are empirical constants that determine the volumetric dependence of the attractive pressure term (Kontogeorgis and Folas, 2009; Michelsen and

Møllerup, 2007), and $\alpha(T)$ is a fluid-specific, temperature-dependent parameter calculated by fitting Eq. 2.12 to experimental data. When $\delta_1 = \delta_2 = 0$ and $\alpha = 1$, Eq. 2.12 reduces to the vdW CEoS. When $\delta_1 = 1$ and $\delta_2 = 0$, Eq. 2.12 yields the RK CEoS (Redlich and Kwong, 1949); and, when $\delta_1 = 1+(2)^{0.5}$ and $\delta_2 = 1-(2)^{0.5}$, Eq. 2.12 yields the PR CEoS (Peng and Robinson, 1976).

The parameters b and a_c in Eq. 2.12 are calculated by solving Eq. 2.11. The expressions for b and a_c are given by:

$$b = \Omega_b \frac{R\,T_c}{(P_c)} \tag{2.13}$$

$$a_c = \Omega_a \frac{(R\,T_c)^2}{(P_c)} \tag{2.14}$$

The values of Ω_b and Ω_a for the vdW, RK and PR CEoS are given in Table 2.1. A brief discussion on the application of the RK and PR CEoS in engineering calculations is provided in the following sections.

Table 2.1: Constants for the generalized cubic equation of state (Eq. 2.12). Z_c is the critical compressibility factor ($Z_c = P_c * V_c / R * T_c$).

Equation	Ω_α	Ω_β	Z_c	δ_1	δ_2
Van Der Waals	0.422	0.125	0.375	0	0
Redlich-Kwong	0.427	0.087	0.333	1	0
Peng–Robinson	0.457	0.078	0.307	$1+(2)^{0.5}$	$1-(2)^{0.5}$

2.4.3 The Redlich-Kwong Cubic Equation of State

Redlich and Kwong (Redlich and Kwong, 1949) modified the volume function in the denominator of the attractive term of the vdW CEoS (Eq. 2.10). They reintroduced temperature dependency for α as initially recommended by Clausius (Clausius, 1880). Clausius reasoned that the magnitude of

the attraction between pairs of molecules decreases with increasing temperature and approaches zero at infinite temperature. Based on Clausius' reasoning, Redlich and Kwong (Redlich and Kwong, 1949) proposed an empirical parameter known as α to account for the effect of the temperature on the attractive term of a CEoS. The proposed α parameter is given by:

$$\alpha(T) = \frac{1}{(T_r)^{0.5}} \tag{2.15}$$

where T_r is the reduced temperature, compared to the VdW CEoS, the RK CEoS produces more accurate P^{sat} of pure components (the procedure for calculating P^{sat} is covered in section 3.2); however, the RK CEoS produces poor results for high molecular weight and polar components (Wilson, 1966; Zudkevitch and Joffe, 1970). To improve the accuracy of the RK CEoS, Soave (Soave, 1972a) proposed the following expression for the calculation of α:

$$\alpha(T) = \left(1 + m_{RK}(1 - (T_r)^{0.5})\right)^{0.5} \tag{2.16}$$

where m_{RK} is a fluid-specific parameter fitted to match the P^{sat} of a pure component at $T_r = 0.7$ and can be correlated to the ω as follows:

$$m_{RK} = 0.480 + 1.574\omega - 0.176\omega^2 \tag{2.17}$$

where ω is the acentric factor, the RK CEoS with the α parameter calculated from Eq. 2.16 is commonly referred to as the Soave-Redlich-Kwong (SRK) CEoS. Note that the α parameter calculated from Eq 2.16 does not approach zero at a high reduced temperature as required by Clausius' postulate regarding attractive interactions between molecules (Clausius, 1880)

2.4.4 The Peng-Robinson Cubic Equation of State

Peng and Robinson (Peng and Robinson, 1976) modified the attractive pressure term of the RK CEoS, intending to produce 1) more accurate saturated liquid density values and 2) a critical compressibility factor (Z_c) closer to that of hydrocarbons. The resulting equation, the PR CEoS, produces better saturated liquid densities and a lower Z_c than those from the RK or SRK CEoS, as shown in Table 2.1. Although saturated liquid densities calculated from the PR CEoS are more satisfactory than those calculated from the RK or SRK CEoS, the calculated liquid densities are not accurate enough for wide use in process design and simulation without the use of volume translation (Whitson and Brulé, 2000). Regarding Z_c, the PR CEoS predicts a fixed value 0.307, somewhat closer to the experimental value of heavier hydrocarbons found in crude oils. The fixed Z_c value predicted by the RK and SRK CEoS is 0.333, which is considered too high for applications in the petroleum industry. This difference in Z_c values is why the PR CEoS is used in the petroleum industry. However, when properly tuned, the PR and the SRK CEoS produce similar vapour-liquid equilibrium results (Whitson and Brulé, 2000).

Peng and Robinson (Peng and Robinson, 1976) also proposed an expression for α similar to that developed by Soave (Eq. 2.16 and 2.17). The value of m_{PR} in Eq. 2.18 was fitted to match the P^{sat} of pure components from the normal boiling point to the critical point, whereas Soave fitted m_{RK} to match the P^{sat} only at $T_r = 0.7$. The fitted value of m_{PR} for the PR CEoS is defined below (Peng and Robinson, 1976):

$$m_{PR} = 0.3746 + 1.5422\omega - 0.2699\omega^2 \qquad (2.18)$$

2.4.5 Advantages, and Limitations of The Redlich-Kwong and Peng-Robinson Cubic Equations of State

The key factors that have contributed to the widespread application of CEoS in process design, simulation and optimization are 1) their relative simplicity, 2) ease of use, and 3) numerical efficiency (Kontogeorgis and Folas, 2009; Prausnitz and Tavares, 2004; Valderrama, 1990). Additionally, highly optimized, reliable, and easily applicable algorithms, like those proposed by Michelsen and Møllerup (Michelsen and Møllerup, 2007), are readily available for calculating all commonly used thermodynamic properties. Table 2.2 presents a list of the advantages and disadvantages of CEoS.

Table 2.2: Advantages, and limitations of the Redlich-Kwong and Peng-Robinson cubic equations of state (Kontogeorgis and Folas, 2009; Valderrama, 2003)

Advantages	Disadvantages
Simple models capable of fast calculations.	It cannot be easily extended to 'more complex' molecules like electrolytes and biomolecules.
Capable of describing properties of compounds in both liquid and vapour phases.	Do not produce good results for solid phases and hydrates.
Well-established mixing rules for the calculation of mixture phase behaviour.	Predictions for binary mixtures often require interaction parameters fitted to experimental data.
Satisfactory results for both low- and high-pressure vapor-liquid equilibrium.	Poor correlation of complex vapour-liquid equilibrium of mixtures containing polar components.
For most applications, CEoS can be tuned to give acceptable values for thermodynamic properties.	Do not yield accurate liquid volumes unless a volume translation is used.
Present correct limiting behaviour: as $V \rightarrow b$, $P \rightarrow \infty$ in all Van Der Waals type equations.	The temperature dependency of α is not well established; b seems density-dependent, but the dependence is unknown.
Many existing databases and correlations are available for binary interaction parameters,	It is challenging to develop generalized binary interaction parameters for predictive applications.
Cubic equations are suitable for applying modern mixing rules that include Gibbs free energy models or concentration-dependent parameters.	Several interaction parameters might be required in applications to complex mixtures, even with modern mixing rules.
Good multicomponent VLE prediction for mixtures containing hydrocarbons, gases, and other non-polar compounds	Calculations can be sensitive to the interaction parameter, especially for gas-hydrocarbons

Several studies suggest that most of the limitations presented in Table 2.2 could be overcome by proposing more flexible expressions for the calculation of the parameter α that allow a more accurate fitting of the CEoS to experimental data (Le Guennec *et al.*, 2016; Twu *et al.*, 1995a, 1995b; Young *et al.*, 2016). A review of the most widely used expressions for the calculation of α, or α-functions, is presented in the following section.

2.5 An Overview of Common α-Functions

The introduction of α-functions has been paramount to improving the accuracy and versatility of CEoS. The most popular α-function currently in use is that proposed by Soave (Soave, 1972a), Eq. 2.16. The widespread use of the Soave α-function emerges from the fact that the fluid-specific parameter m in Eq.2.16 can be easily correlated to ω, as seen in Eq. 2.17, making the Soave α-function predictive. However, the Soave α-function does not produce a satisfactory correction for polar components, and, consequently, the predicted P^{sat} for these components has higher deviations (Le Guennec *et al.*, 2016; Mathias and Copeman, 1983a; Young *et al.*, 2016). Moreover, the calculation of inaccurate pure component P^{sat} affects the calculation of the mixture's Helmholtz energy, potentially producing thermodynamically inconsistent results or fake phase behaviour predictions (Van Ness *et al.*, 1973; Whitson and Brulé, 2000). Therefore, the convenience and simplicity of the Soave α-function come at the cost of accuracy when dealing with complex systems. To address these shortfalls, researchers have proposed numerous α-functions. The *following subsections briefly discuss the α-functions widely used in engineering calcula*tions.

2.5.1 The Mathias α-Function

Mathias(Mathias, 1983) proposed an α-function that attempts to correct the inaccuracies of the Soave α-function at T_r different from 0.7, with a focus on improving prediction for polar components:

$$\alpha(T) = \left[1 + m_m\left(1 + (T_r)^{0.5}\right) - p\,(1 - T_r)(0.7 - T_r)\right]^{0.5} \qquad (2.19)$$

$$m_m = 0.48508 + 1.5519\omega - 0.15613\omega^2 \qquad (2.20)$$

where p, known as the polar parameter, is a component-specific adjustable parameter fitted to experimental P^{sat} (Mathias, 1983). The Mathias α-function is more accurate than the function developed by Soave due to its flexibility arising from the additional adjustable parameter p (Mathias, 1983; Young *et al.*, 2016). However, the Mathias α-function is not widely used because there is no correlation for calculating parameter p.

2.5.2 The Mathias−Copeman α-Function

Mathias and Copeman (Mathias and Copeman, 1983b) proposed an α-function with three adjustable parameters:

$$\alpha(T) = \left[1 + C_1\,(1 - (T_r)^{0.5}) + C_2\,(1 - (T_r)^{0.5})^2 + C_3(1 - (T_r)^{0.5})^3\right]^2 \qquad (2.21)$$

where C_1, C_2, and C_3 are fluid-specific adjustable parameters calculated by fitting experimental P^{sat} data. The introduction of these three parameters makes Eq. 2.21 very flexible and capable of effectively fitting the Psat of polar and non-polar components, producing more accurate results. However, there is no generalized correlation for calculating parameters C1, C2, and C3, making Eq. 2.21 non-predictive and consequently unsuitable for engineering calculations.

2.5.3 The Stryjek−Vera α-Function

Stryjek and Vera (Stryjek and Vera, 1986) proposed the following α-function for the PR CEoS:

$$\alpha(T) = k_o + k_1(1 + (T_r)^{0.5})(0.7 - T_r) \qquad (2.22)$$

$$k_o = 0.378893 + 1.4897153\omega - 0.17131848\omega^2 + 0.0196554\omega^3 \qquad (2.23)$$

where k_1 is an adjustable parameter fitted to P^{sat} data, Stryjek and Vera tested their α-function on 90 pure components of industrial interest, including 37 hydrocarbons, 10 ketones, 12 alcohols, 10 ethers, and 17 components from assorted chemical families (Stryjek and Vera, 1986). Stryjek and Vera reported that deviations usually fell below 1% for P^{sat}. Stryjek and Vera recommend using a value of $k_1=0$ for a T_r higher than 0.7; however, there is no correlation for calculating k_1 at reduced temperatures below 0.7, which renders the equation unsuitable for predictive applications.

2.5.4 The Trebble−Bishnoi α-Function

Trebble and Bishnoi (Trebble and Bishnoi, 1987) proposed the following exponential expression for the calculation of α as an attempt to capture the exponential behaviour depicted by thermodynamic properties near the critical point as described by Valderrama (Valderrama, 2003):

$$\alpha(T) = exp[m_{TB}(1 - Tr)] \qquad (2.24)$$

where m_{TB} is the only fluid-specific adjustable parameter and can be fitted to P^{sat} data. The Trebble−Bishnoi function is a single parameter α-function and, as indicated in preceding subsections, results in limited flexibility when handling polar components. Trebble and Bishnoi (Trebble and Bishnoi, 1987) also proposed a generalized expression for calculating m_{TB} using P^{sat} data from 75 polar and non-polar components (Trebble and Bishnoi, 1987).

The Trebble−Bishnoi α-function has unfortunately been reported to result in high errors (relative to other α-functions) when used to evaluate P^{sat}. Coquelet *et al.* (Coquelet *et al.*, 2004) tested the correlation proposed by Trebble and Bishnoi on the PR CEoS for P^{sat} of 15 hydrocarbons, 4 polar, and 3 other components. Coquelet *et al.* (Coquelet *et al.*, 2004) reported an overall average

absolute relative deviation (AARD) (Eq. 3.19) of 3.30%, which is notably higher than the Soave, Mathias-Copeman, Stryjek-Ver, and Twu α-functions which typically give an oval value of 2% AARD (Valderrama, 2003).

2.5.5 The Twu α-Function

Another exponential α-function was proposed by Twu *et al.* (Twu *et al.*, 1995b) and is defined below:

$$\alpha(T) = T_r^{N(M-1)}\, exp\left(L(1 - T_r^{NM})\right) \tag{2.25}$$

where *N, M,* and *L* are all component-specific adjustable parameters that are calculated by fitting them to pure component P^{sat}. The Twu α-function gets its flexibility from utilizing three adjustable fluid-specific parameters at the cost of complexity. Compared to other α-functions, the Twu α-function produces better results for non-polar and polar components, especially when compared to the Soave α-function (Valderrama, 2003; Young *et al.*, 2016). Furthermore, as described by Le Guennec *et al.* (Le Guennec *et al.*, 2017), if adequately constrained, the Twu α-function can produce consistent values (discussion of consistent α curves is further discussed in Section 2.6). The Twu α-function, however, is not predictive as there is no general correlation for calculating the three parameters *N, M* and *L*.

2.5.6 Updated Soave α-Function

Pina-Martinez *et al.* (Pina-Martinez *et al.*, 2019a) updated the expression for calculating parameter *m* of the Soave α-function to improve its predictions. The Soave α-function's general expression

(Eq. 2.17) was initially fitted using a slim number of components consisting mainly of hydrocarbons at a T_r of 0.7 (Soave, 1972b). Pina-Martinez *et al.* evaluated 1,721 pure components of various chemical families within the subcritical range (Pina-Martinez *et al.*, 2019a). Pina-Martinez *et al.* proposed the following correlation for *m* for the PR and RK CEoS:

$$m_{PR-pina} = 0.3919 + 1.4996\omega - 0.2721\omega^2 + 0.1063\omega^3 \quad (2.26)$$

$$m_{RK-pina} = 0.4810 + 1.5963\omega - 0.2963\omega^2 + 0.1233\omega^3 \quad (2.27)$$

where $m_{PR\text{-}Pina}$ and $m_{RK\text{-}Pina}$ are correlations intended for the PR and RK CEoS, respectively. Pina-Martinez *et al.* reported that when parameter *m* is calculated from Eq. 2.26 or 2.27, the calculated P^{sat} of pure components from the PR and RK CEoS are more accurate than those obtained when *m* is calculated from their respective original expressions shown in Eq. 2.18 and 2.17.

2.5.7 Comparison of α-Functions

Young *et al.*(Young *et al.*, 2016) evaluated 20 α-functions using the PR CEoS, including all the α-functions discussed in this section. Young *et al.* tested the α-functions on 56 components from assorted chemical families, including hydrocarbons, non-condensable gases, alcohols, organic acids, and other organic polar components. Table 2.3 summarizes errors for the 5 different α-functions discussed here. In the study by Young et al., the Trebble-Bishnoi and Soave α-functions exhibited suboptimal performance. Specifically, the Trebble-Bishnoi α-function had the highest overall AARD (Eq. 3.19), except water, among all chemical family groups tested. An overall AARD of 2.33% was reported for the Trebble-Bishnoi α-function. The Soave α-function, too, demonstrated subpar performance, exhibiting an overall AARD of 2.03%. However, the Mathias-Copeman, Twu, and Stryjek-Vera α-functions were much more accurate, with reported overall

AARD of 0.60, 0.66, and 0.75% respectively. The study conducted by Young *et al.* supports the observation that α-functions with three parameters show better performance when calculating thermodynamic properties due to their superior flexibilities. The observation is particularly apparent when modelling polar and associating components.

Table 2.3: Performance Overview of selected α-functions reporting average absolute relative deviations (AARD), in %. NC is the number of components (Young *et al.*, 2016)

Family group	**NC**	**α-functions AARD, %**					
		Soave	**Mathias-Copeman**	**Stryjek-Vera**	**Trebble-Bishnoi**	**Twu**	***Overall***
Alkanes	10	0.72	0.45	0.56	1.82	0.45	0.80
Hydrocarbon	18	0.97	0.41	0.70	2.10	0.44	0.92
Water	01	1.91	0.19	0.25	0.59	0.21	0.63
Permanent Gases	08	1.12	0.19	0.31	1.94	0.27	0.77
Alcohol	04	4.51	1.21	1.14	4.40	1.33	2.52
Organic Acid	02	4.62	1.25	1.60	3.27	1.47	*2.44*
Polar	08	1.02	0.61	0.77	2.21	0.60	*1.04*
C/N	05	1.40	0.50	0.67	2.28	0.54	*1.08*
Overall	*56*	*2.03*	*0.60*	*0.75*	*2.33*	*0.66*	*1.28*

* C/N-Chlorinated / Nitrogenated

2.6 Consistency Check for α-Function

A detailed discussion of thermodynamic inconsistency and the associated consequences was provided in Chapter 1. To ensure a CEoS produces consistent thermodynamic results, the α-function must obey the following thermodynamic constraints (Le Guennec *et al.*, 2017):

$$\alpha \geq 0 \; and \; \alpha(T) \; is \; continuous \tag{2.28}$$

$$\frac{d\alpha}{dT_r} \leq 0 \; and \; \frac{d\alpha}{dT_r} \; is \; continuous \tag{2.29}$$

$$\frac{d^2\alpha}{dT_r^2} \geq 0 \; and \; \frac{d^2\alpha}{dT_r^2} \; is \; continuous \tag{2.30}$$

$$\frac{d^3\alpha}{dT_r^3} \leq 0 \tag{2.31}$$

The assertion of the continuity of α (Eq. 2.28) and the derivatives of α (Eq. 2.29 and 2.30) are required to avoid discontinuities in the calculated state functions (Le Guennec *et al.*, 2016). Equation 2.28 asserts that α-functions must be positive and continuous. The attractive term (2nd term of Eq. 2.12), which strongly depends on the value of the α-function, must always decrease the system's total pressure. Therefore, a sign change would result in physically inconsistent behaviour (Deiters, 2013). This constraint can also be observed in Figure 2.4, which illustrates a consistent α-function plotted against the T_r. Equation 2.28 ensures that the curve shown in Figure 2.4 is continuous, positive, and free of discontinuities. Equation 2.29 ensures the α-function approaches zero as the reduced temperature approaches infinity, as seen in Figure 2.4. By doing so, Eq. 2.29 satisfies the theoretical requirement demanding only repulsive forces at infinite temperature (the attractive term in Eq. 2.12 cancels out when α=0). Le Guennec *et al.* (Le Guennec *et al.*, 2016) also demonstrated that Eq. 2.30 and 2.31 are vital in ensuring the reliability of calculations derived from the cubic equation of state (CEoS). Specifically, Equation 2.30 guarantees that the C_p^{sat} values are positive, while Eq. 2.31 verifies that the calculated temperature trends do not display inconsistent inflection points in the supercritical region, aligning with the observed behaviour in experimental C_p^{sat} data, which does not showcase any inflection points in the supercritical region.

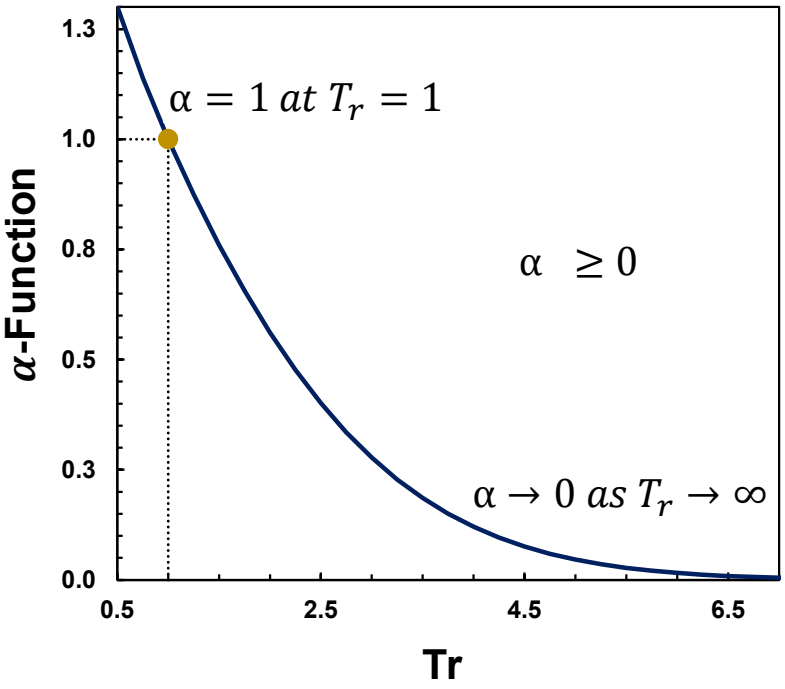

Figure 2.4: Schematic of a thermodynamically consistent α-function

2.7 Summary

EoS saw significant developments over the past century, from the original vdW CEoS to more recent EoS like the RK and PR CEoS. CEoS are not purely grounded in theoretical principles like the Virial EoS. They also do not adequately account for molecular association due to polar or electrostatic interactions. Nevertheless, a CEoS can provide an acceptable approximation of thermodynamic properties across the phase diagram. A CEoS is the preferred choice for most engineering applications due to its simplicity and versatility. Since Soave originally developed his α-function, which can still be found in modern-day process simulators, numerous authors have proposed new α-functions to improve the accuracy of the calculations. Among these, the α-function proposed by Twu *et al.* is one of the best alternatives to the popular Soave α-function due to its flexibility and improved accuracy for polar and non-polar components. Furthermore, as

proven by Le Guennec *et al.* (Le Guennec *et al.*, 2016), the Twu α-function can be constrained to satisfy the consistency check presented in Eq. 2.28 to 2.31.

3 Modelling Methodology

This chapter reviews the different modelling techniques and algorithms designed to fit the PR and RK equations of state with α parameter from the Twu function to experimental data. The chapter first reviews the calculation of saturation pressure, enthalpy of vaporization and heat capacity from a cubic equation of state; then, it presents the optimization algorithm used to fit the equation to data; and, finally, it describes the experimental dataset used for fitting in this study.

3.1 The Generalized Cubic Equation of State

For computational calculations, it's advantageous to formulate the generalized CEoS in terms of the reduced Helmholtz function, a thermodynamic potential that quantifies the system's available energy to perform useful work while at a constant V and T. Using A^r facilitates the calculation of all thermodynamic properties as they can be calculated explicitly from the partial derivatives of the Helmholtz function. The generalized CEoS in terms of A^r is given by (Michelsen and Møllerup, 2007).

$$\frac{A^r(T,v^\beta)}{RT} = -ln\left(1-\frac{b}{v^\beta}\right) - \frac{\alpha(T)}{RTb(\delta_1-\delta_2)} ln\left(\frac{1+\frac{\delta_1 b}{v^\beta}}{1+\frac{\delta_1 b}{v^\beta}}\right) \tag{3.1}$$

The pressure explicit EoS presented in Eq.2.12 and Eq. 3.1 are related as follows:

$$P = -\left(\frac{\partial A^r(T,v)}{\partial v}\right)_T + \frac{RT}{v} \tag{3.2}$$

The parameter $\alpha(T)$ in Eq. 3.1 is given by:

$$\alpha(T) = \alpha\, a_c \tag{3.3}$$

In this study, the parameter α (*or* $\alpha(T)$) was calculated using the Twu (Twu *et al.*, 1991b, 1991a) correlation:

$$\alpha(T) = T_r^{\alpha_1}\, exp\left(\alpha_2\left(1 - T_r^{\alpha_3}\right)\right) \tag{3.4}$$

where α_1, α_2 and α_3 are fluid-specific parameters calculated by fitting the generalized CEoS, Eq. 3.1, with parameter α calculated from Eq. *3.4* to experimental P^{sat}, ΔH_v and C_p^{sat} as recommended by Pina-Martinez *et al.* (Pina-Martinez *et al.*, 2018). Pina-Martinez *et al.* highlighted the importance of combining three thermodynamic properties, P^{sat}, ΔH_v, and C_p^{sat} to optimize the accuracy of an α-function's parameters. While P^{sat} data is a fundamental requirement, the inclusion of the other two types (ΔH_v and C_p^{sat}) significantly enhances the accuracy of the CEoS. ΔH_v and C_p^{sat} also improve derivative thermodynamic property prediction. The calculation of ΔH_v (Eq. 3.7-3.11) requires computing the first derivative of α, whereas C_p^{sat} (Eq. 3.12-3.16) is a function of the second derivative. Therefore, it is possible to assess the accuracy of the calculated derivatives through these properties.

3.2 Flash Calculations

In Eq *3.4*, the P^{sat}, H_v and C_p^{sat} required for fitting α_1, α_2 and α_3 were calculated from an isothermal two-phase flash algorithm. The flash algorithm uses the accelerated successive substitution method developed by Michelsen and Møllerup (Michelsen and Møllerup, 2007) to find the pressure that satisfies the following equation at a given temperature:

$$\left(\frac{\phi^{v(T,P)}}{\phi^{l(T,P)}} - 1\right)^2 = 0 \qquad (3.5)$$

where ϕ is the fugacity coefficient of the pure component and superscripts v and l stand for the vapour and liquid phases, respectively. Equation 3.5 is only satisfied when the fugacity of the pure component in the vapour phase is equal to that in the liquid phase (equal fugacity criteria of equilibrium, Eq. 2.3). The fugacity coefficient in the vapour and liquid phases is calculated as follows:

$$ln\left(\phi^{\beta}\right) = \left(\frac{A^r}{RT}\right)^{\beta} + Z^{\beta} - 1 - \ln\left(Z^{\beta}\right) \qquad (3.6)$$

where A^r/RT is calculated from Eq. 3.1, Z is the compressibility factor, and β is the vapour or liquid phase. For instance, to calculate ϕ in the vapour phase using Eq. 3.6 at a given T and P, A^r/RT is calculated using the v of the vapour phase and the T, and Z is calculated using the v of the vapour phase, the T, and the P. The P at equilibrium is unknown. Therefore, an iterative method (or flash calculation) was used to find the P that satisfies the equal fugacity criteria shown by Eq. 3.5. The solution of Eq. 3.5 produces the P^{sat} and the compressibility factors of the vapour, Z^v, and liquid, Z^l, phases at equilibrium. The flash calculations (iterative procedure to solve Eq. 3.5) were performed in MATLAB (R2021b-R2023a) using the accelerated substitution method proposed by Michelsen and Mollerup (Michelsen & Mollerup, 2007). This algorithm's average speed was 3000 flash calculations per second with an Intel(R) Core (TM) i7-9700 CPU @ 3.00GHz processor.

The enthalpy of vaporization, ΔH_v, was calculated using P^{sat}, Z^v and Z^l as inputs, according to:

$$\Delta H_v = H^v - H^l \tag{3.7}$$

$$H^\beta = A^r\left(T, v^\beta\right) + T\,S^{res}\left(T, v^\beta\right) + P^{sat}v^\beta - RT + H^{ideal\ gas} \tag{3.8}$$

$$v^\beta = Z^\beta \frac{RT}{P^{sat}} \tag{3.9}$$

$$\frac{S^{res}\left(T,v^\beta\right)}{R} = -T\left[\frac{\partial F}{\partial T}\right] - F \tag{3.10}$$

$$F = \frac{A^r(T,v_{liq})}{RT} \tag{3.11}$$

where superscript β stands for vapour, v, or liquid, l, phases; S^{res} is the residual entropy; and $H^{ideal\ gas}$ is the enthalpy of the ideal gas at the system T. The $H^{ideal\ gas}$ cancels out when evaluating Eq. 3.7 and, therefore, does not need to be evaluated. The C_p^{sat} was calculated as follows:

$$C_p^{sat} = C_p^{sat\ (res)} + C_p^{ideal\ gas} \tag{3.12}$$

$$C_p^{sat\ (res)} = C_{V_{liq}}^{res} - T\frac{\left(\frac{\partial P}{\partial T}\right)_{V_{liq}}^2}{\left(\frac{\partial P}{\partial V_{liq}}\right)_T} - R \tag{3.13}$$

$$C_{V_{liq}}^{res} = \left(-T^2\left(\frac{\partial^2 F}{\partial T^2}\right)_{V_{liq}} - 2T\left(\frac{\partial F}{\partial T}\right)_{V_{liq}}\right)R \tag{3.14}$$

$$\left(\frac{\partial P}{\partial T}\right)_{V_{liq}} = -RT\left(\frac{\partial^2 F}{\partial T \partial V_{liq}}\right) + \frac{P}{T} \tag{3.15}$$

$$\left(\frac{\partial P}{\partial V_{liq}}\right)_T = -RT\left(\frac{\partial^2 F}{\partial V_{liq}^2}\right)_T - \frac{RT}{V_{liq}^2} \tag{3.16}$$

$C_p^{ideal\ gas}$ is the heat capacity of the ideal gas at the system's absolute T and is calculated using the correlation proposed by Yaws (Yaws, 2015).

$$C_P^{ideal\ gas} = A_{Cp} + B_{Cp}T + C_{Cp}T^2 + D_{Cp}T^3 \qquad (3.17)$$

where A_{cp}, B_{cp}, C_{cp}, and D_{cp} are fluid-specific parameters reported by Yaws (Yaws, 2015). The flash algorithm implemented in this study calculates P^{sat}, ΔH_v, and C_p^{sat} using the following inputs: 1) the absolute T of the system; 2) constants A_{cp}, B_{cp}, C_{cp}, and D_{cp} in Eq. 3.17; 3) the T_c and P_c of the pure component for the calculation of a_c and b using Eq. 2.14 and 2.13, respectively; and 4) parameters α_1, α_2, and α_3 for the calculation of $\alpha(T)$ from Eq. *3.4*. All the required inputs are known except for parameters α_1, α_2 and α_3.

3.3 Optimization Algorithm

The parameters α_1, α_2 and α_3 in Eq. 3.4 were calculated by minimizing the following objective function, *OF*:

$$OF = W_{f\,P^{sat}}\left(\frac{AARD_{P^{sat}}}{100}\right)^2 + W_{f\,\Delta H^{vap}}\left(\frac{AARD_{\Delta H^{vap}}}{100}\right)^2 + W_{f\,Cp^{sat}}\left(\frac{AARD_{Cp^{sat}}}{100}\right)^2 \qquad (3.18)$$

where W_f is the property weighting factor, and AARD is the average absolute relative deviation calculated as:

$$AARD(\%) = \frac{100}{NP}\sum_1^{NP}\left|\frac{X_{exp} - X_{calc}}{X_{exp}}\right| \qquad (3.19)$$

where subscripts *calc* and *exp* refer to calculated and experimental values, respectively; X is the property under study; and NP is the number of experimental data points. The advantage of using AARD in Eq. 3.18 instead of another deviation metric (for instance, the absolute error or deviation) is that the objective function (Eq. 3.18) is dimensionless. The values of W_f are unknown and were determined as follows. The three weighting factors in Eq. 3.18 were changed from 0 to 1 with increments of 0.1 until a tridimensional grid was constructed. Then, Eq. 3.18 was minimized at each one of the nodes of the tridimensional grid (or combination of weighting factors) by using a non-linear optimization algorithm (fmincon) in MATLAB™ constrained to satisfy the thermodynamic consistency criteria shown in Eq. 2.28 to 2.31. The following constraints were imposed on the weighting factors to eliminate redundant nodes and ensure accurate values of P^{sat}:

$$\sum W_f = W_{f\,P^{sat}} + W_{f\,\Delta H^{vap}} + W_{f\,Cp^{sat}} = 1 \qquad (3.20)$$

$$W_{f\,P^{sat}} \geq 0.5 \qquad (3.21)$$

$$W_{f\,\Delta H^{vap}}\ and\ W_{f\,Cp^{sat}} \neq 0 \qquad (3.22)$$

The first constraint, Eq. *3.20*, significantly eliminates the number of redundant sets. The second constraint, Eq. *3.21*, ensures that the optimizer will prioritize the minimization of errors associated with the P^{sat} over the ΔH_v, or C_p^{sat}; and the third constraint, Eq. *3.22*, ensures that the ΔH_v and C_p^{sat} influence the optimization procedure. It is required to produce highly accurate values of P^{sat} at the pure component level for engineering applications to ensure that when the CEoS is extended to mixtures, it still produces accurate mixtures' phase boundaries and phase compositions. Accurate phase boundaries and phase compositions are needed to simulate absorption, liquid extraction, and distillation operations.

The minimization of the objective function (Eq. 3.18) at each node produced a solution consisting of a set of three Twu α-function parameters (α_1, α_2, α_3). The optimum set of Twu α-function parameters (or optimum solution) was the one that produced 1) the global minimum of the objective function and 2) a lower overall average absolute deviation (AAD) for the P^{sat} compared to that for the C_p^{sat}. The overall AAD was calculated according to:

$$AAD = \frac{1}{NP}\sum_1^{NP}\left|X_{exp} - X_{calc}\right| \qquad (3.23)$$

The overall AAD was the preferred error metric for selecting the optimum solution because the error distribution of AAD is not as biased as AARD's. High AARD values are typically found at T_r below 0.4 and decrease almost exponentially with T. In the case of AAD, high AAD values are found at intermediate temperatures (typically, at T_r between 0.4 and 0.9), where most industrial processes are usually operated.

The properties required as input in Eq. 3.18 were calculated according to the flash algorithm described in Section 3.2. The experimental properties were collected primarily from the NIST Database (NIST, 2017). Details on the development of the dataset used in this study for fitting are presented in the following section.

3.4 Development of the Thermophysical Properties Dataset

The Twu correlation (Eq. *3.4*) was fitted to a development dataset containing experimental P^{sat}, ΔH_v and C_p^{sat} of 9 alcohols, 4 aldehydes, 16 alkanes, 10 amines, 15 aromatics, 7 branched alkanes, 11 carboxylic acids, 12 cyclic alkanes, 15 heterocyclic nitrogen-containing compounds, 9 heterocyclic sulphur-containing compounds,16 ketones, 6 nitriles, 15 thiols, water, and ammonia.

Most of the experimental data were collected from the NIST database (NIST, 2017), with some components utilizing supplementary ΔH_v and C_p^{sat} data from the databases compiled by Zábranský *et al* (Zábranský *et al.*, 1996) and Acree and Chickos (Acree and Chickos, 2010). Other pure component properties, such as P_c and T_c and $C_p^{ideal\ gas}$ coefficients in Eq. 3.18, required as inputs for the flash algorithm, were collected from the Yaws' Handbook of Thermodynamic and Physical Properties of Chemical Compounds (Yaws, 2015). Values of the acentric factor, ω, were also included in this dataset as they were used as input for the calculation of α for the Soave function (Eq. 2.16), which was used for comparison purposes. The experimental data collected from the NIST database (NIST, 2017), Zábranský *et al.* (Zábranský *et al.*, 1996) , and Acree and Chickos (Acree and Chickos, 2010) were screened to eliminate outliers. The screening procedure used for outlier elimination is described in Section 3.5. To aid in the analysis of the results, the components in this dataset were classified into three groups according to the nature of the intermolecular interactions: 1) non-polar, 2) polar, and 3) hydrogen bonding components. The components in group 2 are polar but do not exhibit hydrogen bonding interactions. Table 3.1 summarizes relevant information about the Development Dataset.

Table 3.1: Summary of relevant information for the chemical families in the Development Dataset. NC and NP refer to the number of components and the number of data points, respectively; and Tr is the reduced temperature. This dataset was screened to eliminate outliers.

Family	NC	P^{sat} / kPa		ΔH / kJ mol^{-1}		C_p^{sat} / kJ kmol^{-1} K^{-1}	
		NP	Tr range	NP	Tr range	NP	Tr range
Group 1: Non-polar							
Alkanes	16	10635	0.231 – 1.000	292	0.373 – 0.970	1577	0.221 – 0.997
Aromatics	7	1065	0.388 – 1.000	83	0.445 – 0.934	355	0.158 – 0.717
Branched Alkanes	12	2624	0.024 – 1.000	91	0.388 – 0.813	353	0.246 – 0.629
Cyclic Alkanes	18	6999	0.306 – 1.000	346	0.343 – 0.936	939	0.117 – 0.969
Group 2: Polar							
HSCC	9	714	0.330 – 0.997	56	0.409 – 0.842	241	0.254 – 0.995
Thiols	14	404	0.410 – 0.997	51	0.432 – 0.913	639	0.177 – 0.644
Pyridines	11	1444	0.390 – 0.994	85	0.392 – 0.714	460	0.321 – 0.977
Aldehydes	4	368	0.393 – 0.894	22	0.429 – 0.783	60	0.317 – 0.619
Ketones	16	3437	0.331 – 1.000	186	0.349 – 0.964	492	0.253 – 0.967
Nitriles	6	548	0.334 – 0.999	36	0.426 – 0.858	96	0.297 – 0.643
Group 3: Hydrogen Bonding							
Amines	10	1031	0.414 – 1.000	38	0.475 – 0.902	165	0.371 – 0.674
HNCC	4	698	0.365 – 0.996	20	0.524 – 0.824	136	0.330 – 0.639
Alcohols	11	9924	0.295 – 1.000	272	0.414 – 0.939	895	0.195 – 0.954
H2O/NH3	2	2256	0.389 – 1.000	62	0.456 – 0.801	181	0.311 – 0.997
Acids	11	3088	0.372 – 0.985	72	0.393 – 0.897	244	0.375 – 0.744
Total	*151*	*45,235*		*1,712*		*6,833*	

HNCC=Hydrogen-Bonding Heterocyclic Nitrogen-Containing Compound; HSCC=Heterocyclic Sulfur Containing Compound

Figure 3.1, Figure 3.2 and Figure 3.3 show the distribution of the data points in the Development Dataset for P^{sat}, ΔH and C_p^{sat}, respectively, versus the T_r range. The T_r range for P^{sat} and ΔH was from 0.3 to 1.0, which covers temperatures from near the triple point and extends to the critical point. However, for $C_p^{sat,}$ a constrained range was used from 0.3 to 0.8 because C_p^{sat} calculated from CEoS typically deviates significantly from the experimental data at temperatures above 0.8 as described by Kontogeorgis and Folas (Kontogeorgis and Folas, 2009). As seen in Figure 3.1 to Figure 3.3, most data points for the three studied properties are reported at T_r within the range of 0.5 and 0.8.

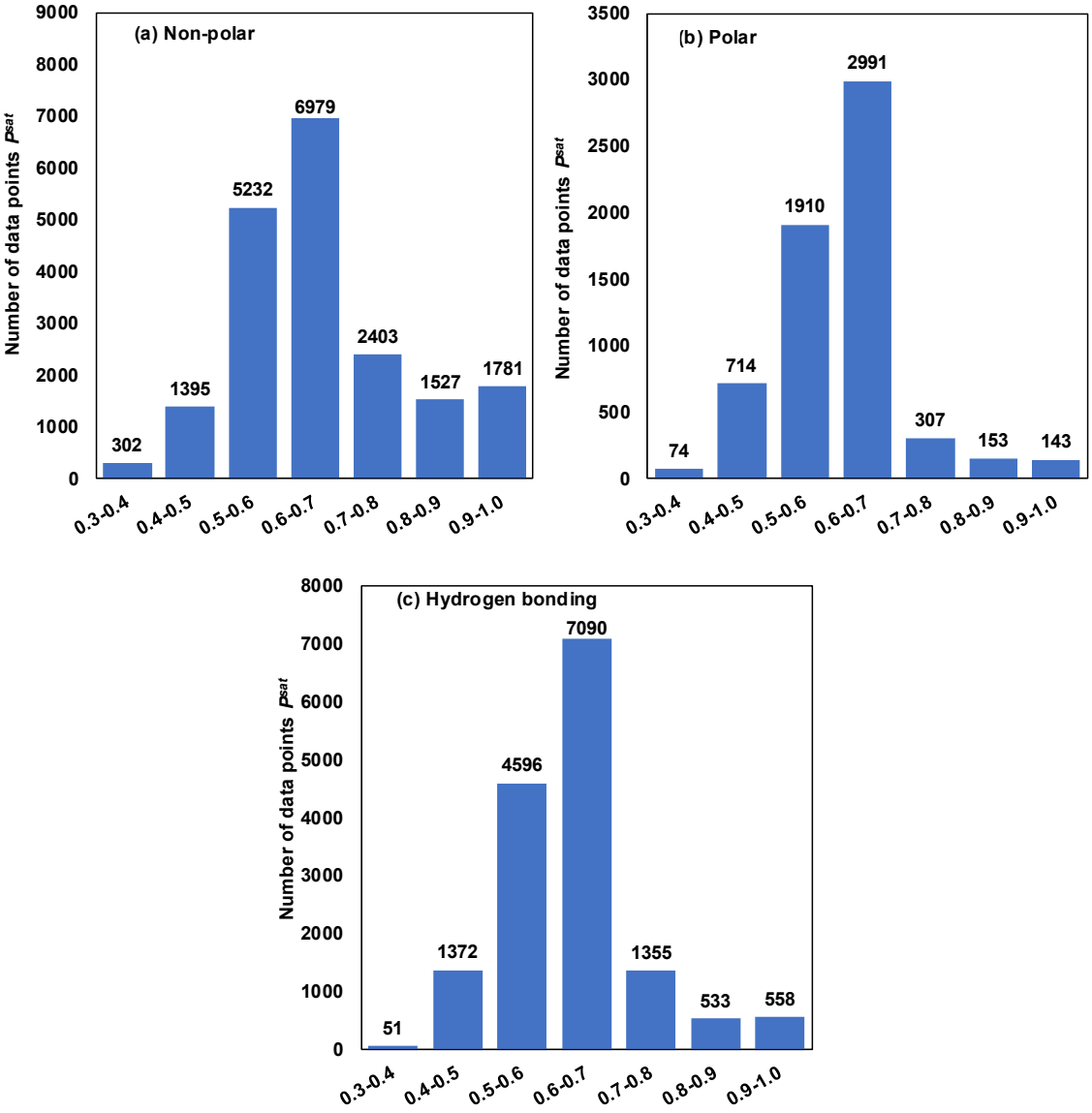

Figure 3.1: Plots representing the count of data points at varying ranges of reduced temperature (X-axis). The Y-axis indicates the number of data points for the saturation pressure (P^{sat}). Plot-a displays the P^{sat} count for Group 1: nonpolar components, plot-b Group 2: polar components, and plot-C Group 3: hydrogen bonding components.

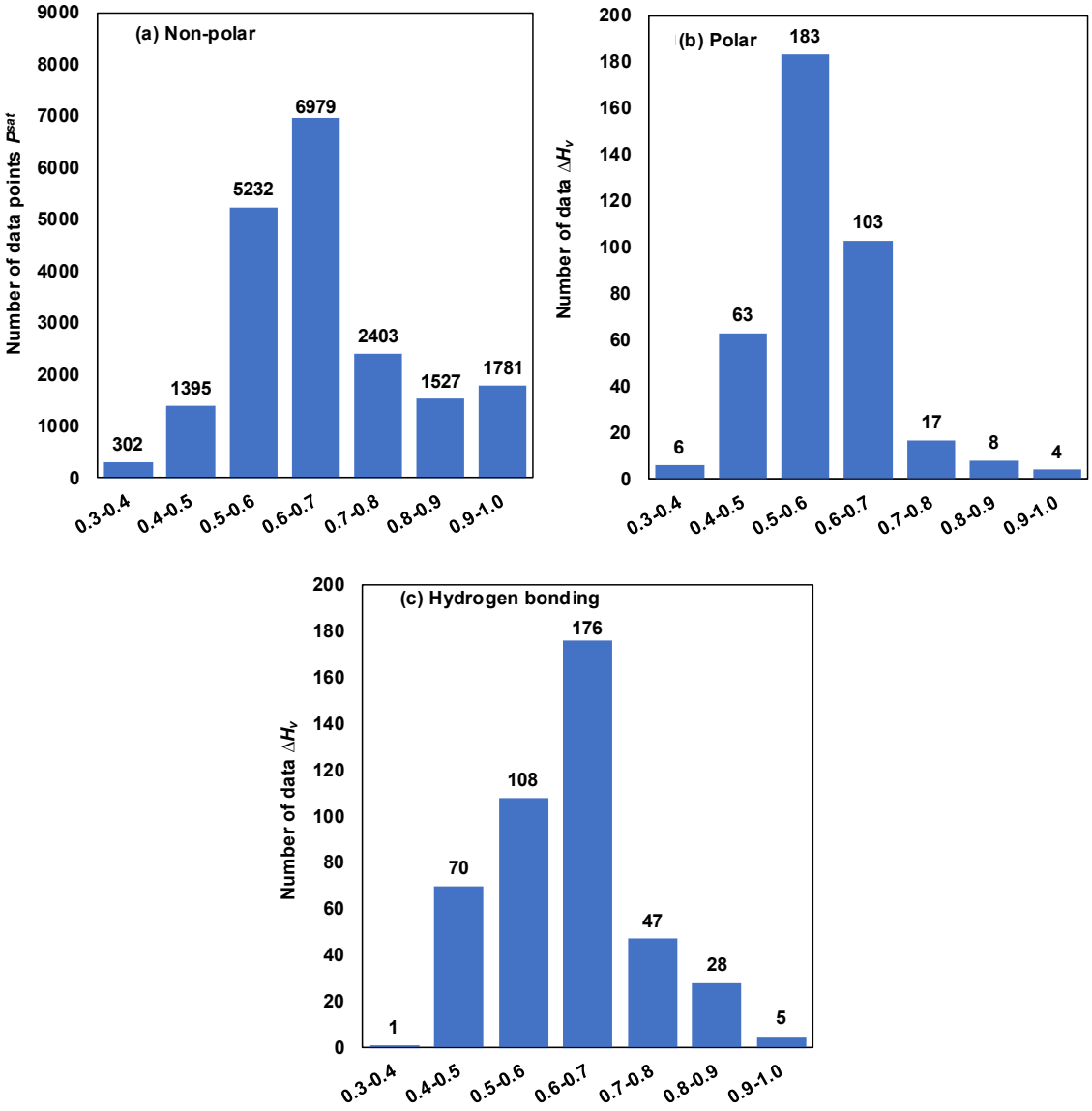

Figure 3.2: Plots representing the count of data points at varying ranges of reduced temperature (X-axis). The Y-axis indicates the number of data points for the vaporization enthalpy (ΔH_v). Plot-a displays the ΔH_v count for Group 1: nonpolar components, plot-b Group 2: polar components, and plot-C Group 3: hydrogen bonding components.

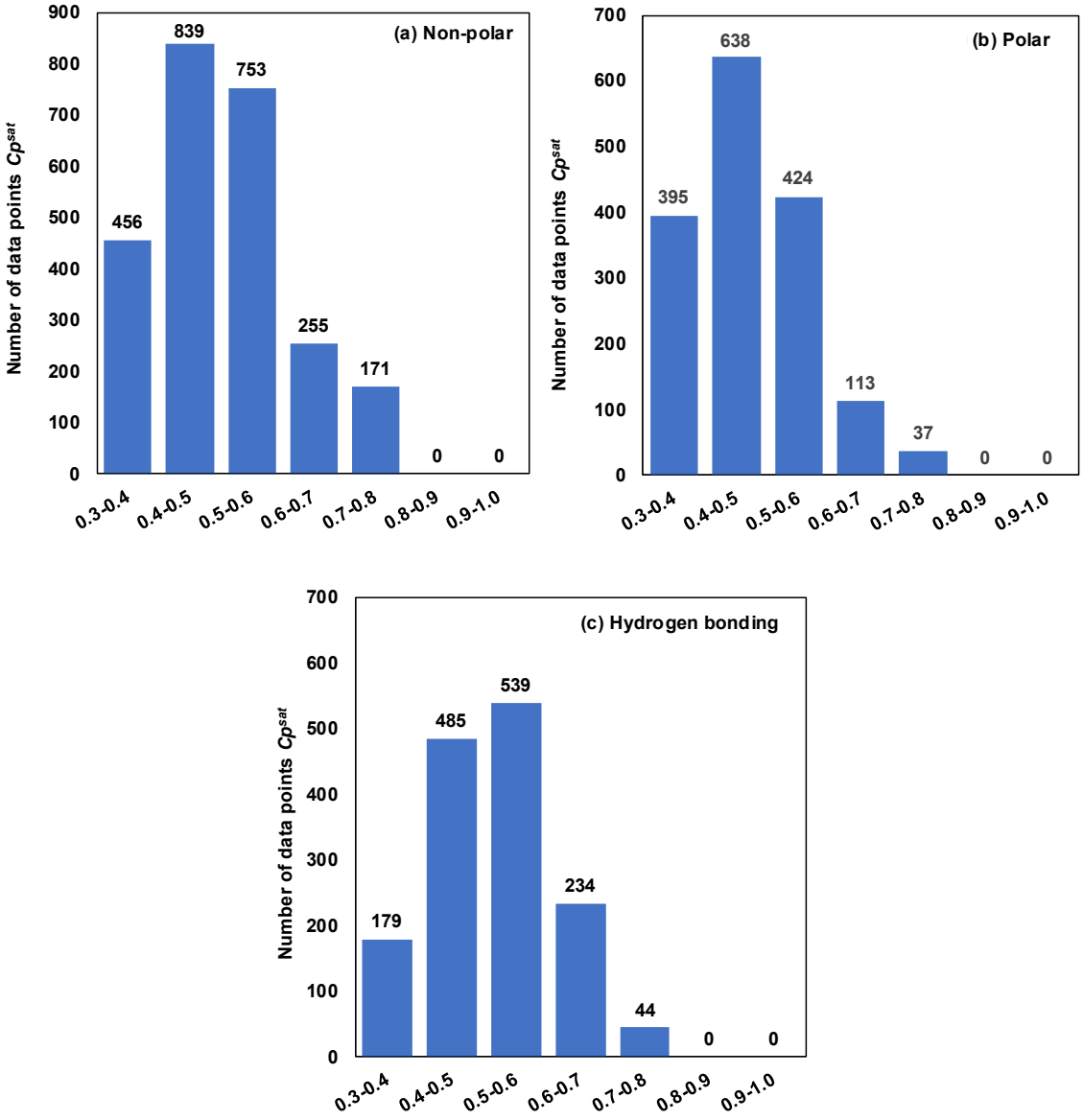

Figure 3.3: Plots representing the count of data points at varying ranges of reduced temperature (X-axis). The Y-axis indicates the number of data points for the Saturated liquid heat capacity. (C_p^{sat}). Plot-a displays the C_p^{sat} count for Group 1: nonpolar components, plot-b Group 2: polar components, and plot-C Group 3: hydrogen bonding components.

3.5 Data Screening and Outlier Elimination

The accuracy of the calculated parameters α_1, α_2 and α_3 depends significantly on the quality of the experimental data used in the optimization algorithm. The presence of outliers in the datasets can negatively affect the fitting procedure and, consequently, the α parameters, which in turn dictate

the performance of the CEoS. In this study, a quantile regression algorithm was implemented in MATLAB™, which played a crucial role in detecting outliers within the dataset. This algorithm works by determining the upper and lower limits that define an outlier using experimental values of the thermodynamic variable for a specific quantile, as initially proposed by (Meinshausen, 2006). Essentially, data points that lie outside of these set boundaries may indicate the presence of an outlier. To illustrate this procedure, one can refer to Figure 3.4.

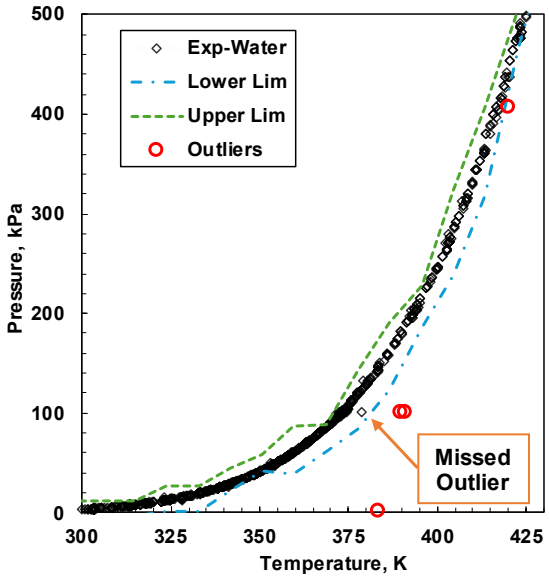

Figure 3.4: Bounds and Outliers Detected Using a Quartile Regression Algorithm: The green line represents the upper limit, while the blue line marks the lower limit. Diamonds denote experimental data for water, and circles represent outliers.

In Figure 3.4, green and blue lines represent the upper and lower boundaries, respectively, while the experimental data is depicted as diamonds. Notably, outliers identified in this stage are depicted as circles. In Figure 3.4, the quantile regression algorithm identifies several erroneous outliers, emphasizing that most evaluated data has been retained. Moreover, it illustrates a limitation, as it can be observed that possible outliers have been missed during the initial screening process. Further steps to capture this outlier could involve manual removal of the undetected outlier or

rerunning the quartile regression algorithm after eliminating the most prominent outliers. It is crucial to manually verify the outliers detected by the algorithm and discard them from the dataset if an apparent deviation is observed, ensuring the precision and reliability of the analysis.

3.6 Testing The Consistency of The Fitted Twu Correlation Parameters

The consistent calculation of thermodynamic properties across the phase diagram highly depends on the ability of an EoS to produce qualitatively correct trends for its first and second derivatives. Derivative properties are those calculated from the derivatives of the EoS, such as isothermal compressibility, thermal expansion, Waring number (W) and speed of sound(u) (Bell *et al.*, 2018; Velasco *et al.*, 2012; Waring, 1954). Therefore, comparing experimental and calculated derivative properties assesses the accuracy of derivatives calculated from an EoS and provides a qualitative consistency test.

This study evaluated the consistency of the first and second derivatives calculated from the CEoS with fitted Twu correlation parameters by calculating the Waring number, W, and the saturated liquid speed of sound, u. These two properties were chosen because W can be used to check if the shape of the calculated P^{sat} curve is consistent with the Clapeyron equation, and u is considered the most demanding test to check the performance of any EoS as it depends on the first and second derivatives of the equation(Kontogeorgis and Folas, 2009). A brief review of the calculation of W and u is presented below.

3.6.1 The Waring Number

Waring (Waring, 1954) proposed an empirical method to assess the consistency of calculated pure component P^{sat}. Subsequently, the following empirical parameter, known as the Waring (W) number in kJ mol$^{-1,}$ was defined.:

$$W = \frac{RT^2}{P}\left(\frac{\partial P}{\partial T}\right) \tag{3.24}$$

The Clapeyron equation can be written in terms of W as:

$$\frac{\Delta H_v}{\Delta Z^{vap}} = W \tag{3.25}$$

where Z^{vap} is the difference in compressibility factors of saturated vapour and liquid, Waring (Waring, 1954) calculated W numbers for numerous pure components using highly accurate experimental values for ΔH_v and ΔZ^{vap} and plotted the calculated W values versus the T_r from the graphs, Waring concluded that to satisfy the Clapeyron equation, the plotted curves must be: 1) convex and continuous; 2) have a minimum value consistent with the inflection point of the curve log(P) versus 1/T as noted by Thodos (Thodos, 1950); and 3) produce a finite W number at the critical point. These observations are empirical but have been used by several authors to verify the thermodynamic consistency of calculated pure component P^{sat} (Bell *et al.*, 2018; Velasco *et al.*, 2012; Waring, 1954). This study calculated the W number from Eq. 3.25 using the derivative calculated from the CEoS with fitted Twu correlation parameters. Then, W was plotted versus the reduced temperature, and the produced curves' consistency was assessed using the three criteria previously outlined.

3.6.2 The Speed of Sound

The speed of sound, u in m/s, is calculated as follows (Michelsen and Møllerup, 2007):

$$u = \sqrt{-\frac{v_{liq}^2}{M_w}\left(\frac{C_p^{sat}}{C_v{}^{sat}}\right)\left(\frac{\partial P}{\partial V}\right)} \qquad (3.26)$$

where M_w is the molecular weight; v_{liq}, $C_P{}^{sat}$, and $C_v{}^{sat}$ are the saturated liquid volume, isobaric heat capacity and isochoric heat capacity, respectively; and $(\partial P/\partial V)$ is the derivative of pressure with respect to the saturated liquid molar volume. In this study, the consistency of the CEoS for the calculation of u was assessed by comparing calculated and experimental values for 90 pure components from a similar set of assorted chemical families described in section 3.5, excluding thiols (no experimental data are reported for these components). The speed of sound was calculated from Eq. 3.26 using v^{sat}, $C_p{}^{sat}$, $C_v{}^{satt,}$ and $(\partial P/\partial V)$ calculated from the CEoS with fitted Twu correlation parameters. The calculated speed of sound was compared with experimental data collected from the NIST Database (NIST, 2017). Table 3.2 presents details of the experimental dataset used.

Table 3.2. Speed of Sound Analysis Dataset, NC and NP denote the number of components and data points respectively, while Tr symbolizes reduced temperature. The *u* signifies the speed of sound in m s^{-1}. Outliers have been diligently excluded from this dataset.

Family	**NC**	**NP**	***Speed of Sound***	
			***u*, m/s range**	**Tr range**
Group 1: Non-polar				
Alkanes	16	854	68 - 2106	0.243 - 1.000
Aromatics	7	53	1012 - 1491	0.434 - 0.621
Branched Alkanes	12	120	100 - 1391	0.364 - 0.969
Cyclic Alkanes	18	455	81 - 1818	0.313 - 1.000
Group 2: Polar				
HSCC	9	23	1249 - 1503	0.402 - 0.480
Thiols	14	-	-	-
Pyridines	11	80	1278 - 1488	0.454 - 0.537
Aldehydes	4	9	1367 - 1479	0.422 - 0.465
Ketones	16	161	467 - 1521	0.403 - 0.887
Nitriles	6	60	573 - 1572	0.423 - 0.870
Group 3: Hydrogen Bonding				
Amines	10	45	1045 - 1702	0.494 - 0.632
HNCC	4	43	1050 - 1600	0.375 - 0.617
Alcohols	11	631	97 - 1676	0.343 - 0.998
H2O/NH3	2	40	294 - 1996	0.494 - 0.999
Acids	11	42	4 - 1312	0.422 - 0.597
Total	*90*	*2616*		

HNCC=Heterocyclic Nitrogen Containing Compound; HSCC=Heterocyclic Sulfur Containing Compound

4 Analysis of Subcritical Region

The first part of this chapter presents the results of fitting the PR and RK CEoS with α parameter calculated from the Twu correlation (Eq. 3.4 and 2.25) to experimental P^{sat}, ΔH_v and C_p^{sat} of the components listed in Table 3.1 in Chapter 3. The components summarized in Table 3.1 were classified into three groups according to intermolecular interactions: Group 1, non-polar; Group 2, polar; and Group 3, hydrogen-bonding components. This classification allowed us to study the performance of the CEoS in fitting the properties of non-polar, polar, and hydrogen-bonding components. These components' properties were compared using the PR and RK CEoS with the α parameter calculated from the Soave correlation (Eq. 2.16 and 2.17). The performance of the different CEoS was assessed by comparing deviations between experimental and calculated data. The second part of this chapter presents the results of a consistency check performed by calculating W and u. The Waring number is a parameter that assesses if the CEoS produces trends that satisfy the Clapeyron equation. The speed of sound was used to assess the quality of the derivative of the CEoS and function as a rigorous test of thermodynamic consistency.

4.1 Analyzing The Performance of The Redlich-Kwong and Peng-Robinson Cubic Equations of State With α Parameter from The Twu and Soave α-Functions

The following nomenclature will be used throughout this chapter to refer to the different CEoS used in this study: PR-Twu and PR-Soave refer to the PR CEoS with α parameter calculated from the Twu and Soave correlations, respectively, and RK-Twu and RK-Soave refer to the RK CEoS with α parameter calculated from the Twu and Soave correlations, respectively. The three fluid-specific coefficients in the Twu correlation (Eq. *3.4*) were calculated by fitting the respective model to experimental data as described in Section 3.2. The Soave parameter *m,* which is used for the PR-Soave and RK-Soave models, was predicted from a correlation proposed by Pina *et al.*

(Pina-Martinez *et al.*, 2019b) and is defined in Eq. 2.18 and Eq. 2.15. All the fitted Twu correlation parameters are summarized in Appendix B2- Fitted Twu Parameter and calculated Absolute Average Relative Deviations (AARD).

4.1.1 Analysis of Group 1: Non-Polar Components

Figure 4.1 presents the summary of the overall absolute relative deviation (AARD, %) (Eq. *3.19*) for the non-polar components in Group 1. In the case of P^{sat}, Figure 4.1a, PR-Twu and RK-Twu produced lower AARD results than those from PR-Soave and RK-Soave for all the components in Group 1. PR-Twu and RK-Twu fitted the data with relatively low AARD values when predicting the properties of normal and branched alkanes. Slightly higher errors are observed for normal alkanes than branched alkanes due to the large quantity of heavier alkanes in the normal family relative to the branched family. Heavier alkanes have been reported to interact more strongly (a direct consequence of London dispersion forces) and tend to result in higher errors for the P^{sat} (Kumar and Okuno 2012; Li and Yang 2010). If a comparison is made between the AARD values of cyclic alkanes and aromatics, it can be observed that RK-Twu produces lower AARD relative to those from PR-Twu. Among the non-polar components in Group 1, the aromatics showed the most significant AARD, suggesting that the PR and RK equations, regardless of the α-function, cannot fully capture the attractive interactions exhibited by aromatic molecules. PR-Twu and RK-Twu fitted the P^{sat} data in Group 1 with overall AARD values of 3.4 and 3.7%, respectively, and PR-Soave and RK-Soave with overall AARD values of 8.2 and 7.9%, respectively.

In the case of ΔH_v, PR-Twu and RK-Twu generally produced lower AARD than PR-Soave and RK-Soave. PR-Twu and RK-Twu fitted the ΔH_v of the components in Group 1 with overall AARD

values of 1.5 and 1.6% relative to the values of 2.5 and 2.3% obtained from the PR-Soave and RK-Soave, respectively. In the case of C_p^{sat}, PR-Twu and RK-Twu produced results that are, on average, six to seven times lower compared to those obtained from PR-Soave and RK-Soave, suggesting the Twu α-function is more suitable for the calculation of C_p^{sat} due to its greater flexibility. PR-Twu and RK-Twu fitted the C_p^{sat} of the components in Group 1 with overall AARD values of 1.0 and 1.1%, respectively, and PR-Soave and RK-Soave predicted the C_p^{sat} with overall AARD values of 7.5 and 6.2%, respectively.

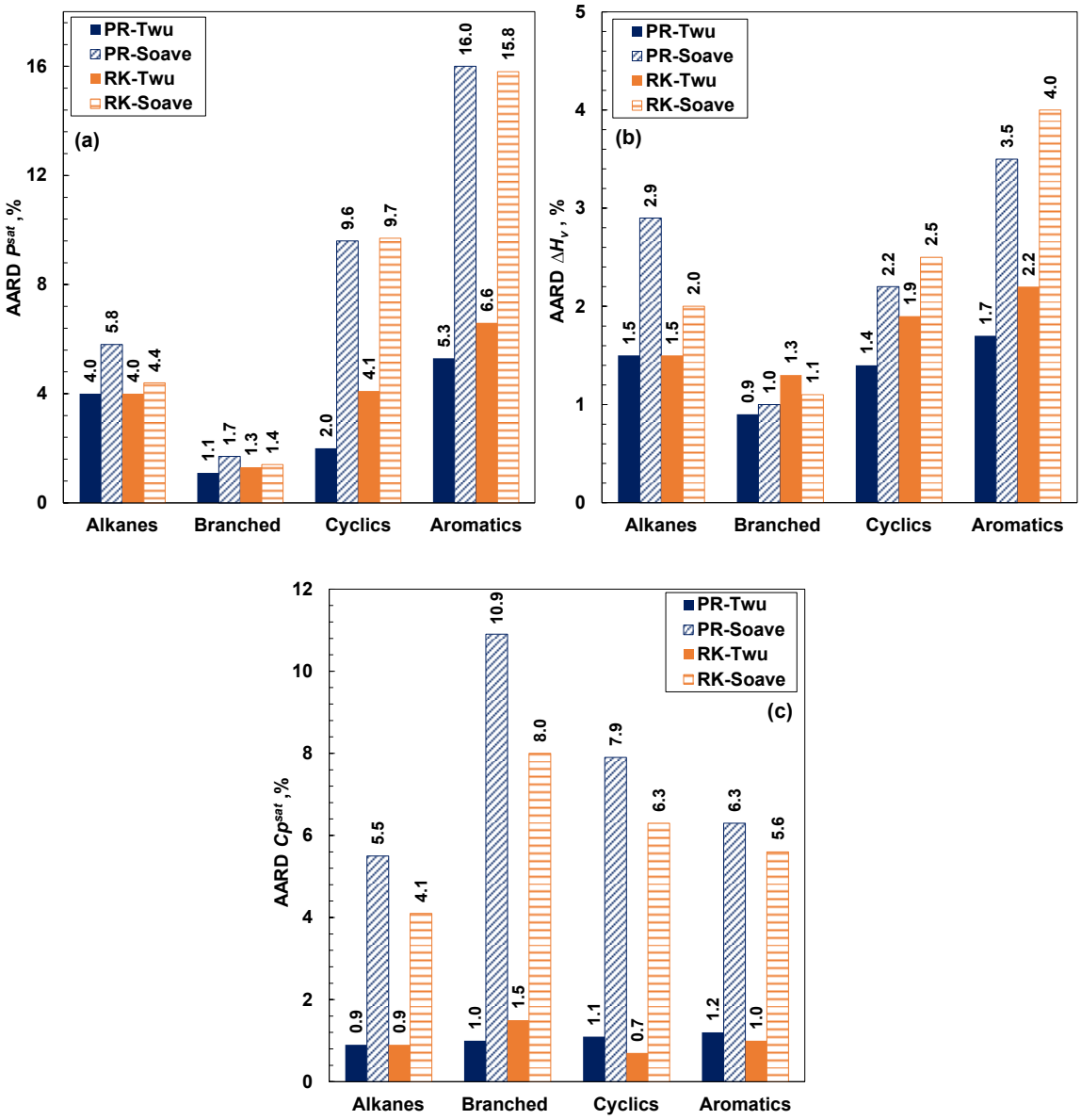

Figure 4.1: Summary of the overall average absolute relative deviation (AARD, %) for (a) saturation pressure (P^{sat}), (b) enthalpy of vaporization (ΔH_v) and (c) saturated liquid heat capacity (C_p^{sat}) for the chemical families in Group 1. In each figure, families are ordered from the least polar (family on the far left) to the most polar (family on the far right). Alkanes, Branched and Cyclic refer to normal, branched, and cyclic alkanes, respectively.

4.1.2 Analysis of Group 2: Polar Components

Figure 4.2 presents the overall AARD values for the P^{sat} (panel a), ΔH_v (panel b) and $C_p^{sat.}$ (panel c) for the chemical families in Group 2. The chemical families in Group 2 contain polar

components unable to self-associate via hydrogen bonding, and they are ordered in Figure 4.2 from left to right in terms of increasing polarity. PR-Twu and RK-Twu produced results with lower AARD compared to those from PR-Soave and RK-Soave for the three properties (P^{sat}, ΔHv, and C_p^{sat}). In the case of P^{sat}, PR-Twu and RK-Twu produced significantly lower AARD values than those from PR-Soave and RK-Soave, showing that the Twu α-function is more appropriate for polar components due to its flexibility. PR-Twu and RK-Twu produced comparatively higher AARD values for ketones, nitriles, and aldehydes (Figure 4.2a). We hypothesize that this was not because of their higher polarity but because of scattering in the experimental data; additional data is needed to evaluate these models' performance when evaluating ketones, nitriles, and aldehydes. PR-Twu and RK-Twu fitted the P^{sat} of the components in Group 2 with overall AARD values of 5.1 and 4.6%, respectively, and PR-Soave and RK-Soave with AARD values of 26.5 and 26.7%, respectively. For ΔH_v and C_p^{sat}, PR-Twu and RK-Twu produce results with lower AARD than those obtained from PR-Soave and RK-Soave for all the families in Group 2, Figure 4.2a and b. PR-Twu and RK-Twu fitted the ΔH_v of the components in Group 2 with overall AARD values of 3.1 and 3.0%, respectively; they both fitted their C_p^{sat} with an overall AARD value of 1.7%. PR-Soave and RK-Soave predicted ΔH_v with overall AARD values of 6.7 and 7.7%, respectively, and C_p^{sat} with overall AARD values of 7.9 and 6.6%, respectively.

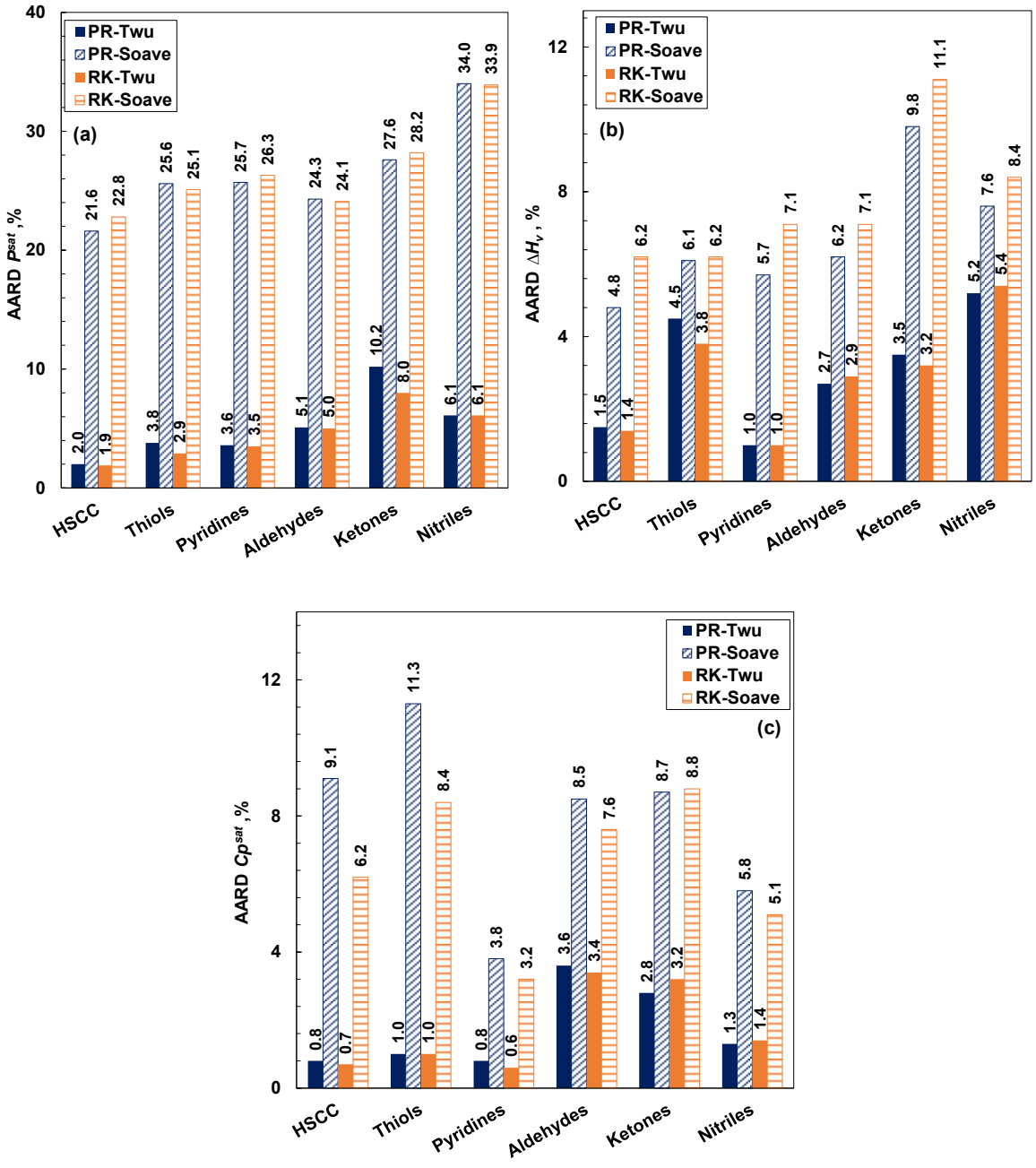

Figure 4.2: Summary of the overall average absolute relative deviation (AARD, %) for (a) saturation pressure (P^{sat}), (b) enthalpy of vaporization (ΔH_v) and (c) saturated liquid heat capacity (C_p^{sat}) for the chemical families in Group 2. In each figure, families are ordered from the least polar (family on the far left) to the most polar (family on the far right). HSCC stands for heterocyclic sulfur containing compounds.

4.1.3 Analysis of Group 3: Hydrogen-Bonding Components

The chemical families included in Group 3 contain components that self-associate through hydrogen bonding. The C_p^{sat} of alcohols was one of the most challenging properties because PR-Twu and RK-Twu originally produced very high deviations. The fitting approach for the C_p^{sat} of alcohols was modified to address this issue so that only C_p^{sat} data at a T_r below 0.5 (instead of 0.8) was utilized for fitting; however, the AARD was calculated for data points up to a T_r of 0.8 to ensure consistency with other C_p^{sat}, which were also evaluated up to a T_r of 0.8 Figure 4.4 presents the overall AARD values for P^{sat}, ΔH_v and C_p^{sat} for the different chemical families in Group 3. PR-Twu and RK-Twu predict properties with lower AARD than those from PR-Soave and RK-Soave, except for the P^{sat} and ΔH_v of the carboxylic acids. This observation agrees with results reported by Bell *et al.* (Bell *et al.*, 2018) and Le Guennec *et al.* (Le Guennec, Privat, *et al.*, 2016), where both authors report relatively high AARD values amongst their tested databases for strongly associating fluids such as carboxylic acids. The errors reported by Bell *et al.* (Bell *et al.*, 2018), Le Guennec *et al.* (Le Guennec, Privat, *et al.*, 2016) and the value reported in this study further highlight the inadequacy of the Twu α-function for representing thermodynamic properties of carboxylic acids. The PR and RK CEoSail correctly model the thermodynamic properties of carboxylic acids because these acids form dimers (Twu *et al.*, 1993). Figure 4.3 shows a schematic of the monomeric (Figure 4.3a) and dimeric units (Figure 4.3b) for acetic acid, where solid lines represent chemical bonds and dashed lines represent hydrogen bonding. The dimeric units comprise two monomers bound by two hydrogen bonds (J. A. Davies *et al.*, 2019; M. M. Davies and Sutherland, 1938). Traditional CEoS do not account for dimerization, thereby not representing the actual thermodynamic behaviour of carboxylic acids. As a result, high errors are obtained in VLE calculations (Twu *et al.*, 1993).

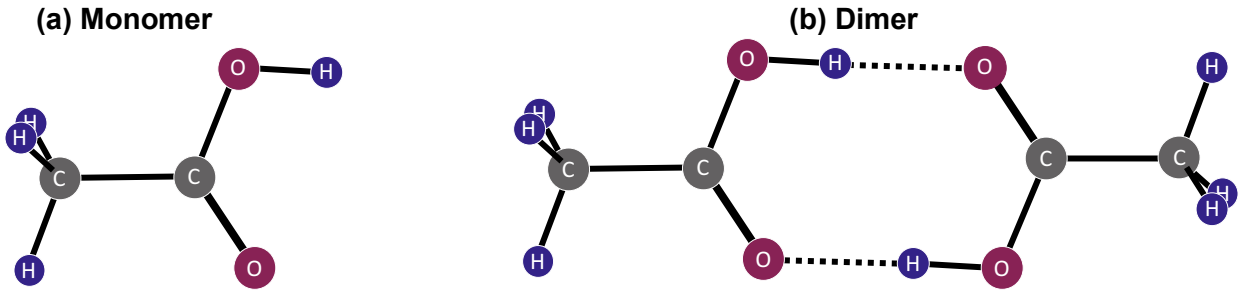

Figure 4.3: Representation of monomeric and dimeric units for acetic acid: Monomer (a) and dimer (b). Elements are denoted as O for oxygen, H for hydrogen, and C for carbon. Solid lines depict chemical bonds, while dashed lines signify hydrogen bonding.

The PR-Twu model fitted the P^{sat}, ΔH_v and C_p^{sat} of the components in Group 3 with overall AARD values of 16.1, 4.2 and 3.3%, respectively, and the RK-Twu model fitted the same three properties with overall AARD values of 13.7, 3.8 and 3.3%, respectively. The PR-Soave model predicted the P^{sat}, ΔH_v and C_p^{sat} of the components in Group 3 with overall AARD values of 26.3, 6.7 %, and 11.2%, respectively, and the RK-Soave model with overall AARD values of 23.6, 6.4 and 12.1%, respectively.

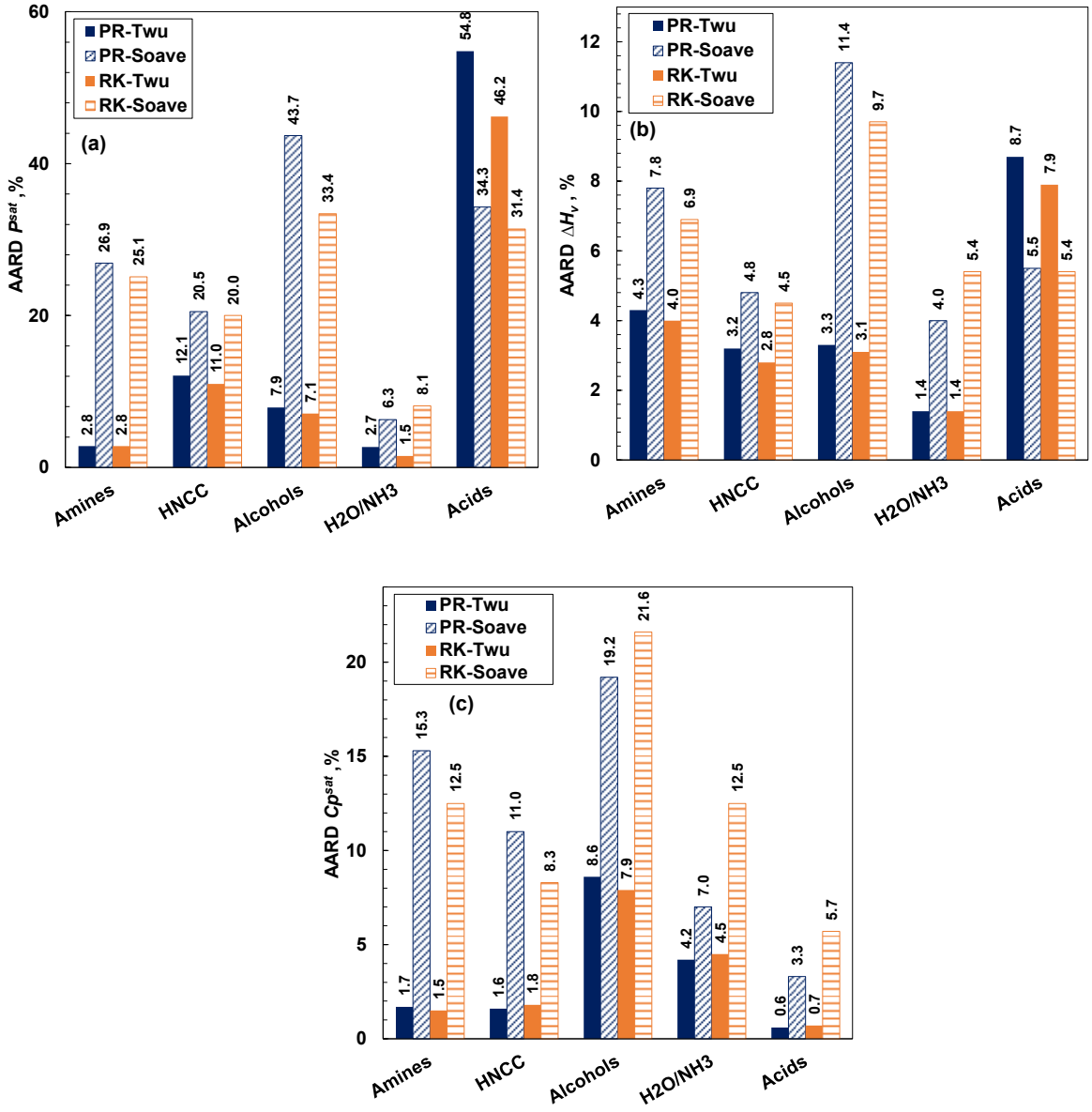

Figure 4.4: Summary of the overall average absolute relative deviation (AARD, %) for (a) saturation pressure (P^{sat}), (b) enthalpy of vaporization (ΔH_v) and (c) liquid heat capacity (C_p^{sat}) for the chemical families in Group 3. In each figure, families are ordered from the least polar (far left) to the most polar (far right). HNCC stands for heterocyclic nitrogen containing compounds.

Figure 4.5 shows the C_p^{sat} of alcohols fitted to PR-Twu and predicted by PR-Soave. RK-Twu and RK-Soave were not included in Figure 4.5 because they performed similarly to PR-Twu and PR-Soave, respectively. Ammonia and Water, also hydrogen-bonding components from Group 3, were

also included in Figure 4.5a and b, respectively, for comparison. Figure 4.5 shows a good agreement between data and fitted PR-Twu for Ammonia, Water, Methanol and Ethanol with AARD of 2.8, 5.8, 2.3 and 8.1, respectively. However, the quality of the fitting decreases as the molecular weight of the alcohol increases, as seen in Figure 4.5, with AARD ranging from 16.5% for pentanol to 18.7% for 1-dodecanol. In the case of PR-Soave, the AARD for Ammonia and Water is 3.7 and 10.7, respectively. The AARD was higher than 20% for alcohols, even for low molecular weight alcohols such as Methanol and Ethanol. The lower deviations found for the CEoS coupled with the Twu α-function result from its higher flexibility; however, the Twu α-function cannot capture the C_p^{sat} of alcohols, and neither is the Soave α-function.

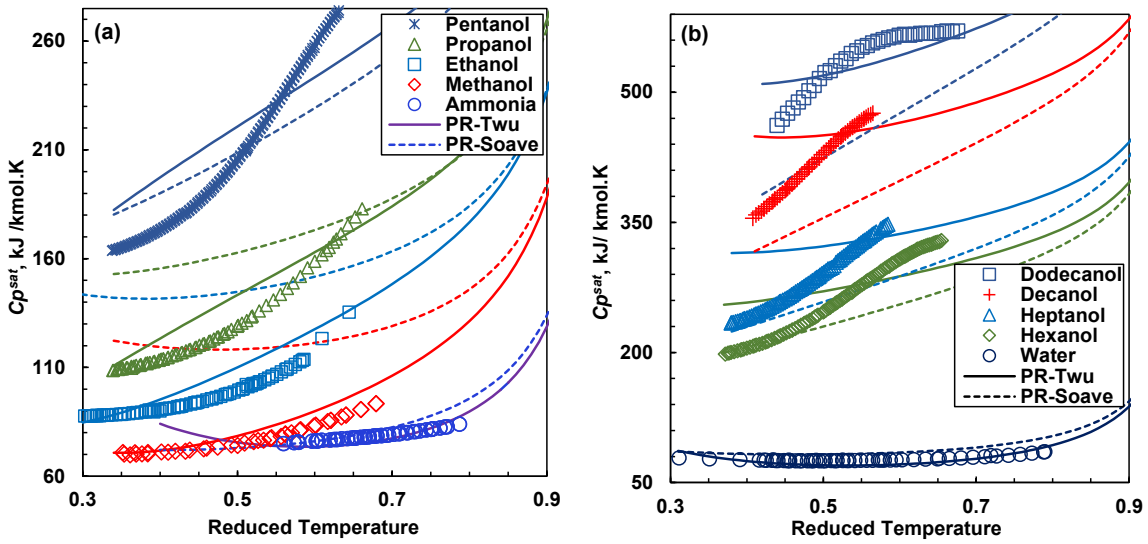

Figure 4.5: Heat capacity plotted against reduced temperature for alkanols, H_2O and NH_3: Symbols indicate experimental data, dashed lines represent the Peng-Robinson (PR) cubic equation of sate (CEoS) coupled with the Twu α-function (PR-Twu), and solid lines denote the PR CEoS coupled with the Soave α-function (RK-Soave).

Figure 4.6 shows the experimental and calculated ΔHv (panel a) and Cpsat (panel b) of four components in Group 3. These components are butanoic acid, butanol, pyrrolidine (cyclic secondary amine) and diethylamine (normal secondary amine); they all have a carbon number of

four and are self-associated through hydrogen bonding. The ΔH_v and C_p^{sat} shown in Figure 4.6 were calculated from RK-Twu and RK-Soave. PR-Twu and PR-Soave are not shown in Figure 4.6 as their performance is comparable to RK-Twu and RK-Soave, respectively. RK-Twu and RK-Soave can capture the correct trends for the ΔH_v of the four components and exhibit a good agreement with the experimental data, Figure 4.6a. In the case of C_p^{sat}, Figure 4.6b, RK-Twu can adeptly capture the correct trends for all components except for butanol. As shown in Fig. 4.6b, the experimental C_p^{sat} capacity of butanol increases more rapidly with the temperature compared to the other components in Figure 4.6b. Interestingly, PR-Twu and RK-Twu can capture the C_p^{sat} of hydrogen bonding components except for normal alcohols with carbon numbers higher than 3, as seen in Figure 4.5 and Figure 4.6. The results of this study further indicate that the Twu α-function is adequate, due to its flexibility, to capture the effect of hydrogen bonding on C_p^{sat} when hydrogen bonding is the most dominant intermolecular interaction, as in the case of ammonia, water, and low molecular weight alcohols. However, high molecular weight alcohols do not only self-associate through hydrogen bonding but also stronger dispersion forces arising from the interactions between the paraffinic chains, as suggested by Cerdeiriña *et al.* (Cerdeiriña *et al.*, 2004). The Twu α-function can not capture these dispersion forces and, consequently, is inadequate in predicting C_p^{sat} for high molecular weight alcohols.

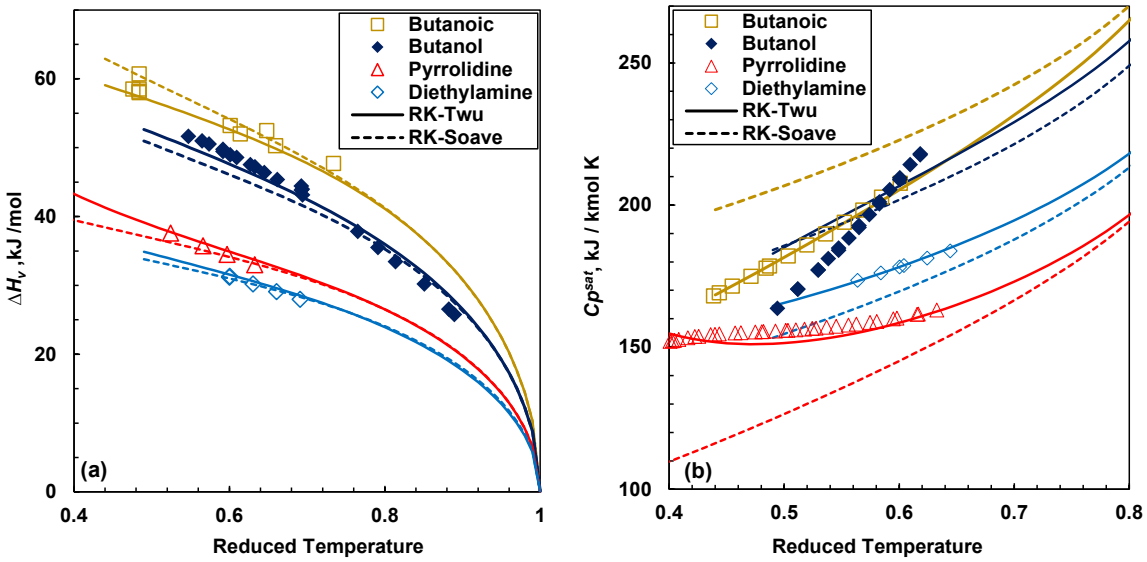

Figure 4.6: (a) Vaporization enthalpy (ΔHv) vs. reduced temperature and (b) Saturated heat capacity (C_p^{sat}) vs. reduced temperature. Symbols represent experimental data. Dashed lines depict the Redlich-Kwong (RK) cubic equation of state (CEoS) coupled with the Twu α-function (RK-Twu), while solid lines denote the RK CEoS coupled with the Soave α-function (RK-Soave). The plots include components from the carboxylic acids, alcohols, pyridines, and amines families with equivalent carbon chain lengths.

4.2 Investigating the performance of The Redlich-Kwong and Peng-Robinson Cubic Equations of State

Table 4.1 summarizes the overall AARD per Group for the three properties calculated from PR-Twu and RK-Twu. The results in Table 4.1 suggest no significant difference between the performance of PR-Twu and RK-Twu in the fitting of P^{sat}, ΔH_v and C_p^{sat} of pure components. A similar conclusion is drawn from the deviations summarized in Table 4.2. Therefore, according to the results in this study, the PR and RK CEoS produce similar results for pure components, with lower deviations observed when CEoS is coupled with the Twu α-function. The work done by Ghanbari *et al.* (Ghanbari *et al.*, 2017) and Twu *et al.* (Twu *et al.*, 1998) came to similar conclusions after comparing the RK and PR CEoS. The highest deviations for CEoS were found for the P^{sat} of carboxylic acids in Group 3.

Table 4.1: Absolute Average Relative Deviation (AARD) Summary. Table details chemical Group, number of components (NC), and the AARD for the Peng-Robinson (PR) and Redlich-Kwong (RK) cubic equations of state (CEoS) coupled with the Twu α-function. PR-Twu and RK-Twu AARD are broken down into saturation pressure (P^{sat}), vaporization enthalpy (ΔH_v), and saturated liquid heat capacity (C_p^{sat}) AARD values.

Chemical Group	**NC**	**PR-Twu AARD, %**			**RK-Twu AARD, %**		
		P^{sat}	ΔHv	Cp^{sat}	P^{sat}	ΔHv	Cp^{sat}
Group 1 (non-polar)	53	3.4	1.5	1.1	4.4	1.8	1.0
Group 2 (polar)	44	5.5	3.1	1.6	4.7	2.9	1.7
Group 3 (H-bonding)	54	20.3	5.0	3.5	17.1	4.6	3.4
Overall	*151*	*9.7*	*3.2*	*2.1*	*8.7*	*3.1*	*2.0*

Table 4.2: Absolute Average Relative Deviation (AARD) Summary. Table details chemical Group, number of components (NC), and the AARD for the Peng-Robinson (PR) and Redlich-Kwong (RK) cubic equations of state (CEoS) coupled with the Soave α-function. PR-Soave and RK-Soave AARD are broken down into saturation pressure (P^{sat}), vaporization enthalpy (ΔH_v), and saturated liquid heat capacity (C_p^{sat}) AARD values.

Chemical Group	**NC**	**PR-Soave AARD, %**			**RK-Soave AARD, %**		
		P^{sat}	ΔHv	Cp^{sat}	P^{sat}	ΔHv	Cp^{sat}
Group 1 (non-polar)	53	8.9	2.6	7.1	8.5	2.6	5.6
Group 2 (polar)	44	26.3	7.0	8.2	26.6	8.0	6.8
Group 3 (H-bonding)	54	32.2	7.7	12.1	28	7.0	13.0
Overall	*151*	*22.5*	*5.8*	*9.1*	*21.0*	*5.9*	*8.5*

Figure 4.7 shows experimental and calculated C_p^{sat} for five 6-carbon components from the three Groups tested in this study. The C_p^{sat} was calculated from PR-Twu and PR-Soave. For all the components included in Figure 4.7, PR-Twu can capture the correct trends and produce lower deviations compared to those from PR-Soave. As the polarity of the component increases, it is evident that PR-Twu is better suited to describe the C_p^{sat} than PR-Soave because of its higher flexibility. In the case of high molecular weight alcohols, such as hexanol in Figure 4.7, both

equations fail to capture the correct trend, and there is poor agreement with the experimental data. Similar conclusions apply to RK-Twu and RK-Soave.

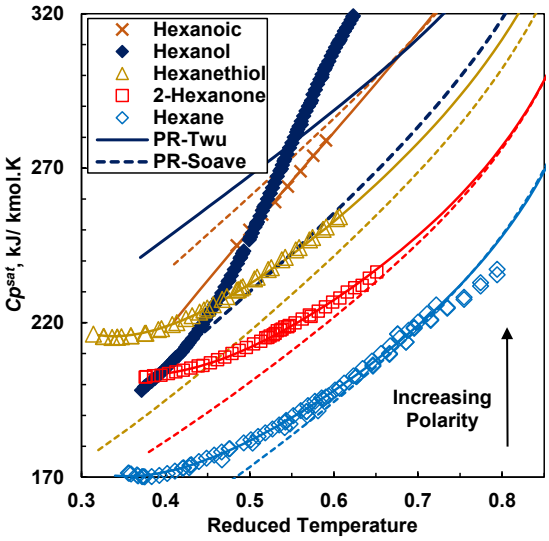

Figure 4.7: Saturated heat capacity (C_p^{sat}) vs. reduced temperature for 6-carbon components from alkanes, thiols, ketones, alcohols, and carboxylic acids. Symbols are experimental data; solid lines are the Peng-Robinson (PR) cubic equation of state (CEoS) with Twu α-function (PR-Twu), and dashed lines represent PR CEoS with Soave α-function (PR-Soave).

4.3 Evaluating the Consistency of The Redlich-Kwong and Peng-Robinson Cubic Equations of State

As discussed in Section 1.1, the consistency of the fitted Twu α-function parameters was tested by calculating the Waring number for the component in the Development Dataset (Table 3.1) and the saturated liquid speed of sound (u) for the components summarized in the Test Dataset (Table 3.2). The Waring number (W) results are presented first, and those for the speed of sound second.

4.4 Analysis of Waring Numbers

The Waring number (Waring, 1954) was calculated for all the components in the Development Dataset (Table 3.1) according to Eq. 3.25 using parameters calculated from PR-Twu and RK-Twu. For comparison purposes, the Waring number was also calculated using parameters from PR-

Soave and RK-Soave. To help in the analysis, the ratio W/W_{min} was defined as the Waring number divided by the minimum Waring number (W_{min}) (Waring number with the lowest numerical value amongst the values calculated) and plotted against the reduced temperature as shown in Figure 4.8 for selected components in Group 1 (non-polar). Note dividing by W_{min} does not affect the shape of the trends but rather normalizes the values so that $W=1$ when $W=W_{min,}$ as proposed by Bell *et al.* (Bell *et al.*, 2018). As concluded by Waring, and as seen in Figure 4.8, the Waring Number (W) is: 1) convex and continuous, 2) has a minimum value, and 3) produces a finite W number at the critical point ($T_r=1$). Similar trends were observed for all components in Group 2 (polar) and 3 (hydrogen-bonding), demonstrating that the PR and RK CEoS with this study's fitted Twu parameters produce qualitatively consistent behaviour as seen in Fig. 4.9 for selected alcohols (Panel a) and acids (Panel b) from Group 3. This trend is also observed in Fig. A.1, in Appendix A, for selected components in Group 2. Figure 4.8 does not show the Waring number calculated from PR-Twu and PR-Soave to avoid clutter. Nonetheless, these two models produced very similar trends as those from RK-Twu and RK-Soave shown in Figure 4.8. A similar observation applies to Figure 4.9.

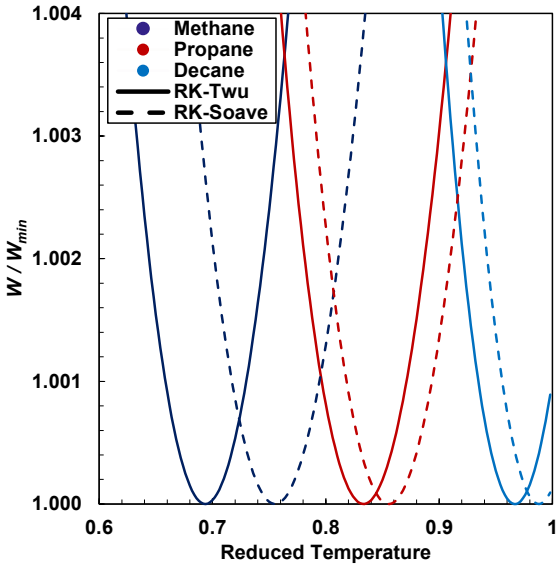

Figure 4.8: The Waring Number (W)/minimum Waring Number (W_{min}) is plotted against reduced temperature for alkanes ranging from methane to pentadecane. In plot-a, the Redlich-Kwong (RK) cubic equation of state (CEoS) and Twu α-function (RK-Twu) is used, and in plot-b, the RK CEoS is coupled with the Soave (RK-Soave) α-function.

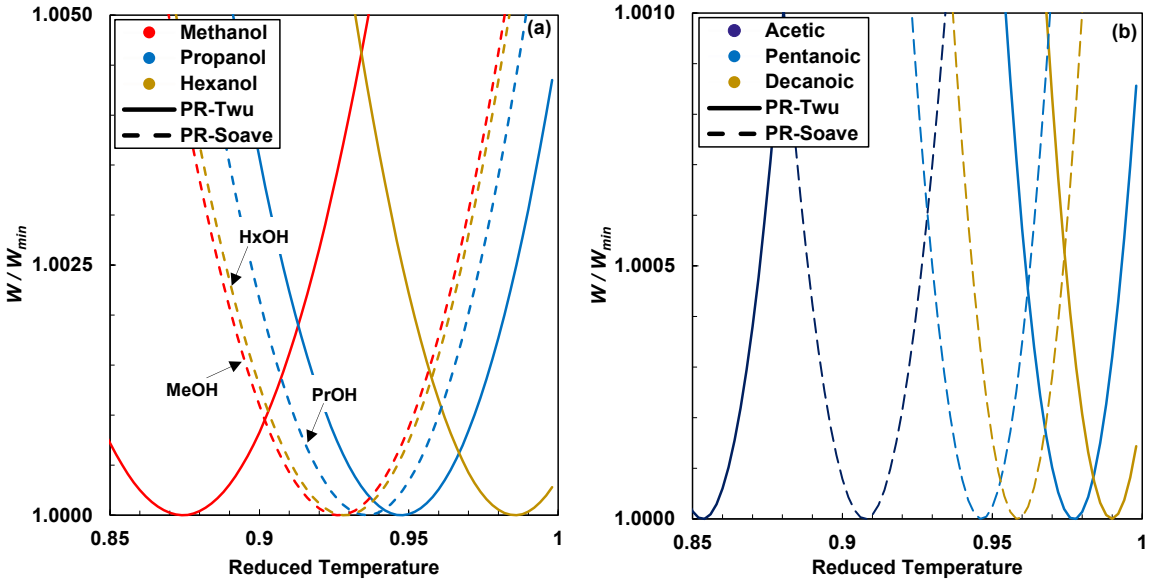

Figure 4.9: Two plots of the Waring Number (W) /minimum Waring Number (W_{min}) against reduced temperature for linear alcohols (a) and carboxylic acids (b). Using Peng-Robinson (PR) cubic equation of state (CEoS); solid lines indicate that the PR CEoS is coupled with the Twu α-function (PR-Twu), and dashed lines indicates that the PR CEoS was used with Soave (PR-Soave)

As seen in Figure 4.8 and Figure 4.9b for alkanes and carboxylic acids, respectively, the location of W_{min} shifts to higher reduced temperatures as the molecular weight of the component increases regardless of the model used. However, in the case of alcohols, as seen in Figure 4.9a, the location of W_{min} does not follow this trend when PR-Soave is used, which might be related to a potential inconsistency of the Soave α-function for alcohols. The nature of this inconsistency is unknown; however, it could be the reason behind the high deviations found for alcohol when calculating the P^{sat} and ΔH_v using either the PR-Soave or RK-Soave, as shown in Figure 4.4. Interestingly, despite the high deviations found for the P^{sat} and ΔH_v of carboxylic acids from PR-Twu and RK-Twu, Figure 4.4, the location of W_{min} increases with molecular weight. This trend indicates that despite the high error, the shape of the C_p^{sat} is still thermodynamically consistent from evaluating the Waring number trends.

4.4.1 Analysis of Saturated Liquid Speed of Sounds

The saturated liquid speed of sound (u) for the components in the Test Dataset is summarized in Table 3.2 was calculated from Eq. *3.26* using parameters calculated from PR-Twu and RK-Twu. PR-Soave and RK-Soave were also used for calculating the u for comparison purposes. In general, the four models tested produce qualitatively consistent trends for the u for all the components in the Test Dataset, *i.e.*, the models predict that the u of a saturated liquid decreases with temperature, as shown in Figure 4.10. However, as seen in Figure 4.10, the models cannot produce accurate results by comparing experimental data to model predictions. In addition, the models produce similar results regardless of the α-function, or the CEoS used, as shown in Figure 4.10a. The high deviations could be the result of the very well-known fact that CEoS produce wildly inaccurate liquid densities or volumes (Kontogeorgis and Folas, 2009; Péneloux *et al.*, 1982; Saeed and Ghader, 2019; Yan *et al.*, 2021) that are used as input for the calculation of u from Eq. *3.26*.

Inaccurate liquid densities will negatively affect the predicted *u* quality, as Liang et al. suggested (Liang *et al.*, 2012). It is essential to know that these errors do not impede the qualitative assessment of the speed of sound curves, which was the goal of this assessment. However, after observing these errors, a future evaluation of the *u* value using volume translation parid with the optimized consistent α calculated seems justified for further analysis of u predictions using CEoS.

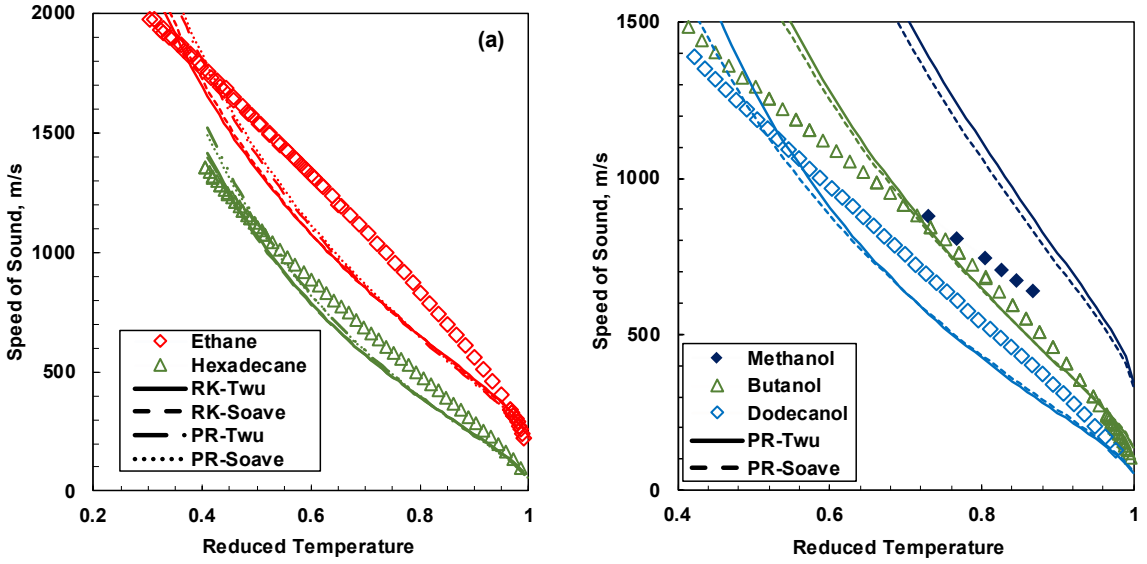

Figure 4.10: Comparative plots of the speed of sound (in m/s) against the Reduced Temperature. Plot-a contains alcohols and plot-b alkanes. For modeling: solid lines denote Peng-Robinson (PR) with the Twu α-function (PR-Twu); dashed lines PR with Soave α-function (PR-Soave); dash-dot-dot lines signify Redlich-Kwong (RK) with the Twu α-function (RK-Twu); and dotted lines RK with Soave α-function (RK-Soave).

In the case of alkanes and alcohols from Groups 1 and 3, the four models produced the highest deviations for components with carbon numbers below four, with lower deviations for components with higher carbon numbers, as seen in Figure 4.10a and b, respectively. Figure 4.10c shows experimental and calculated *u* for selected components from Groups 2 (pyridine, butyronitrile and tetrahydrothiophene) and 3 (hexanoic acid), respectively. For the components in Group 2, the deviations were comparable to those obtained for alkanes of similar carbon number.

5 Conclusions and Recommendations

This chapter summarizes the conclusions drawn from this study and recommendations for future research projects in this field.

5.1 Conclusions

In this study, the Peng-Robinson (PR) and the Redlich-Kwong (RK) cubic equations of state (CEoS) with α-parameter calculated from the Twu α-function (Eq. 3.4) were fitted to saturation pressure (P^{sat}), enthalpy of vaporization (ΔH_v) and saturated liquid heat capacity (C_p^{sat}) of 151 pure components. The pure components were classified according to intermolecular interaction into three groups: Group 1, containing 53 non-polar components; Group 2, containing 44 polar components; and Group 3, Containing 54 hydrogen-bonding components. For comparison purposes, the P^{sat}, ΔH_v, and C_p^{sat} of all the components in the dataset were predicted using the PR and RK CEoS with α-parameter calculated from the updated Soave correlation (Eq. 2.26 and Eq. 2.27) proposed by Pina-Martinez *et al.* (Pina-Martinez *et al.*, 2019b). Most of the experimental data were collected from the NIST database (NIST, 2017), with some components utilizing supplementary ΔH_v and C_p^{sat} data from the databases compiled by Zábranský *et al* (Zábranský *et al.*, 1996) and Acree and Chickos (Acree and Chickos, 2010). All the data utilized from these databases were measured experimentally rather than generated through correlations (pseudo-experimental). Before being used in this study, the data were screened using a quantile regression algorithm implemented in MATLAB™ that detected and eliminated any outliers that could affect the quality of the fitting procedure. A flash algorithm for the calculation of P^{sat}, ΔH_v and C_p^{sat}, as well as a constrained optimization routine for fitting the CEoS to data, was developed in this study using MATLAB™. The optimization algorithm was constrained to ensure the fitted Twu α-

function parameters satisfied the thermodynamic consistency requirements proposed by Le Guenec *et al.* (Le Guennec *et al.*, 2016) and presented in Eq. 2.28 to 2.31. The four models used in this study were PR-Twu, PR-Soave, RK-Twu, and RK-Soave, referring to the CEoS and the α-function used, respectively.

In general, PR-Twu and RK-Twu fitted the P^{sat}, $\Delta H_{v,}$ and saturated C_p^{sat} of all the components in the dataset with significantly lower deviations than those obtained from PR-Soave and RK-Soave. Comparing the overall average absolute relative deviations (AARD, %) between PR-Twu and RK-Twu, both models perform with similar accuracy for the three thermodynamic properties tested in this study. Consequently, there is no advantage of one model over the other. A similar observation is applicable when comparing PR-Soave and RK-Soave according to the results presented in this study. The Twu was found to produce more accurate results than the Soave α-function. When comparing the deviations for C_p^{sat}, it is evident that the Twu α-function produces significantly more accurate results than those from the Soave α-function for all the components tested in this study. The improved accuracy is due to the higher flexibility of the Twu α-function arising from its three-adjustable parameters. However, in the case of the carboxylic acids in Group 3, both α-function produced very high deviation for P^{sat} and ΔH_v of carboxylic acids. This result indicates that the Twu α-function is not adequate for carboxylic acids. PR-Twu fitted the P^{sat}, $\Delta H_{v,}$ and C_p^{sat} of all the components in the dataset with overall AARD values of 9.7, 3.2 and 2.1%, respectively, and RK-Twu fitted the same three properties with overall AARD values of 8.7, 3.1 and 2.0%, respectively. PR-Soave predicted the P^{sat}, $\Delta Hv,$ and C_p^{sat} of all the components in the dataset with overall AARD values of 22.5, 5.8 and 9.1%, respectively, and RK-Soave predicted the same three properties with overall AARD values of 21.0, 5.9 and 8.5%, respectively.

The fitted Twu α-function parameters were subjected to two additional checks to assess their consistency for calculating derivative properties. The first check was calculating the Waring number (W), a qualitative test related to the Clapeyron equation. The second check predicted the u, which depends on the second derivative of the CEoS. The calculated W for all the components in the dataset was plotted against the reduced temperature, and the resulting trends produced the qualitative correct behaviour: 1) convex and continuous, 2) have a minimum value, and 3) produce a finite W number at the critical point. It was found that the location of the minimum value of the W shifted to higher reduced temperatures as the molecular weight of the component increased when the Twu α-function was used. This trend with the increasing molecular weight was also observed when the Soave α-function was used for all the components in the dataset except for alcohols. This result could indicate that the Soave α-function may not be appropriate for alcohols. The u was predicted for 90 components grouped in the Test Dataset. The four models tested in this study (PR-Twu, RK-Twu, PR-Soave, and RK-Soave) produced results with similar deviations and reproduced the qualitative correct trends. However, the accuracy of the results is inadequate for all models because of the very well-known fact that cubic equations of state produce wildly inaccurate liquid densities or molar volumes (Kontogeorgis and Folas, 2009; Péneloux *et al.*, 1982; Saeed and Ghader, 2019; Yan *et al.*, 2021), that are used as input for the calculation of the u (Eq. 3.26). The highest deviations were found for carboxylic acids, indicating some inadequacies of CEoS to predict accurate liquid densities for these highly associated fluids.

5.2 Recommendations

The recommendations for future studies are as follows:

1. The evaluation of the saturated liquid speed of sound (u) faced challenges due to the selected models' shortcomings in accurately predicting liquid densities. This discovery highlights the need to reevaluate the use of volume-translated variations of the CEoS being examined.

2. The potential inconsistencies found for the Waring number of alcohols calculated from PR-Soave and RK-Soave need to be further investigated to shed light on the applicability of these two models for predicting the phase behaviour of alcohols. It is then required to examine other derivative properties in the subcritical, critical, and supercritical regions to determine if these potential inconsistencies affect the calculation of the thermophysical properties of alcohols.

3. Analysis of the Waring Number indicates potential discrepancies in the P^{sat} curve. These discrepancies suggest that the imposed constraints might be inadequate to ensure consistent P^{sat} curves, implying that further model refinement might be required to achieve the desired consistency.

4. An immediate and logical extension of this research would be to explore the supercritical region. Such an endeavour would present a more stringent assessment of thermodynamic consistency, especially considering the potential challenges of extrapolating from the subcritical to the supercritical domain.

5. Further advancing this research would involve a detailed examination of mixtures and their properties in the subcritical domain, utilizing the α-parameters and approaches established in this investigation.

References

Abudour, A. M., Mohammad, S. A., Robinson, R. L., and Gasem, K. A. M. (2014). Generalized binary interaction parameters for the Peng-Robinson equation of state. *Fluid Phase Equilib*, **383**, 156–173. https://doi.org/10.1016/j.fluid.2014.10.006

Acree, W., and Chickos, J. S. (2010). Phase Transition Enthalpy Measurements of Organic and Organometallic Compounds. Sublimation, Vaporization and Fusion Enthalpies From 1880 to 2010. *J Phys Chem Ref Data*, **39**, 043101. https://doi.org/10.1063/1.3309507

Aghaie, M., Rezaei, N., and Zendehboudi, S. (2019). Assessment of carbon dioxide solubility in ionic liquid/toluene/water systems by extended PR and PC-SAFT EOSs: Carbon capture implication. *J. Mol. Liq.*, **275**, 323–337. https://doi.org/10.1016/J.MOLLIQ.2018.11.038

Anderson, T. F., and Prausnitz, J. M. (1978). Application of the UNIQUAC Equation to Calculation of Multicomponent Phase Equilibria. 1. Vapor-Liquid Equilibria. *Ind. Eng. Chem. Process. Des. Dev.*, **17**, 552–561. https://doi.org/10.1021/I260068A028/ASSET/I260068A028.FP.PNG_V03

Barker, J. A., Leonard, P. J., and Pompe, A. (1966). Fifth Virial Coefficients. *J. Chem. Phys.*, **44**, 4206–4211. https://doi.org/10.1063/1.1726606

Bell, I. H., Satyro, M., and Lemmon, E. W. (2018). Consistent Twu Parameters for More than 2500 Pure Fluids from Critically Evaluated Experimental Data. *J. Chem. Eng. Data*, **63**, 2402–2409. https://doi.org/10.1021/ACS.JCED.7B00967/SUPPL_FILE/JE7B00967_SI_003.PDF

Benjamin, K. M., Schultz, A. J., and Kofke, D. A. (2006). Gas-Phase Molecular Clustering of TIP4P and SPC/E Water Models from Higher-Order Virial Coefficients†. *Ind. Eng. Chem. Res.*, **45**, 5566–5573. https://doi.org/10.1021/IE051160S

Benjamin, K. M., Singh, J. K., Schultz, A. J., and Kofke, D. A. (2007). Higher-Order Virial Coefficients of Water Models. *J. Phys. Chem. B*, **111**, 11463–11473. https://doi.org/10.1021/JP0710685

Bourne, T. (2016). *Applications of the Virial Equation of State to Determining the Structure* and *Phase Behaviour of Fluids*. University of Manchester.

Brush, S. G., and Hall, N. S. (2003). *The kinetic theory of gases: an anthology of classic papers with historical commentary*, **1**. Imperial College Press.

Cai, J., Qiu, D., Zhang, L., and Hu, Y. (2006). Vapor-liquid critical properties of multi-component fluid mixture. *Fluid Phase Equilib*, **241**, 229–235. https://doi.org/10.1016/j.fluid.2005.11.003

Castier, M. (2011). Thermodynamic speed of sound in multiphase systems. *Fluid Phase Equilib*, **306**, 204–211. https://doi.org/10.1016/J.FLUID.2011.04.002

Cerdeiriña, C. A., González-Salgado, D., Romani, L., Del Carmen Delgado, M., Torres, L. A., and Costas, M. (2004). Towards an understanding of the heat capacity of liquids. A simple two-state model for molecular association. *J. Chem. Phys.*, **120**, 6648–6659. https://doi.org/10.1063/1.1667469

Chapman, W. G., Gubbins, K. E., Jackson, G., and Radosz, M. (1989). SAFT: Equation-of-state solution model for associating fluids. *Fluid Phase Equilib*, **52**, 31–38. https://doi.org/10.1016/0378-3812(89)80308-5

Clausius, R. (1880). Ueber das Verhalten der Kohlensäure in Bezug auf Druck, Volumen und Temperatur. Annalen Der Physik, **245**, 337–357. https://doi.org/10.1002/ANDP.18802450302

Cohen, E. G. D. (1993). Fifty years of kinetic theory. *Physica A*, **194**, 229–257. https://doi.org/10.1016/0378-4371(93)90357-A

Coquelet, C., Chapoy, A., and Richon, D. (2004). Development of a new alpha function for the Peng-Robinson equation of state: Comparative study of alpha function models for pure gases (natural gas components) and water-gas systems. *Int J Thermophys*, **25**, 133–158. https://doi.org/10.1023/B:IJOT.0000022331.46865.2F

Davies, J. A., Hanson-Heine, M. W. D., Besley, N. A., Shirley, A., Trowers, J., Yang, S., and Ellis, A. M. (2019). Dimers of acetic acid in helium nanodroplets. *Phys. Chem. Chem. Phys.*: PCCP, **21**, 13950–13958. https://doi.org/10.1039/C8CP05934A

Davies, M. M., and Sutherland, G. B. B. M. (1938). The Infra-Red Absorption of Carboxylic Acids in Solution I. Qualitative Features. *J. Chem. Phys.*, **6**, 755–766. https://doi.org/10.1063/1.1750166

Deiters, U. K. (2013). Comments on the modeling of hydrogen and hydrogen-containing mixtures with cubic equations of state. *Fluid Phase Equilib*, **352**, 93–96. https://doi.org/10.1016/J.FLUID.2013.05.032

Economou, I. G., and Donohue, M. D. (1992). Thermodynamic Inconsistencies in and Accuracy of Chemical Equations of State for Associating Fluids. *Ind. Eng. Chem. Res.*, **31**, 1203–1211. https://doi.org/10.1021/IE00004A035/ASSET/IE00004A035.FP.PNG_V03

F. Ely, J., and Marrucho, I. M. F. (2000). 8 The corresponding-states principle. *Experimental Thermodynamics*, **5**, 289–320. https://doi.org/10.1016/S1874-5644(00)80019-3

Feng, C., Schultz, A. J., Chaudhary, V., and Kofke, D. A. (2015). Eighth to sixteenth virial coefficients of the Lennard-Jones model. *J. Chem. Phys.*, **143**, 44504. https://doi.org/10.1063/1.4927339/15500522/044504_1_ACCEPTED_MANUSCRIPT.PDF

Gao, G., Daridon, J. L., Saint-Guirons, H., Xans, P., and Montel, F. (1992). A simple correlation to evaluate binary interaction parameters of the Peng-Robinson equation of state: binary light hydrocarbon systems. *Fluid Phase Equilib*, **74**, 85–93. https://doi.org/10.1016/0378-3812(92)85054-C

George Hayden, J., and O'Connell, J. P. (1975). A Generalized Method for Predicting Second Virial Coefficients. *Ind. Eng. Chem. Process. Des. Dev.*, **14**, 209–216. https://doi.org/10.1021/I260055A003/SUPPL_FILE/I260055A003_SI_001.PDF

Ghanbari, M., Ahmadi, M., and Lashanizadegan, A. (2017). A comparison between Peng-Robinson and Soave-Redlich-Kwong cubic equations of state from modification perspective. *Cryogenics*, **84**, 13–19. https://doi.org/10.1016/j.cryogenics.2017.04.001

Ghosh, P. (1999). Prediction of Vapor-Liquid Equilibria Using Peng-Robinson and Soave-Redlich-Kwong Equations of State. *Chem Eng Technol*, **22**, 379–399.

Gokul, N., Schultz, A. J., and Kofke, D. A. (2021). Properties of supercritical N2, O2, CO2, and NH3 mixtures from the virial equation of state. *AIChE J*, **67**, e17072. https://doi.org/10.1002/AIC.17072

Graboski, M. S., and Daubert, T. E. (1978). A Modified Soave Equation of State for Phase Equilibrium Calculations. 1. Hydrocarbon Systems. *Ind. Eng. Chem. Process. Des. Dev.*, **17**, 443–448. https://doi.org/10.1021/I260068A009/ASSET/I260068A009.FP.PNG_V03

Gross, J., and Sadowski, G. (2001). Perturbed-Chain SAFT: An Equation of State Based on a Perturbation Theory for Chain Molecules. *Ind. Eng. Chem. Res.*, **40**, 1244–1260. https://doi.org/10.1021/IE0003887

Guggenheim, E. A. (1952). Mixtures: *The theory of the equilibrium properties of some simple classes of mixtures, solutions,* and *alloys*. Clarendon Press.

Harandi, M. N., and Haghtalab, A. (2021). Thermodynamic modeling of CO 2 solubility into an aqueous solution of N-methyldiethanolamine using EoS/G E approach and different Alpha-functions. *Fluid Phase Equilib*, **539**, 113030. https://doi.org/10.1016/j.fluid.2021.113030

Huang, S. H., and Radosz, M. (1991). Equation of state for small, large, polydisperse, and associating molecules: extension to fluid mixtures. *Ind. Eng. Chem. Res.*, **30**, 1994–2005. https://doi.org/10.1021/IE00056A050

Jaubert, J.-N., and Mutelet, F. (2004). VLE predictions with the Peng-Robinson equation of state and temperature dependent k ij calculated through a group contribution method. *Fluid Phase Equilib*, **224**, 285–304. https://doi.org/10.1016/j.fluid.2004.06.059

Jaubert, J.-N., and Privat, R. (2010). Relationship between the binary interaction parameters (kij) of the Peng-Robinson and those of the Soave-Redlich-Kwong equations of state: Application to the definition of the PR2SRK model. *Fluid Phase Equilib*, **295**, 26–37. https://doi.org/10.1016/j.fluid.2010.03.037

Kontogeorgis, G. M., and Folas, G. K. (2009). *Thermodynamic Models for Industrial Applications: From Classical and Advanced Mixing Rules to Association Theories*. wiley. https://doi.org/10.1002/9780470747537

Kunz, O., and Wagner, W. (2012). The GERG-2008 wide-range equation of state for natural gases and other mixtures: An expansion of GERG-2004. *J. Chem. Eng. Data*, **57**, 3032–3091. https://doi.org/10.1021/JE300655B/ASSET/IMAGES/MEDIUM/JE-2012-00655B_0029.GIF

Le Guennec, Y., Lasala, S., Privat, R., and Jaubert, J. N. (2016). A consistency test for α-functions of cubic equations of state. *Fluid Phase Equilib*, **427**, 513–538. https://doi.org/10.1016/J.FLUID.2016.07.026

Le Guennec, Y., Privat, R., and Jaubert, J.-N. (2016). Development of the translated-consistent tc-PR and tc-RK cubic equations of state for a safe and accurate prediction of volumetric, energetic and saturation properties of pure compounds in the sub- and super-critical domains. *Fluid Phase Equilib*, **429**, 301–312. https://doi.org/10.1016/j.fluid.2016.09.003

Le Guennec, Y., Privat, R., Lasala, S., and El Jaubert, J.-N. (2017). On the imperative need to use a consistent a-function for the prediction of pure-compound supercritical properties with a cubic equation of state. *Fluid Phase Equilib*, **445**, 45–53. https://doi.org/10.1016/j.fluid.2017.04.015

Liang, X., Maribo-Mogensen, B., Thomsen, K., Yan, W., and Kontogeorgis, G. M. (2012). Approach to improve speed of sound calculation within PC-SAFT framework. *Ind. Eng. Chem. Res.*, **51**, 14903–14914. https://doi.org/10.1021/IE3018127/SUPPL_FILE/IE3018127_SI_001.PDF

Marshall, B. D. (2019). A PC-SAFT model for hydrocarbons IV: Water-hydrocarbon phase behavior including petroleum pseudo-components. *Fluid Phase Equilib*, **497**, 79–86. https://doi.org/10.1016/J.FLUID.2019.06.007

Marshall, B. D. (2020). A PC-SAFT model for hydrocarbons V: Alcohol-hydrocarbon phase behavior with application to petroleum pseudo-components. *Fluid Phase Equilib*, **507**, 112420. https://doi.org/10.1016/J.FLUID.2019.112420

Mathias, P. M. (1983). A versatile phase equilibrium equation of state. *Ind. Eng. Chem. Process Des. Dev.; (United States)*, **22:3**, 385–391. https://doi.org/10.1021/I200022A008

Mathias, P. M., and Copeman, T. W. (1983a). Extension of the Peng-Robinson equation of state to complex mixtures: Evaluation of the various forms of the local composition concept. *Fluid Phase Equilib*, **13**, 91–108. https://doi.org/10.1016/0378-3812(83)80084-3

Mathias, P. M., and Copeman, T. W. (1983b). Extension of the Peng-Robinson equation of state to complex mixtures: Evaluation of the various forms of the local composition concept. *Fluid Phase Equilib*, **13**, 91–108. https://doi.org/10.1016/0378-3812(83)80084-3

Meinshausen, N. (2006). Quantile Regression Forests. *J Mach Learn Res*, **7**, 983–999.

Meng, L., Duan, Y. Y., and Li, L. (2004). Correlations for second and third virial coefficients of pure fluids. *Fluid Phase Equilib*, **226**, 109–120. https://doi.org/10.1016/J.FLUID.2004.09.023

Michelsen, M. L., and Møllerup, J. (2007). Thermodynamic Models: Fundamentals and Computational Aspects. Tie-Line Publications, **2**

Nishiumi, H., Arai, T., and Takeuchi, K. (1988). Generalization of the binary interaction parameter of the Peng-Robinson equation of state by component family. *Fluid Phase Equilib*, **42**, 43–62. https://doi.org/10.1016/0378-3812(88)80049-9

National Institute of Standards and Technology (NIST). (2017). Standard Reference Database.

Nothnagel, K. H., Abrams, D. S., and Prausnitz, J. M. (1973). Generalized Correlation for Fugacity Coefficients in Mixtures at Moderate Pressures. Application of Chemical Theory of Vapor imperfections. *Ind. Eng. Chem. Process. Des. Dev.*, **12**, 25–35. https://doi.org/10.1021/I260045A006/ASSET/I260045A006.FP.PNG_V03

Peneloux, A., Abdoul, W., and Rauzy, E. (1989). Excess functions and equations of state. *Fluid Phase Equilib*, **47**, 115–132. https://doi.org/10.1016/0378-3812(89)80172-4

Péneloux, A., Rauzy, E., and Fréze, R. (1982). A consistent correction for Redlich-Kwong-Soave volumes. *Fluid Phase Equilib*, **8**, 7–23. https://doi.org/10.1016/0378-3812(82)80002-2

Peng, D. Y., and Robinson, D. B. (1976). A New Two-Constant Equation of State. Industrial and Ind. *Eng. Chem. Fundam.*, **15**, 59–64. https://doi.org/10.1021/I160057A011

Pina-Martinez, A., Le Guennec, Y., Privat, R., Jaubert, J. N., and Mathias, P. M. (2018). Analysis of the Combinations of Property Data That Are Suitable for a Safe Estimation of Consistent Twu α-Function Parameters: Updated Parameter Values for the Translated-Consistent tc-PR and tc-RK Cubic Equations of State. *J. Chem. Eng. Data*, **63**, 3980–3988. https://doi.org/10.1021/ACS.JCED.8B00640/SUPPL_FILE/JE8B00640_SI_001.PDF

Piña-Martinez, A., Privat, R., and Jaubert, J. N. (2022). Use of 300,000 pseudo-experimental data over 1800 pure fluids to assess the performance of four cubic equations of state: SRK, PR, tc-RK, and tc-PR. *AIChE J*, **68**, e17518. https://doi.org/10.1002/AIC.17518

Pina-Martinez, A., Privat, R., Jaubert, J. N., and Peng, D. Y. (2019a). Updated versions of the generalized Soave α-function suitable for the Redlich-Kwong and Peng-Robinson equations of state. *Fluid Phase Equilib*, **485**, 264–269. https://doi.org/10.1016/J.FLUID.2018.12.007

Prausnitz, J. M., Lichtenthaler, R. N., and Gomes de Azevedo, E. (1998). *Molecular Thermodynamics of Fluid-Phase Equilibria*. **2**. Prentice-Hall Inc.

Prausnitz, J. M., and Tavares, F. W. (2004). Thermodynamics of fluid-phase equilibria for standard chemical engineering operations. *AIChE J*, **50**, 739–761. https://doi.org/10.1002/AIC.10069

Redlich, O., and Kwong, J. N. S. (1949). On the thermodynamics of solutions. V. An equation of state. Fugacities of gaseous solutions. *Chem. Rev.*, **44**, 233–244. https://doi.org/10.1021/cr60137a013

Saeed, A., and Ghader, S. (2019). Calculation of density, vapor pressure and heat capacity near the critical point by incorporating cubic SRK EoS and crossover translation. *Fluid Phase Equilib*, **493**, 10–25. https://doi.org/10.1016/J.FLUID.2019.03.027

Sarkoohaki, B., Almasi, M., and Karimkhani, M. (2019). Theoretical and experimental study of physicochemical behavior of binary mixtures: SAFT and PC-SAFT models. *J Chem Sci*, **131**, 1–5. https://doi.org/10.1007/S12039-019-1630-9/METRICS

Soave, G. (1972a). Equilibrium constants from a modified Redlich-Kwong equation of state. *Chem. Eng. Sci.*, **27**, 1197–1203. https://doi.org/10.1016/0009-2509(72)80096-4

Soave, G. (1972b). Equilibrium constants from a modified Redlich-Kwong equation of state. *Chem. Eng. Sci.*, **27**, 1197–1203. https://doi.org/10.1016/0009-2509(72)80096-4

Sokovnin, O. M., Zagoskina, N. V., and Zagoskin, S. N. (2022). Mathematical Models of the State of a Real Gas. *J. Eng. Phys. Thermophys.*, **95**, 806–820. https://doi.org/10.1007/S10891-022-02539-2/METRICS

Stryjek, R., and Vera, J. H. (1986). PRSV: An improved peng—Robinson equation of state for pure compounds and mixtures. *Can J Chem Eng*, **64**, 323–333. https://doi.org/10.1002/CJCE.5450640224

Tassios, D. P. (1993). *Applied Chemical Engineering Thermodynamics*. Springer Berlin Heidelberg. https://doi.org/10.1007/978-3-662-01645-9

Thiesen, M. (1885a). Untersuchungen über die Zustandsgleichung. *Ann Phys*, **260**, 467–492. https://doi.org/10.1002/ANDP.18852600308

Thiesen, M. (1885b). Untersuchungen über die Zustandsgleichung. *Ann Phys*, **260**, 467–492. https://doi.org/10.1002/ANDP.18852600308

Thodos, G. (1950). Vapor Pressures of Normal Saturated Hydrocarbons. *J Ind Eng Chem*, **42**, 1514–1526. https://doi.org/10.1021/IE50488A019

Trebble, M. A., and Bishnoi, P. R. (1987). Development of a new four-parameter cubic equation of state. *Fluid Phase Equilib*, **35**, 1–18. https://doi.org/10.1016/0378-3812(87)80001-8

Trusler, J. P. M. (2000a). 3 The virial equation of state. *Experimental Thermodynamics*, **5**, 35–74. https://doi.org/10.1016/S1874-5644(00)80014-4

Trusler, J. P. M. (2000b). 3 The virial equation of state. *Experimental Thermodynamics*, **5**, 35–74. https://doi.org/10.1016/S1874-5644(00)80014-4

Tsochantaris, E., Liang, X., and Kontogeorgis, G. M. (2020). Evaluating the Performance of the PC-SAFT and CPA Equations of State on Anomalous Properties of Water. *J. Chem. Eng. Data*, **65**, 5718–5734. https://doi.org/10.1021/ACS.JCED.0C00689/ASSET/IMAGES/MEDIUM/JE0C00689_0012.GIF

Twu, C. H., Bluck, D., Cunningham, J. R., and Coon, J. E. (1991a). A cubic equation of state with a new alpha function and a new mixing rule. *Fluid Phase Equilib*, **69**, 33–50. https://doi.org/10.1016/0378-3812(91)90024-2

Twu, C. H., Bluck, D., Cunningham, J. R., and Coon, J. E. (1991b). A cubic equation of state with a new alpha function and a new mixing rule. *Fluid Phase Equilib*, **69**, 33–50. https://doi.org/10.1016/0378-3812(91)90024-2

Twu, C. H., Coon, J. E., and Bluck, D. (1998). Comparison of the Peng−Robinson and Soave−Redlich−Kwong Equations of State Using a New Zero-Pressure-Based Mixing Rule for the Prediction of High-Pressure and High-Temperature Phase Equilibria. *Ind. Eng. Chem. Res.*, **37**, 1580–1585. https://doi.org/10.1021/IE9706424

Twu, C. H., Coon, J. E., and Cunningham, J. R. (1993). An equation of state for carboxylic acids. *Fluid Phase Equilib*, **82**, 379–388. https://doi.org/10.1016/0378-3812(93)87161-S

Twu, C. H., Coon, J. E., and Cunningham, J. R. (1995a). A new generalized alpha function for a cubic equation of state Part 1. Peng-Robinson equation. *Fluid Phase Equilib*, **105**, 49–59. https://doi.org/10.1016/0378-3812(94)02601-V

Twu, C. H., Coon, J. E., and Cunningham, J. R. (1995b). A new generalized alpha function for a cubic equation of state Part 2. Redlich-Kwong equation. *Fluid Phase Equilib*, **105**, 61–69. https://doi.org/10.1016/0378-3812(94)02602-W

Valderrama, J. O. (1990). A Generalized Patel-Teja Equation of State for Polar and Nonpolar Fluids and Their Mixtures. *J. Chem. Eng. Japan*, **23**, 87–91. https://doi.org/10.1252/JCEJ.23.87

Valderrama, J. O. (2003). The state of the cubic equations of state. *Ind. Eng. Chem. Res.*, **42**, 1603–1618. https://doi.org/10.1021/IE020447B

van Beijeren, H., and Ernst, M. H. (1979). Kinetic theory of hard spheres. *J Stat Phys*, **21**, 125–167. https://doi.org/10.1007/BF01008695/METRICS

Van der Waals, J.D. (1873) Over de Continuiteit van den Gas-en Vloeistoftoestand (On the Continuity of the Gas and Liquid State). Ph.D. Thesis, University of Leiden, Leiden.

Van Der Waals, J. D., and Rowlinson, J. S. (1988). *On the continuity of the gaseous* and *liquid states.* Elsevier Science Pub

Van Ness, H. C., Byer, S. M., and Gibbs, R. E. (1973). Vapor-Liquid equilibrium: Part I. An appraisal of data reduction methods. *AIChE J*, **19**, 238–244. https://doi.org/10.1002/AIC.690190206

Varzandeh, F., Stenby, E. H., and Yan, W. (2016). Comparison of GERG-2008 and simpler EoS models in calculation of phase equilibrium and physical properties of natural gas related systems. *Fluid Phase Equilib*, **434**, 21-43. https://doi.org/10.1016/j.fluid.2016.11.016

Velasco, S., White, J. A., Srinivasan, K., and Dutta, P. (2012). Waring and Riedel functions for the liquid-vapor coexistence curve. *Ind. Eng. Chem. Res*., **51**, 3197–3202. https://doi.org/10.1021/IE2028393/SUPPL_FILE/IE2028393_SI_001.PDF

Waring, W. (1954). Form of a Wide-Range Vapor Pressure Equation. *J Ind Eng Chem*, 46, 762–**763**. https://doi.org/10.1021/IE50532A042

Wertheim, M. S. (1986). Fluids with highly directional attractive forces. III. Multiple attraction sites. *J Stat Phys*, **42**, 459–476. https://doi.org/10.1007/BF01127721

Whitson, C. H., and Brulé, M. R. (2000). *Phase Behavior*. https://doi.org/10.2118/9781555630874

Wilson, G. M. (1966). Calculation of Enthalpy Data from a Modified Redlich-Kwong Equation of State. *ACRE*, **11**, 392–400. https://doi.org/10.1007/978-1-4757-0522-5_43

Xu, L., Li, Z., Yang, Z., and Duan, Y. Y. (2022). Empirical correlations for the third virial coefficients of nonpolar, polar and quantum fluids in a wide temperature range. *Fluid Phase Equilib*, **559**. https://doi.org/10.1016/J.FLUID.2022.113477

Xu, L., Liu, H. T., Yang, Z., and Duan, Y. Y. (2021). Empirical correlations for second virial coefficients of associated and quantum fluids covering a wide temperature range. *Fluid Phase Equilib,* **547**, 113133. https://doi.org/10.1016/J.FLUID.2021.113133

Yan, W., Regueira, T., Liu, Y., and Stenby, E. H. (2021). Density Modeling of High-Pressure Mixtures using Cubic and Non-Cubic EoS and an Excess Volume Method. *Fluid Phase Equilib*, **532**, 112884. https://doi.org/10.1016/J.FLUID.2020.112884

Yaws, C. L. (2015). *The Yaws H*and*book of Physical Properties for Hydrocarbons* and *Chemicals*, **2**, Gulf Professional Publishing

Young, A. F., Pessoa, F. L. P., and Ahón, V. R. R. (2016). Comparison of 20 Alpha Functions Applied in the Peng-Robinson Equation of State for Vapor Pressure Estimation. *Ind. Eng. Chem. Res*., **55**, 6506–6516. https://doi.org/10.1021/ACS.IECR.6B00721/ASSET/IMAGES/LARGE/IE-2016-00721S_0004.JPEG

Zábranský, Milan., (1996). *Heat capacity of liquids: critical review* and *recommended values.* American Chemical Society., American Institute of Physics., National Institute of Standards and

Technology (U.S.), and International Union of Pure and Applied Chemistry. Commission on Thermodynamics.

Zhao, W., Xia, L., Sun, X., and Xiang, S. (2019). A Review of the Alpha Functions of Cubic Equations of State for Different Research Systems. *Int J Thermophys*, **40**, 1–25. https://doi.org/10.1007/S10765-019-2567-4/TABLES/4

Zudkevitch, D., and Joffe, J. (1970). Correlation and prediction of vapor-liquid equilibria with the redlich-kwong equation of state. *AIChE J*, **16**, 112–119. https://doi.org/10.1002/AIC.690160122

Appendix

Appendix A- Plots of the speed of sound for selected components in Group 2

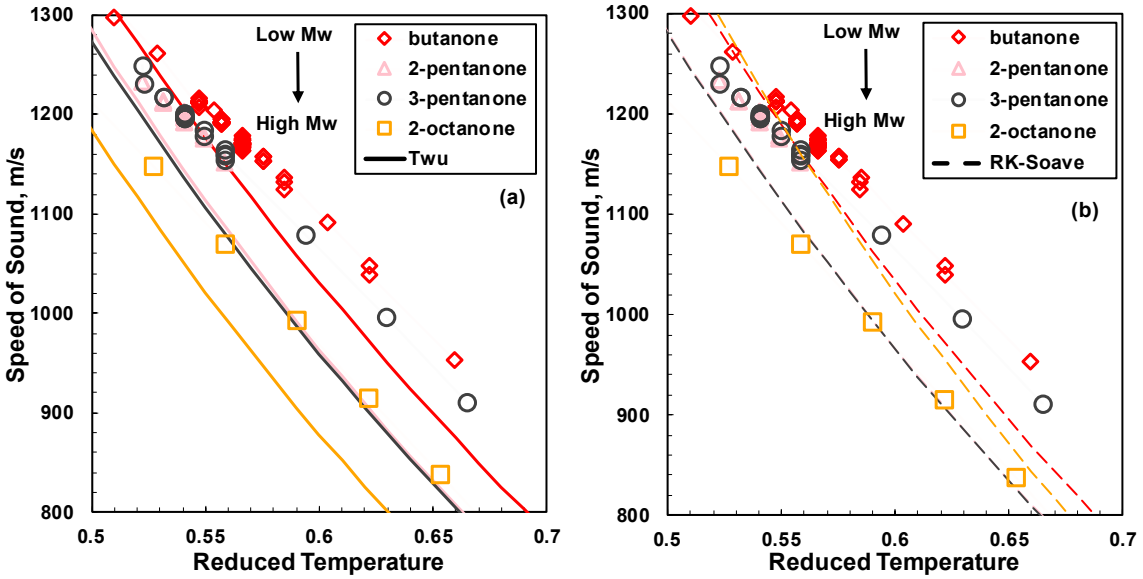

Figure A.1: Plots of the speed of sound (u) against reduced temperature for linear Ketones. Plot (a) utilizes the Peng-Robinson equation with the Twu α-function (PR-Twu), while Plot (b) employs the Soave α-function (PR-Soave). Experimental data is represented by symbols, model predictions are depicted using lines, and Mw is the molecular weight.

Appendix B1- Inputs for CEoS

Table B1.1: Inputs for Group 1 Non-Polar components, where A, B, C, D, E are constants for the ideal heat capacity (Eq. 3.17).

Component	CAS	Mw, g/mol	Family	ω	Tc, K	Pc, kPa	A_{Cp}	B_{Cp}	C_{Cp}	D_{Cp}	E_{Cp}
methane	74-82-8	16.043	Alkanes	0.0120	190.56	4599	3.4942E+01	-3.9957E-02	1.9184E-04	-1.5300E-07	3.9321E-11
ethane	74-84-0	30.070	Alkanes	0.1000	305.32	4872	2.8146E+01	4.3447E-02	1.8946E-04	-1.9080E-07	5.3349E-11
propane	74-98-6	44.097	Alkanes	0.1520	369.83	4248	2.8277E+01	1.1600E-01	1.9597E-04	-2.3270E-07	6.8669E-11
butane	106-97-8	58.123	Alkanes	0.2000	425.12	3796	2.0056E+01	2.8153E-01	-1.3143E-05	-9.4570E-08	3.4149E-11
pentane	109-66-0	72.150	Alkanes	0.2520	469.70	3370	2.6671E+01	3.2324E-01	4.2820E-05	-1.6640E-07	5.6036E-11
hexane	110-54-3	86.177	Alkanes	0.3010	507.60	3025	2.5924E+01	4.1927E-01	-1.2491E-05	-1.5920E-07	5.8784E-11
heptane	142-82-5	100.204	Alkanes	0.3500	540.20	2740	2.6984E+01	5.0387E-01	-4.4748E-05	-1.6840E-07	6.5183E-11
octane	111-65-9	114.231	Alkanes	0.4000	568.70	2490	2.9053E+01	5.8016E-01	-5.7103E-05	-1.9550E-07	7.6614E-11
nonane	111-84-2	128.258	Alkanes	0.4440	594.60	2290	2.9687E+01	6.6821E-01	-9.6492E-05	-2.0010E-07	8.2200E-11
decane	124-18-5	142.285	Alkanes	0.4920	617.70	2110	3.1780E+01	7.4489E-01	-1.0945E-04	-2.2670E-07	9.3458E-11
undecane	1120-21-4	156.312	Alkanes	0.5300	639.00	1950	1.2521E+02	3.1401E-01	7.9137E-04	-9.1410E-07	2.7568E-10
dodecane	112-40-3	170.338	Alkanes	0.5760	658.00	1820	7.1498E+01	7.2559E-01	1.1553E-04	-4.1200E-07	1.4141E-10
tridecane	629-50-5	184.365	Alkanes	0.6170	675.00	1680	1.1040E+02	5.3321E-01	7.3984E-04	-1.0210E-06	3.2423E-10
tetradecane	629-59-4	198.392	Alkanes	0.6430	693.00	1570	1.1550E+02	6.0882E-01	6.8043E-04	-9.7090E-07	3.0756E-10
pentadecane	629-62-9	212.419	Alkanes	0.6860	708.00	1480	1.2465E+02	6.2706E-01	8.3164E-04	-1.1690E-06	3.7326E-10
hexadecane	544-76-3	226.446	Alkanes	0.7170	723.00	1400	1.3175E+02	6.7397E-01	8.7770E-04	-1.2430E-06	3.9785E-10
benzene	71-43-2	78.114	Aromatics	0.2100	562.05	4895	-3.1368E+01	4.7460E-01	-3.1137E-04	8.5240E-08	-5.0524E-12
toluene	108-88-3	92.141	Aromatics	0.2640	591.75	4108	-2.4097E+01	5.2187E-01	-2.9827E-04	6.1220E-08	1.2576E-12
ethylbenzene	100-41-4	106.167	Aromatics	0.3040	617.15	3609	-2.0527E+01	5.9578E-01	-3.0849E-04	3.5620E-08	1.2409E-11
o-xylene	95-47-6	106.167	Aromatics	0.3100	630.30	3732	1.8200E-01	5.1344E-01	-2.0212E-04	-2.1610E-08	2.3212E-11
propylbenzene	103-65-1	120.194	Aromatics	0.3440	638.35	3200	-1.0933E+01	6.4349E-01	-2.7829E-04	-1.4430E-08	2.8143E-11
naphthalene	91-20-3	128.174	Aromatics	0.3020	748.40	4050	6.7099E+01	4.3239E-02	9.1740E-04	-1.0020E-06	3.0896E-10
n-butylbenzene	104-51-8	134.221	Aromatics	0.3940	660.50	2890	2.6627E+01	5.3108E-01	3.7958E-05	-2.7950E-07	1.0200E-10
2-methylnaphthalene	91-57-6	142.200	Aromatics	0.3780	761.00	3500	-8.9900E-01	6.1854E-01	-1.8095E-04	-1.1450E-07	5.9208E-11

Component	CAS	Mw, g/mol	Family	ω	Tc, K	Pc, kPa	A_{Cp}	B_{Cp}	C_{Cp}	D_{Cp}	E_{Cp}
Acenaphthene	83-32-9	154.211	Aromatics	0.4750	803.15	2976	-6.1063E+01	9.6388E-01	-7.2100E-04	2.6230E-07	-3.6857E-11
1,8-dimethylnaphthalene	569-41-5	156.227	Aromatics	0.3950	792.00	3100	-4.4770E+01	9.4224E-01	-6.6284E-04	1.8840E-07	0.0000E+00
2,7-dimethylnaphthalene	582-16-1	156.227	Aromatics	0.4840	794.22	2914	-4.9867E+01	1.0029E+00	-7.9843E-04	3.3600E-07	-5.8987E-11
n-hexylbenzene	1077-16-3	162.275	Aromatics	0.5080	723.61	2305	3.9655E+01	6.4328E-01	6.6681E-05	-3.5560E-07	1.2779E-10
diphenylmethane	101-81-5	168.238	Aromatics	0.4820	760.00	2710	-1.0030E+02	1.2250E+00	-1.0670E-03	4.8040E-07	-8.7845E-11
isopentane	78-78-4	72.150	Branched	0.2280	460.40	3380	-8.8100E-01	4.7498E-01	-2.4797E-04	6.7510E-08	-8.5343E-12
3-methylpentane	96-14-0	86.177	Branched	0.2740	504.43	3124	-7.1230E+00	5.8327E-01	-3.0338E-04	6.8020E-08	-3.9778E-12
2,3-dimethylpentane	565-59-3	100.204	Branched	0.2960	537.30	2910	3.8654E+01	3.7259E-01	2.7632E-04	-4.3150E-07	1.3811E-10
3-methylhexane	589-34-4	100.204	Branched	0.3200	535.20	2810	-1.2841E+01	7.1358E-01	-4.2021E-04	1.2000E-07	-1.2906E-11
2-methylhexane	591-76-4	100.204	Branched	0.3280	530.40	2740	-3.2490E+00	6.6625E-01	-3.3836E-04	6.0490E-08	2.5385E-12
4-methylheptane	589-53-7	114.231	Branched	0.3710	561.74	2542	-1.7581E+01	8.3526E-01	-5.1418E-04	1.5100E-07	-1.5855E-11
2-methylheptane	592-27-8	114.231	Branched	0.3770	559.64	2484	-3.3670E+00	7.5824E-01	-3.8216E-04	5.7360E-08	8.0178E-12
cyclopropane	75-19-4	42.081	Cyclic	0.1270	397.91	5495	2.1172E+01	6.3106E-02	2.9197E-04	-3.2710E-07	9.9730E-11
spiropentane	157-40-4	68.119	Cyclic	0.2300	499.74	4819	-4.1488E+01	5.3877E-01	-3.8261E-04	1.0920E-07	0.0000E+00
cyclohexane	110-82-7	84.161	Cyclic	0.2080	553.80	4080	1.3783E+01	2.0742E-01	5.3682E-04	-6.3010E-07	1.8988E-10
methylcyclopentane	96-37-7	84.161	Cyclic	0.2300	532.79	3785	-9.9390E+00	4.2528E-01	1.2521E-05	-1.8860E-07	6.4751E-11
methylcyclohexane	108-87-2	98.188	Cyclic	0.2360	572.10	3480	4.2960E+00	4.2716E-01	2.1058E-04	-3.9990E-07	1.3121E-10
ethylcyclopentane	1640-89-7	98.188	Cyclic	0.2700	569.50	3400	-2.8514E+01	5.7607E-01	-9.4379E-05	-1.6440E-07	6.9435E-11
cycloheptane	291-64-5	98.188	Cyclic	0.2410	604.20	3820	9.4470E+00	3.5261E-01	3.7699E-04	-5.3870E-07	1.6956E-10
propylcyclopentane	2040-96-2	112.215	Cyclic	0.3440	591.80	2966	-5.1866E+01	7.8827E-01	-3.5255E-04	-6.8550E-09	3.1314E-11
propylcyclohexane	1678-92-8	126.242	Cyclic	0.3740	623.48	2613	2.5567E+01	5.2828E-01	2.3719E-04	-4.6760E-07	1.5413E-10
butylcyclopentane	2040-95-1	126.242	Cyclic	0.3740	618.48	2677	-1.1673E+02	1.3097E+00	-1.2439E-03	5.2920E-07	0.0000E+00
butylcyclohexane	1678-93-9	140.269	Cyclic	0.4170	648.16	2453	9.0421E+01	2.3264E-01	9.4595E-04	-1.0570E-06	3.1928E-10

Table B1.2: Inputs for Group 2 Polar components, where A, B, C, D, E are constants for the ideal heat capacity (Eq. 3.17).

Component	CAS	Mw, g/mol	Family	ω	Tc, K	Pc, kPa	A_{Cp}	B_{Cp}	C_{Cp}	D_{Cp}	E_{Cp}
propanal	123-38-6	58.080	Aldehydes	0.2560	504.40	5516	5.8911E+01	4.8385E-03	3.3514E-04	-3.0510E-07	8.3305E-11
butanal	123-72-8	72.107	Aldehydes	0.2770	537.20	4320	6.4374E+01	6.4776E-02	3.5143E-04	-3.5370E-07	1.0082E-10
hexanal	66-25-1	100.161	Aldehydes	0.3870	591.00	3460	7.1773E+01	2.0294E-01	3.4761E-04	-4.1610E-07	1.2259E-10
benzaldehyde	100-52-7	106.124	Aldehydes	0.5640	695.00	4508	-8.9000E-01	4.4758E-01	-1.8566E-04	-3.6200E-08	3.1110E-11
thietane	287-27-4	74.147	HSCC	0.2180	602.00	6108	-1.9537E+01	3.6008E-01	-2.2545E-04	5.4990E-08	0.0000E+00
dimethyl sulfoxide	67-68-5	78.135	HSCC	0.4010	729.00	6987	2.7816E+01	2.4839E-01	-1.3176E-04	2.3840E-08	1.6501E-12
thiophene	110-02-1	84.142	HSCC	0.1970	579.35	5690	2.2037E+01	1.2481E-01	2.4505E-04	-3.3890E-07	1.1175E-10
tetrahydrothiophene	110-01-0	88.174	HSCC	0.2570	632.00	5520	-6.1610E+00	3.7746E-01	-1.3544E-04	-3.9010E-08	2.5996E-11
2-methylthiophene	554-14-3	98.169	HSCC	0.2820	606.20	4691	-1.9124E+01	4.7660E-01	-3.3969E-04	9.6830E-08	0.0000E+00
3-methylthiophene	616-44-4	98.169	HSCC	0.2820	610.80	4738	-2.3147E+01	4.9802E-01	-3.7681E-04	1.1370E-07	0.0000E+00
thiane	1613-51-0	102.200	HSCC	0.2910	661.07	4662	-5.2045E+01	6.3212E-01	-3.3873E-04	6.1030E-08	0.0000E+00
2-methyltetrahydrothiophene	1795-09-1	102.200	HSCC	0.2910	661.07	4488	-4.0320E+01	6.2493E-01	-3.9430E-04	9.6600E-08	0.0000E+00
benzothiophene	95-15-8	134.202	HSCC	0.3600	754.00	4435	-4.7900E+01	8.1457E-01	-8.0881E-04	4.1420E-07	-8.5298E-11
acetone	67-64-1	58.080	Ketones	0.3060	508.20	4702	3.5918E+01	9.3896E-02	1.8730E-04	-2.1640E-07	6.3174E-11
butanone	78-93-3	72.107	Ketones	0.3240	535.50	4154	3.7369E+01	2.3045E-01	5.7387E-06	-8.8170E-08	2.9637E-11
cyclopentanone	120-92-3	84.118	Ketones	0.2880	624.50	4600	-2.9270E+01	5.0540E-01	-3.4447E-04	1.3120E-07	-2.6198E-11
4-butanolide	96-48-0	86.090	Ketones	0.4510	739.00	6008	2.2370E+01	1.7297E-01	2.4826E-04	-3.3530E-07	1.0555E-10
2-pentanone	107-87-9	86.134	Ketones	0.3430	561.08	3694	4.2356E+01	2.7425E-01	6.3786E-05	-1.6870E-07	5.5342E-11
3-pentanone	96-22-0	86.134	Ketones	0.3450	560.90	3740	4.9800E+01	2.6897E-01	5.0669E-05	-1.5230E-07	4.9510E-11
1,3-dioxolan-2-one	96-49-1	88.063	Ketones	0.4630	806.00	8975	-4.2285E+00	3.2157E-01	-7.6693E-05	-1.4810E-07	8.7872E-11
cyclohexanone	108-94-1	98.145	Ketones	0.3060	664.30	4600	-1.2337E+01	4.0837E-01	1.0597E-04	-2.9620E-07	1.0088E-10
3-Penten-2-one, 4-methyl-	141-79-7	98.145	Ketones	0.5210	600.00	3587	1.6062E+01	5.8779E-01	-6.0312E-04	4.4460E-07	-1.4943E-10
methyl isobutyl ketone	108-10-1	100.161	Ketones	0.3560	574.60	3270	2.4040E+00	5.8495E-01	-3.7647E-04	1.2420E-07	-1.7051E-11
3-hexanone	589-38-8	100.161	Ketones	0.3800	582.82	3320	7.3031E+01	2.2148E-01	2.7912E-04	-3.6880E-07	1.1286E-10
2-hexanone	591-78-6	100.161	Ketones	0.3850	587.61	3287	4.5050E+01	3.5513E-01	4.8896E-05	-1.9810E-07	6.4005E-11
4-heptanone	123-19-3	114.188	Ketones	0.6060	602.00	2886	3.8840E+00	6.4084E-01	-3.3830E-04	6.3060E-08	0.0000E+00
2-octanone	111-13-7	128.214	Ketones	0.6730	632.70	2603	8.1259E+01	3.2148E-01	3.8818E-04	-5.4650E-07	1.7288E-10

Component	CAS	Mw, g/mol	Family	ω	Tc, K	Pc, kPa	A_{Cp}	B_{Cp}	C_{Cp}	D_{Cp}	E_{Cp}
2,6-Dimethyl-4-heptanone	108-83-8	142.241	Ketones	0.7350	653.74	2290	-1.4330E+00	8.8406E-01	-5.7459E-04	1.9430E-07	-2.8451E-11
benzophenone	119-61-9	182.222	Ketones	0.8920	830.00	2795	-7.5275E+01	1.0612E+00	-7.8307E-04	2.7120E-07	-3.4873E-11
cyanogen	460-19-5	52.036	Nitriles	0.2790	400.15	5980	2.2445E+01	1.6837E-01	-2.3212E-04	1.5780E-07	-4.0479E-11
acetonitrile	107-13-1	53.064	Nitriles	0.3500	540.00	4660	1.8425E+01	1.8336E-01	-1.0072E-04	1.8750E-08	9.1114E-13
propionitrile	107-12-0	55.080	Nitriles	0.2660	564.40	6180	1.7618E+01	2.2119E-01	-1.0707E-04	1.7350E-08	1.0610E-12
butyronitrile	109-74-0	69.107	Nitriles	0.3710	582.35	3790	1.4849E+01	3.4077E-01	-2.0780E-04	6.2990E-08	-7.5521E-12
trimethylacetonitrile	630-18-2	83.133	Nitriles	0.3530	632.96	4011	-9.1300E+00	5.3946E-01	-3.8900E-04	1.1390E-07	0.0000E+00
benzonitrile	100-47-0	103.124	Nitriles	0.3660	699.35	4215	-2.6240E+00	4.5843E-01	-2.6757E-04	4.3710E-08	7.3182E-12
pyridine	110-86-1	79.102	Pyridines	0.2390	619.95	5630	2.3262E+01	1.1251E-01	3.7351E-04	-4.5400E-07	1.4286E-10
4-methylpyridine	108-89-4	93.129	Pyridines	0.3010	646.15	4660	-1.8170E+01	4.7450E-01	-2.4996E-04	3.0280E-08	9.4921E-12
3-methylpyridine	108-99-6	93.129	Pyridines	0.3790	645.00	4371	-1.6136E+01	4.6342E-01	-2.2923E-04	1.6540E-08	1.2749E-11
2-methylpyridine	109-06-8	93.129	Pyridines	0.2990	621.00	4600	-1.7819E+01	4.7591E-01	-2.5380E-04	3.3280E-08	8.7218E-12
2,4-dimethylpyridine	108-47-4	107.155	Pyridines	0.4130	647.00	3529	-1.3020E+01	5.6420E-01	-3.3042E-04	7.4500E-08	0.0000E+00
2,6-dimethylpyridine	108-48-5	107.155	Pyridines	0.4130	623.75	3360	-1.2959E+01	5.3389E-01	-2.5211E-04	1.2260E-08	1.5481E-11
3,4-dimethylpyridine	583-58-4	107.155	Pyridines	0.4130	683.80	3858	-1.3020E+01	5.6420E-01	-3.3042E-04	7.4500E-08	0.0000E+00
2,3-dimethylpyridine	583-61-9	107.155	Pyridines	0.4130	655.40	3642	-1.3020E+01	5.6420E-01	-3.3042E-04	7.4500E-08	0.0000E+00
2,5-dimethylpyridine	589-93-5	107.155	Pyridines	0.4130	644.20	3501	-1.3020E+01	5.6420E-01	-3.3042E-04	7.4500E-08	0.0000E+00
3,5-dimethylpyridine	591-22-0	107.155	Pyridines	0.4130	667.20	3687	-1.3020E+01	5.6420E-01	-3.3042E-04	7.4500E-08	0.0000E+00
isoquinoline	119-65-3	129.162	Pyridines	0.4600	803.15	4384	-1.8255E+01	5.8698E-01	-2.5163E-04	-4.1650E-08	3.9647E-11
methanethiol	74-93-1	48.109	Thiols	0.1580	469.95	7230	4.0307E+01	-3.6753E-03	1.8400E-04	-1.7600E-07	5.0137E-11
propyl mercaptan	107-03-9	76.163	Thiols	0.2240	536.60	4591	3.7035E+01	1.9064E-01	7.2562E-05	-1.4440E-07	4.6182E-11
2-propanethiol	75-33-2	76.163	Thiols	0.2240	535.32	4403	3.1652E+01	2.2715E-01	1.2837E-05	-1.0470E-07	3.6662E-11
1-butanethiol	109-79-5	90.189	Thiols	0.2620	570.10	3919	4.6393E+01	2.2674E-01	1.2687E-04	-1.9440E-07	5.8247E-11
1-propanethiol, 2-methyl-	513-44-0	90.189	Thiols	0.2620	563.95	3838	3.7177E+01	2.8839E-01	1.8512E-05	-1.3850E-07	4.8919E-11
2-butanethiol	513-53-1	90.189	Thiols	0.2620	563.95	3810	4.1398E+01	2.6634E-01	5.7961E-05	-1.6130E-07	5.3327E-11
2-propanethiol, 2-methyl-	75-66-1	90.189	Thiols	0.2620	563.95	3644	3.0326E+01	3.3585E-01	-5.0433E-05	-9.9820E-08	4.0942E-11
cyclopentanethiol	1679-07-8	102.200	Thiols	0.2910	629.00	4327	-3.6386E+01	5.8174E-01	-3.5459E-04	8.4630E-08	0.0000E+00
1-pentanethiol	110-66-7	104.216	Thiols	0.2960	589.61	3353	1.9604E+01	4.6839E-01	-2.0875E-04	4.3240E-08	-7.5836E-12

Component	CAS	Mw, g/mol	Family	ω	Tc, K	Pc, kPa	A_{Cp}	B_{Cp}	C_{Cp}	D_{Cp}	E_{Cp}
2-butanethiol, 2-methyl-	1679-09-0	104.216	Thiols	0.2960	589.61	3272	3.4700E+00	5.6358E-01	-3.3987E-04	7.9360E-08	0.0000E+00
1-butanethiol, 3-methyl-	541-31-1	104.216	Thiols	0.2960	589.61	3322	1.1552E+01	5.1204E-01	-2.7380E-04	5.3400E-08	0.0000E+00
benzenethiol	108-98-5	110.180	Thiols	0.3100	689.50	4898	-5.2590E+00	4.4764E-01	-2.3973E-04	2.2700E-08	1.2746E-11
1-hexanethiol	111-31-9	118.243	Thiols	0.3270	612.95	2940	5.6097E+01	3.5459E-01	1.3831E-04	-2.6780E-07	8.5007E-11
1-heptanethiol	1639-09-4	132.270	Thiols	0.3560	634.43	2621	5.9314E+01	4.3814E-01	8.8964E-05	-2.6170E-07	8.7398E-11

Table B1.3: Inputs for Group 3 Hydrogen bonding components, where A, B, C, D, E are constants for the ideal heat capacity (Eq. 3.17).

Component	CAS	Mw, g/mol	Family	ω	Tc, K	Pc, kPa	A_{Cp}	B_{Cp}	C_{Cp}	D_{Cp}	E_{Cp}
methanol	67-56-1	32.042	Alcohols	0.5640	512.64	8097	4.0046E+01	-3.8287E-02	2.4529E-04	-2.1680E-07	5.9909E-11
ethanol	64-17-5	46.069	Alcohols	0.6450	513.92	6148	2.7091E+01	1.1055E-01	1.0957E-04	-1.5050E-07	4.6601E-11
isopropyl alcohol	67-63-0	60.096	Alcohols	0.6690	508.31	4764	2.5535E+01	2.1203E-01	5.3492E-05	-1.4730E-07	4.9406E-11
1-butanol	71-36-3	74.123	Alcohols	0.5940	563.05	4423	8.1570E+00	4.1032E-01	-2.2645E-04	6.0370E-08	-6.2802E-12
1-pentanol	71-41-0	88.150	Alcohols	0.5730	588.10	3897	9.1750E+00	4.7662E-01	-1.9542E-04	-1.3990E-08	2.0685E-11
cyclohexanol	108-93-0	100.161	Alcohols	0.3690	650.10	4260	1.7124E+01	3.3700E-01	2.8176E-04	-4.2710E-07	1.3215E-10
1-hexanol	111-27-3	102.177	Alcohols	0.5760	610.30	3417	1.0719E+01	5.5767E-01	-2.1818E-04	-3.2300E-08	2.9769E-11
1-heptanol	111-70-6	116.203	Alcohols	0.5670	632.60	3058	1.1810E+01	6.4236E-01	-2.4939E-04	-4.3650E-08	3.7035E-11
1-octanol	111-87-5	130.230	Alcohols	0.5830	652.50	2777	1.3196E+01	7.2493E-01	-2.7623E-04	-5.8380E-08	4.5179E-11
1-decanol	112-30-1	158.284	Alcohols	0.6220	687.30	2315	1.5733E+01	8.9157E-01	-3.3219E-04	-8.6680E-08	6.1276E-11
1-dodecanol	112-53-8	186.338	Alcohols	0.6660	719.40	1994	1.7965E+01	1.0602E+00	-3.9244E-04	-1.1140E-07	7.6380E-11
ammonia	7664-41-7	17.031	H2O/NH3	0.2570	405.40	11353	2.7198E+01	2.2199E-02	2.6395E-05	-2.6421E-08	7.1481E-12
water	7732-18-5	18.015	H2O/NH3	0.3449	647.00	22064	3.3933E+01	-6.4200E-03	2.9900E-05	-1.7800E-08	3.6900E-12
methylamine	74-89-5	31.058	Amines	0.2810	430.05	7460	4.0039E+01	-1.5108E-02	2.5012E-04	-2.3340E-07	6.5582E-11
dimethylamine	124-40-3	45.085	Amines	0.2270	437.20	5712	3.0638E+01	1.0737E-01	1.5824E-04	-1.9420E-07	5.8509E-11
propylamine	107-10-8	59.111	Amines	0.2800	496.95	4740	7.6370E+00	3.3741E-01	-1.6070E-04	2.3840E-08	2.3647E-12
isopropylamine	75-31-0	59.111	Amines	0.2760	471.85	4540	-4.7580E+00	4.0947E-01	-2.8998E-04	1.1550E-07	-2.0187E-11
trimethylamine	75-50-3	59.111	Amines	0.2090	433.25	4073	2.6377E+01	2.1496E-01	1.0135E-04	-1.8840E-07	5.9860E-11
ethylenediamine	107-15-3	60.100	Amines	0.2830	593.00	5115	1.0429E+01	3.2490E-01	-1.9912E-04	6.3560E-08	-8.7124E-12

diethylamine	109-89-7	73.138	Amines	0.3040	496.60	3710	4.0851E+01	2.3495E-01	1.6164E-04	-2.5270E-07	7.9398E-11
1,2-diaminopropane	78-90-0	74.126	Amines	0.3280	585.03	4143	3.6120E+00	4.5467E-01	-3.0830E-04	1.1190E-07	-1.7969E-11
amylamine	110-58-7	87.165	Amines	0.3640	557.66	3728	6.6030E+00	5.2073E-01	-2.5708E-04	3.9760E-08	3.5264E-12
triethylamine	121-44-8	101.192	Amines	0.3160	535.15	3040	5.5793E+01	3.3337E-01	2.2077E-04	-3.4940E-07	1.0838E-10
acetic acid	64-19-7	60.053	Acids	0.4670	591.95	5786	3.4850E+01	3.7626E-02	2.8311E-04	-3.0770E-07	9.2646E-11
butyric acid	107-92-6	88.106	Acids	0.6810	615.70	4064	1.4368E+01	3.9591E-01	-1.8906E-04	-7.6460E-09	2.0812E-11
isobutyric acid	79-31-2	88.106	Acids	0.6140	605.00	3700	-3.2990E+01	5.9238E-01	-5.0629E-04	2.0790E-07	-2.4372E-11
Pentanoic acid	109-52-4	102.133	Acids	0.6980	639.16	3572	-1.2596E+01	6.5474E-01	-5.8609E-04	2.8900E-07	-5.8646E-11
3-methylbutanoic acid	503-74-2	102.133	Acids	0.6820	629.09	3688	-5.8030E+00	5.9939E-01	-4.6602E-04	1.9710E-07	-3.6253E-11
hexanoic acid	142-62-1	116.160	Acids	0.7300	660.20	3380	-9.5590E+00	7.4029E-01	-6.6784E-04	3.7710E-07	-1.0030E-10
heptanoic acid	111-14-8	130.187	Acids	0.7560	677.30	3043	1.1779E+01	6.9196E-01	-4.1039E-04	1.1270E-07	-1.5295E-11
octanoic acid	124-07-2	144.214	Acids	0.7710	694.26	2779	-2.0242E+01	9.9093E-01	-9.2370E-04	5.5030E-07	-1.5434E-10
n-decanoic acid	334-48-5	172.268	Acids	0.8060	722.10	2250	1.6364E+01	9.3012E-01	-4.7163E-04	5.8800E-08	1.1477E-11
undecanoic acid	112-37-8	186.294	Acids	0.9070	749.70	1922	-2.5110E+00	1.0996E+00	-6.4720E-04	1.4770E-07	0.0000E+00
dodecanoic acid	143-07-7	200.321	Acids	0.9560	765.55	1733	-4.2950E+00	1.2373E+00	-8.2209E-04	2.7680E-07	-3.8871E-11
pyrrole	109-97-7	67.091	HNCC	0.3060	639.75	6746	-7.6800E+00	3.1201E-01	-1.1806E-04	-2.7910E-08	2.1314E-11
pyrrolidine	123-75-1	71.122	HNCC	0.2670	568.55	5610	-8.8020E+00	3.1151E-01	6.6087E-05	-2.0530E-07	7.1304E-11
piperidine	110-89-4	85.149	HNCC	0.2430	594.10	4656	-5.3313E+01	7.5541E-01	-5.6470E-04	1.6630E-07	-1.0457E-11
2,4,6-trimethylpyridine	108-75-8	121.182	HNCC	0.4430	689.11	3127	-4.4959E+01	7.5625E-01	-4.7616E-04	1.2070E-07	-5.5157E-12

Appendix B2- Fitted Twu Parameter and calculated Absolute Average Relative Deviations (AARD)

Table B2.1: Fitted Twu Parameter, and Absolute Average Relative Deviations (AARD) For the Twu and Soave α-Functions with the Peng-Robinson Cubic Equation of state, For Group 1 Non-Polar Components.

Component	CAS	MW, g/mol	Family	α_1	α_2	α_3	Twu AARD, %			Soave AARD, %		
							P^{sat}	ΔH_v	C_p^{sat}	P^{sat}	ΔH_v	C_p^{sat}
methane	74-82-8	16.043	Alkanes	-0.1674	0.1493	1.6508	0.81	1.89	1.97	2.46	3.09	3.61
ethane	74-84-0	30.070	Alkanes	-0.1309	0.4173	0.9301	5.89	4.87	2.02	7.12	4.64	6.05
propane	74-98-6	44.097	Alkanes	-0.1235	0.5279	0.8959	3.22	1.83	2.58	4.12	1.78	5.48
butane	106-97-8	58.123	Alkanes	-0.2472	0.3168	1.3424	1.98	1.32	0.99	2.88	1.92	7.19
pentane	109-66-0	72.150	Alkanes	-0.2333	0.4354	1.1497	1.85	1.04	1.27	3.56	1.26	5.87
hexane	110-54-3	86.177	Alkanes	-0.2973	0.3488	1.4892	0.95	0.93	0.62	1.95	1.27	4.35
heptane	142-82-5	100.204	Alkanes	-0.2888	0.4508	1.2856	1.21	0.74	1.00	1.73	0.71	6.72
octane	111-65-9	114.231	Alkanes	-0.3183	0.4310	1.4620	1.01	0.94	1.12	1.67	1.25	5.09
nonane	111-84-2	128.258	Alkanes	-0.2869	0.5725	1.2235	1.26	0.87	0.83	1.91	1.75	6.00
decane	124-18-5	142.285	Alkanes	-0.3290	0.5218	1.3882	5.60	0.97	0.40	6.22	1.84	5.01
undecane	1120-21-4	156.312	Alkanes	-0.3116	0.5681	1.4176	5.95	2.50	0.16	6.66	3.50	4.47
dodecane	112-40-3	170.338	Alkanes	-0.2499	0.7913	1.1428	4.43	1.09	0.30	5.64	4.34	4.86
tridecane	629-50-5	184.365	Alkanes	-0.3287	0.6536	1.3583	4.36	1.12	0.22	5.92	4.16	5.78
tetradecane	629-59-4	198.392	Alkanes	-0.2723	0.8251	1.1730	5.14	1.02	0.39	9.60	4.80	6.19
pentadecane	629-62-9	212.419	Alkanes	-0.3236	0.7417	1.2961	7.06	2.09	0.16	10.20	5.36	6.09
hexadecane	544-76-3	226.446	Alkanes	-0.3486	0.7204	1.3680	13.37	1.14	0.05	20.41	4.46	5.95
benzene	71-43-2	78.114	Aromatics	-0.3120	0.2689	1.3209	0.68	0.45	0.40	2.24	1.49	9.09
toluene	108-88-3	92.141	Aromatics	-0.2506	0.4203	1.1780	2.02	0.85	0.35	3.04	1.31	7.26
ethylbenzene	100-41-4	106.167	Aromatics	-0.2407	0.4936	1.1207	3.03	0.46	0.18	3.58	0.99	8.29
o-xylene	95-47-6	106.167	Aromatics	-0.3426	0.2493	2.0771	5.66	1.24	2.13	4.56	0.97	3.82
propylbenzene	103-65-1	120.194	Aromatics	-0.2802	0.4446	1.3057	2.44	3.75	1.03	3.25	4.50	6.72
naphthalene	91-20-3	128.174	Aromatics	-0.3585	0.2730	1.6503	1.08	2.92	1.36	1.68	3.55	6.43
n-butylbenzene	104-51-8	134.221	Aromatics	-0.1944	0.6815	1.0581	1.50	0.36	0.53	2.51	0.58	4.22
2-methylnaphthalene	91-57-6	142.200	Aromatics	-0.2902	0.3978	1.6334	3.30	2.59	0.68	5.43	3.93	2.01

Component	CAS	MW, g/mol	Family	α_1	α_2	α_3	Twu AARD, %			Soave AARD, %		
							P^{sat}	ΔH_v	C_p^{sat}	P^{sat}	ΔH_v	C_p^{sat}
Acenaphthene	83-32-9	154.211	Aromatics	-0.0009	1.2251	0.7252	1.88	2.66	0.94	36.25	7.65	2.34
1,8-dimethylnaphthalene	569-41-5	156.227	Aromatics	-0.1297	0.9349	0.8692	2.74	1.38	0.33	33.35	4.41	4.80
2,7-dimethylnaphthalene	582-16-1	156.227	Aromatics	-0.0005	1.5620	0.4985	4.59	1.78	3.38	49.80	10.22	1.67
n-hexylbenzene	1077-16-3	162.275	Aromatics	-0.0002	1.5363	0.5813	32.03	1.25	1.34	56.17	4.01	3.06
diphenylmethane	101-81-5	168.238	Aromatics	-0.0739	0.9705	1.0314	7.56	2.71	3.46	6.02	1.86	22.26
isopentane	78-78-4	72.150	Branched	-0.2049	0.4885	0.9851	1.90	1.14	1.36	2.13	1.48	10.48
3-methylpentane	96-14-0	86.177	Branched	-0.1920	0.6094	0.9037	0.78	1.31	1.33	2.19	0.50	11.47
2,3-dimethylpentane	565-59-3	100.204	Branched	-0.0704	0.9734	0.7180	1.34	0.63	1.51	2.07	0.74	11.69
3-methylhexane	589-34-4	100.204	Branched	-0.1189	0.9433	0.7200	1.49	1.78	1.81	1.25	0.72	20.96
2-methylhexane	591-76-4	100.204	Branched	-0.2653	0.4814	1.1832	0.75	0.78	0.43	0.95	0.71	9.43
4-methylheptane	589-53-7	114.231	Branched	-0.3178	0.4169	1.3961	0.37	0.37	0.15	0.94	1.29	4.38
2-methylheptane	592-27-8	114.231	Branched	-0.3024	0.4536	1.3273	0.91	0.36	0.15	2.14	1.25	7.85
cyclopropane	75-19-4	42.081	Cyclic	-0.1893	0.3316	1.1899	5.82	2.05	1.22	6.55	2.13	5.02
spiropentane	157-40-4	68.119	Cyclic	-0.2823	0.3027	1.1322	0.24	0.32	0.12	15.30	3.64	11.17
cyclohexane	110-82-7	84.161	Cyclic	-0.0062	1.1871	0.5422	0.49	0.65	0.69	1.69	2.06	6.40
methylcyclopentane	96-37-7	84.161	Cyclic	-0.2193	0.4455	1.0795	0.17	0.26	0.58	0.97	0.90	12.13
methylcyclohexane	108-87-2	98.188	Cyclic	-0.1860	0.5223	1.0053	0.98	0.43	0.85	2.01	1.59	5.31
ethylcyclopentane	1640-89-7	98.188	Cyclic	-0.2326	0.5249	0.9607	0.62	2.54	0.49	1.29	2.49	19.21
cycloheptane	291-64-5	98.188	Cyclic	-0.0092	1.1143	0.6167	1.02	3.66	0.32	2.29	4.89	4.49
propylcyclopentane	2040-96-2	112.215	Cyclic	-0.3103	0.4149	1.3179	1.21	1.63	0.96	0.46	0.74	14.26
propylcyclohexane	1678-92-8	126.242	Cyclic	-0.0669	0.9955	0.7939	4.85	0.43	1.91	11.89	0.41	1.58
butylcyclopentane	2040-95-1	126.242	Cyclic	-0.3809	0.3091	1.8019	0.47	1.33	0.33	4.50	1.79	14.64
butylcyclohexane	1678-93-9	140.269	Cyclic	-0.0004	1.2272	0.7381	1.47	1.03	0.99	9.69	0.61	0.88
decylcyclohexane	1795-16-0	224.430	Cyclic	-0.0001	1.7993	0.5761	6.53	2.25	5.30	59.08	5.68	0.13

Table B2.2: Fitted Twu Parameter, and Absolute Average Relative Deviations (AARD) For the Twu and Soave α-Functions with the Redlich-Kwong Cubic Equation of state, For Group 1 Non-Polar Components.

Component	CAS	MW, g/mol	Family	α_1	α_2	α_3	Twu AARD, %			Soave AARD, %		
							P^{sat}	ΔH_v	C_p^{sat}	P^{sat}	ΔH_v	C_p^{sat}
methane	74-82-8	16.043	Alkanes	-0.1667	0.2174	1.6486	0.78	2.19	2.39	2.45	3.89	7.93
ethane	74-84-0	30.070	Alkanes	-0.1730	0.3659	1.2855	6.00	4.64	2.58	6.90	3.31	3.26
propane	74-98-6	44.097	Alkanes	-0.1672	0.4585	1.2215	3.39	1.75	3.21	3.57	1.82	3.96
butane	106-97-8	58.123	Alkanes	-0.2686	0.3350	1.6107	2.03	1.80	1.09	3.14	2.11	5.12
pentane	109-66-0	72.150	Alkanes	-0.2615	0.4298	1.4194	1.89	1.50	1.15	2.51	1.85	4.41
hexane	110-54-3	86.177	Alkanes	-0.3180	0.3720	1.7320	0.90	1.24	0.70	2.09	1.92	3.10
heptane	142-82-5	100.204	Alkanes	-0.3195	0.4461	1.5632	1.29	0.99	0.66	1.68	1.25	4.56
octane	111-65-9	114.231	Alkanes	-0.3533	0.4251	1.7760	1.03	1.14	1.04	1.56	1.75	3.59
nonane	111-84-2	128.258	Alkanes	-0.3385	0.5197	1.5573	1.34	0.87	0.50	1.34	0.73	3.90
decane	124-18-5	142.285	Alkanes	-0.3774	0.4869	1.7335	5.65	1.05	0.35	6.18	1.20	3.06
undecane	1120-21-4	156.312	Alkanes	-0.2124	0.8803	1.1608	6.07	0.27	0.44	4.50	1.32	2.50
dodecane	112-40-3	170.338	Alkanes	-0.3255	0.6764	1.4753	4.52	1.20	0.13	3.75	2.07	3.02
tridecane	629-50-5	184.365	Alkanes	-0.3771	0.6133	1.6507	4.43	1.26	0.17	4.63	1.73	3.96
tetradecane	629-59-4	198.392	Alkanes	-0.3414	0.7250	1.4771	5.17	1.00	0.36	5.01	2.18	4.44
pentadecane	629-62-9	212.419	Alkanes	-0.3784	0.6837	1.5810	7.07	2.18	0.07	6.96	2.93	4.39
hexadecane	544-76-3	226.446	Alkanes	-0.3711	0.7418	1.5364	12.66	1.13	0.04	14.08	1.79	4.32
benzene	71-43-2	78.114	Aromatics	-0.3547	0.2531	1.7947	0.72	0.65	0.46	1.12	0.79	6.42
toluene	108-88-3	92.141	Aromatics	-0.2745	0.4266	1.4207	2.16	1.13	0.50	3.24	1.56	4.53
ethylbenzene	100-41-4	106.167	Aromatics	-0.3124	0.3793	1.7851	4.25	0.86	1.93	3.62	1.14	5.69
o-xylene	95-47-6	106.167	Aromatics	-0.3297	0.3396	2.0177	4.62	0.85	1.55	4.99	2.00	1.72
propylbenzene	103-65-1	120.194	Aromatics	-0.2563	0.5609	1.3128	2.70	3.58	0.13	3.24	3.80	4.26
naphthalene	91-20-3	128.174	Aromatics	-0.3911	0.2814	2.0383	1.12	2.90	1.58	1.66	2.97	4.53
n-butylbenzene	104-51-8	134.221	Aromatics	-0.2377	0.6269	1.3155	1.68	0.43	0.89	3.97	1.30	1.97
2-methylnaphthalene	91-57-6	142.200	Aromatics	-0.3207	0.4035	1.9415	3.40	2.93	0.93	6.05	4.84	0.31
Acenaphthene	83-32-9	154.211	Aromatics	-0.2216	0.6254	1.3122	5.59	3.44	0.06	38.33	10.45	4.43

Component	CAS	MW, g/mol	Family	α_1	α_2	α_3	Twu AARD, %			Soave AARD, %		
							P^{sat}	ΔH_v	C_p^{sat}	P^{sat}	ΔH_v	C_p^{sat}
1,8-dimethylnaphthalene	569-41-5	156.227	Aromatics	-0.3449	0.4599	1.7552	0.61	0.52	1.19	22.29	2.22	3.01
2,7-dimethylnaphthalene	582-16-1	156.227	Aromatics	0.0000	1.3000	0.6667	17.48	5.96	0.17	50.99	12.29	3.50
n-hexylbenzene	1077-16-3	162.275	Aromatics	-0.1983	0.8873	0.9349	32.15	1.82	1.82	58.74	6.88	1.12
diphenylmethane	101-81-5	168.238	Aromatics	-0.1099	0.8579	1.3133	9.01	3.02	2.07	6.79	2.27	30.77
isopentane	78-78-4	72.150	Branched	-0.2699	0.3727	1.5384	1.66	1.36	2.93	2.32	1.79	7.36
3-methylpentane	96-14-0	86.177	Branched	-0.2192	0.5878	1.1124	1.06	1.98	1.55	1.71	1.73	8.61
2,3-dimethylpentane	565-59-3	100.204	Branched	-0.1219	0.8240	0.9450	1.87	1.00	2.45	1.41	0.94	8.00
3-methylhexane	589-34-4	100.204	Branched	-0.1572	0.8525	0.9038	2.06	2.65	2.22	1.19	0.79	17.38
2-methylhexane	591-76-4	100.204	Branched	-0.2908	0.4833	1.4212	1.08	1.23	0.72	1.02	1.04	6.85
4-methylheptane	589-53-7	114.231	Branched	-0.3805	0.3639	1.8811	0.43	0.40	0.32	0.81	0.70	2.40
2-methylheptane	592-27-8	114.231	Branched	-0.3290	0.4562	1.5951	0.99	0.44	0.58	1.20	0.65	5.60
cyclopropane	75-19-4	42.081	Cyclic	-0.2146	0.3399	1.4528	5.65	2.08	0.91	4.91	1.93	2.86
spiropentane	157-40-4	68.119	Cyclic	-0.3007	0.3255	1.3860	0.12	0.81	0.13	15.06	5.05	7.69
cyclohexane	110-82-7	84.161	Cyclic	-0.1531	0.6784	0.9174	0.62	0.79	0.68	0.82	0.90	3.94
methylcyclopentane	96-37-7	84.161	Cyclic	-0.2333	0.4746	1.2481	0.14	0.57	0.65	1.06	0.54	8.69
methylcyclohexane	108-87-2	98.188	Cyclic	-0.2129	0.5097	1.2331	0.81	0.24	0.72	1.17	0.28	3.06
ethylcyclopentane	1640-89-7	98.188	Cyclic	-0.2566	0.5174	1.1804	1.00	2.85	0.79	0.89	2.33	15.93
cycloheptane	291-64-5	98.188	Cyclic	-0.1897	0.5753	1.1238	1.01	3.54	0.14	1.57	3.48	1.98
propylcyclopentane	2040-96-2	112.215	Cyclic	-0.3265	0.4416	1.5256	1.56	1.91	1.32	1.39	1.18	11.56
propylcyclohexane	1678-92-8	126.242	Cyclic	-0.1422	0.8078	1.0575	4.65	0.36	1.45	13.00	2.47	2.13
butylcyclopentane	2040-95-1	126.242	Cyclic	-0.3915	0.3525	1.9890	0.64	1.34	0.67	2.45	1.51	12.20
butylcyclohexane	1678-93-9	140.269	Cyclic	-0.0767	1.0107	0.9559	1.18	0.88	0.59	12.22	2.08	3.13
decylcyclohexane	1795-16-0	224.430	Cyclic	-0.0875	1.2899	0.8090	31.48	8.00	0.03	61.69	8.48	1.84

Table B2.3: Fitted Twu Parameter, and Absolute Average Relative Deviations (AARD) For the Twu and Soave α-Functions with the Peng-Robinson Cubic Equation of state, For Group 2 Polar Components.

Component	CAS	MW, g/mol	Family	α_1	α_2	α_3	Twu AARD, %			Soave AARD, %		
							P^{sat}	ΔH_v	C_p^{sat}	P^{sat}	ΔH_v	C_p^{sat}
propanal	123-38-6	58.080	Aldehydes	-0.3331	0.2485	2.0556	9.18	2.82	9.57	17.57	0.48	16.34
butanal	123-72-8	72.107	Aldehydes	-0.0018	1.2409	0.5965	1.58	1.68	2.59	2.06	3.01	7.63
hexanal	66-25-1	100.161	Aldehydes	-0.0003	1.2561	0.7227	4.23	2.57	1.21	6.60	0.46	2.00
benzaldehyde	100-52-7	106.124	Aldehydes	-0.0789	0.9854	0.7232	5.27	3.83	1.07	71.13	20.95	8.00
thietane	287-27-4	74.147	HSCC	-0.2321	0.3637	1.1280	0.35	0.92	0.13	11.81	0.68	11.24
dimethyl sulfoxide	67-68-5	78.135	HSCC	-0.3436	0.2863	2.0791	4.80	1.21	1.32	33.24	7.59	4.27
thiophene	110-02-1	84.142	HSCC	-0.3261	0.1857	1.8451	2.60	1.30	1.64	2.21	1.30	13.24
tetrahydrothiophene	110-01-0	88.174	HSCC	-0.2366	0.3587	1.3303	4.10	0.42	1.46	14.16	3.98	8.75
2-methylthiophene	554-14-3	98.169	HSCC	-0.2335	0.4917	0.9346	0.27	0.59	0.13	16.34	3.60	10.68
3-methylthiophene	616-44-4	98.169	HSCC	-0.2341	0.5020	0.9156	0.23	0.61	0.10	15.52	3.00	12.28
thiane	1613-51-0	102.200	HSCC	-0.0185	1.3583	0.4384	0.40	0.62	0.25	34.25	8.27	6.27
2-methyltetrahydrothiophene	1795-09-1	102.200	HSCC	-0.0012	2.0599	0.2478	3.67	4.41	0.90	51.56	7.73	12.74
benzothiophene	95-15-8	134.202	HSCC	-0.2603	0.4105	1.4863	1.68	3.10	0.93	15.55	6.98	2.00
acetone	67-64-1	58.080	Ketones	-0.2344	0.4731	1.2379	3.51	2.78	0.91	4.15	2.77	6.69
butanone	78-93-3	72.107	Ketones	-0.1048	0.5523	1.4761	3.52	2.85	32.51	1.46	1.30	45.50
cyclopentanone	120-92-3	84.118	Ketones	-0.2659	0.4379	1.1409	2.33	1.15	1.22	2.27	0.60	15.84
4-butanolide	96-48-0	86.090	Ketones	-0.2615	0.3818	1.8876	12.24	2.55	3.02	37.67	11.42	3.95
2-pentanone	107-87-9	86.134	Ketones	-0.2686	0.4865	1.2036	3.94	0.81	0.28	4.15	0.79	8.21
3-pentanone	96-22-0	86.134	Ketones	-0.2537	0.4811	1.2626	8.32	0.95	0.22	7.06	1.00	4.27
1,3-dioxolan-2-one	96-49-1	88.063	Ketones	-0.2310	0.5634	1.5967	25.81	10.64	0.23	22.57	11.39	5.96
cyclohexanone	108-94-1	98.145	Ketones	-0.0863	1.1528	0.6003	22.36	9.21	4.04	16.11	3.41	12.60
3-Penten-2-one, 4-methyl-	141-79-7	98.145	Ketones	-0.3179	0.3078	1.9875	10.74	3.97	0.50	50.65	15.71	9.09
methyl isobutyl ketone	108-10-1	100.161	Ketones	0.0000	1.4937	0.5326	9.51	0.59	0.45	6.17	1.26	7.11
3-hexanone	589-38-8	100.161	Ketones	-0.2441	0.5840	1.1186	3.92	0.70	0.06	5.26	1.06	6.85
2-hexanone	591-78-6	100.161	Ketones	-0.3150	0.4252	1.4233	6.09	0.96	0.23	6.99	1.54	5.48

Component	CAS	MW, g/mol	Family	α_1	α_2	α_3	Twu AARD, %			Soave AARD, %		
							P^{sat}	ΔH_v	C_p^{sat}	P^{sat}	ΔH_v	C_p^{sat}
4-heptanone	123-19-3	114.188	Ketones	-0.3065	0.5823	1.0272	3.79	2.16	0.06	47.52	16.46	1.22
2-octanone	111-13-7	128.214	Ketones	-0.2830	0.5889	1.1814	8.84	1.56	0.10	47.46	17.92	1.96
2,6-Dimethyl-4-heptanone	108-83-8	142.241	Ketones	-0.3455	0.5302	0.4687	31.80	11.23	0.37	97.74	34.45	2.42
benzophenone	119-61-9	182.222	Ketones	0.0000	1.8472	0.4948	5.68	4.22	0.87	84.30	35.77	2.01
cyanogen	460-19-5	52.036	Nitriles	-0.3032	0.3598	1.2662	0.05	2.90	0.28	2.10	3.40	7.62
acetonitrile	107-13-1	53.064	Nitriles	-0.2786	0.3071	1.9072	4.41	2.79	2.85	18.65	12.07	2.80
propionitrile	107-12-0	55.080	Nitriles	-0.2139	0.5540	1.5122	18.75	12.26	0.62	88.91	3.01	7.85
butyronitrile	109-74-0	69.107	Nitriles	-0.2213	0.4363	1.7430	2.01	2.04	1.60	7.30	5.10	9.25
trimethylacetonitrile	630-18-2	83.133	Nitriles	-0.3913	0.0000	0.9995	6.65	9.48	2.46	79.46	19.25	4.35
benzonitrile	100-47-0	103.124	Nitriles	-0.2038	0.5765	1.1980	4.50	2.03	0.22	7.84	2.82	3.10
pyridine	110-86-1	79.102	Pyridines	-0.0014	1.3082	0.5235	1.57	0.73	0.62	3.50	2.53	10.09
4-methylpyridine	108-89-4	93.129	Pyridines	-0.3104	0.3306	1.5141	1.49	0.46	0.72	2.68	0.89	5.84
3-methylpyridine	108-99-6	93.129	Pyridines	-0.1486	0.7624	0.7802	1.64	0.67	0.68	33.74	8.09	2.73
2-methylpyridine	109-06-8	93.129	Pyridines	-0.2368	0.5041	1.0954	0.73	0.59	0.21	1.84	1.01	8.60
2,4-dimethylpyridine	108-47-4	107.155	Pyridines	-0.1419	0.8171	0.8219	1.91	1.14	1.48	31.10	5.17	3.21
2,6-dimethylpyridine	108-48-5	107.155	Pyridines	-0.0014	1.4066	0.5614	2.15	0.97	1.32	31.79	4.75	2.03
3,4-dimethylpyridine	583-58-4	107.155	Pyridines	-0.2075	0.6474	0.9187	0.51	0.27	0.43	28.85	6.55	3.62
2,3-dimethylpyridine	583-61-9	107.155	Pyridines	-0.0102	1.3543	0.5642	1.19	0.79	1.05	31.03	6.46	2.44
2,5-dimethylpyridine	589-93-5	107.155	Pyridines	-0.2474	0.4871	1.1730	23.79	2.85	0.07	31.33	6.26	1.72
3,5-dimethylpyridine	591-22-0	107.155	Pyridines	-0.1595	0.7232	0.9438	1.34	0.89	1.00	30.28	5.17	1.66
isoquinoline	119-65-3	129.162	Pyridines	-0.1287	0.8941	0.6538	3.19	1.53	1.52	56.83	15.74	0.21
methanethiol	74-93-1	48.109	Thiols	-0.1089	0.6447	0.7290	0.57	13.65	0.30	3.58	13.40	10.00
propyl mercaptan	107-03-9	76.163	Thiols	-0.2048	0.5113	0.9295	1.20	0.35	0.26	1.74	0.96	11.42
2-propanethiol	75-33-2	76.163	Thiols	-0.2238	0.4099	0.6020	3.47	6.27	2.50	41.19	6.56	10.95
1-butanethiol	109-79-5	90.189	Thiols	-0.2198	0.5161	1.0052	0.93	0.25	0.12	1.27	1.11	11.88
1-propanethiol, 2-methyl-	513-44-0	90.189	Thiols	-0.0674	1.0913	0.5087	2.02	2.14	0.52	19.12	2.66	10.60
2-butanethiol	513-53-1	90.189	Thiols	-0.0003	1.5354	0.3701	3.77	4.08	0.36	27.81	4.31	11.33
2-propanethiol, 2-methyl-	75-66-1	90.189	Thiols	-0.3173	0.0000	0.2247	8.98	14.43	7.41	66.05	15.26	5.99

Component	CAS	MW, g/mol	Family	α_1	α_2	α_3	Twu AARD, %			Soave AARD, %		
							P^{sat}	ΔH_v	C_p^{sat}	P^{sat}	ΔH_v	C_p^{sat}
cyclopentanethiol	1679-07-8	102.200	Thiols	-0.2800	0.3926	1.1432	0.77	1.30	0.32	11.75	3.42	16.51
1-pentanethiol	110-66-7	104.216	Thiols	-0.3088	0.4066	1.4696	2.46	2.63	0.30	20.22	4.37	12.46
2-butanethiol, 2-methyl-	1679-09-0	104.216	Thiols	-0.1279	1.7715	0.1843	7.68	8.92	0.90	48.58	10.65	10.87
1-butanethiol, 3-methyl-	541-31-1	104.216	Thiols	-0.1401	0.8916	0.6639	0.62	0.68	0.92	5.78	2.90	17.82
benzenethiol	108-98-5	110.180	Thiols	-0.2452	0.5338	0.9458	8.55	2.40	0.16	13.68	2.26	11.10
1-hexanethiol	111-31-9	118.243	Thiols	-0.2780	0.5188	1.3708	4.30	2.41	0.14	31.42	7.79	9.23
1-heptanethiol	1639-09-4	132.270	Thiols	-0.2764	0.5719	1.3606	8.08	3.17	0.08	66.43	9.08	8.42

Table B2.4: Fitted Twu Parameter, and Absolute Average Relative Deviations (AARD) For the Twu and Soave α-Functions with the Redlich-Kwong Cubic Equation of state, For Group 2 Polar Components.

Component	CAS	MW, g/mol	Family	α_1	α_2	α_3	Twu AARD, %			Soave AARD, %		
							P^{sat}	ΔH_v	C_p^{sat}	P^{sat}	ΔH_v	C_p^{sat}
propanal	123-38-6	58.080	Aldehydes	-0.3381	0.3098	2.0669	9.51	3.41	9.58	17.90	1.80	13.08
butanal	123-72-8	72.107	Aldehydes	-0.0021	1.2334	0.6968	1.69	1.28	2.37	1.85	1.75	4.66
hexanal	66-25-1	100.161	Aldehydes	-0.0294	1.1821	0.8497	3.72	3.17	0.96	4.51	1.81	0.86
benzaldehyde	100-52-7	106.124	Aldehydes	-0.1686	0.7424	1.0190	5.16	3.74	0.68	72.18	23.11	11.85
thietane	287-27-4	74.147	HSCC	-0.2528	0.3789	1.3668	0.29	0.68	0.14	11.91	2.56	7.09
dimethyl sulfoxide	67-68-5	78.135	HSCC	-0.3462	0.3486	2.0854	5.31	1.41	1.48	37.17	10.19	0.73
thiophene	110-02-1	84.142	HSCC	-0.2555	0.4183	1.2131	1.44	0.74	0.88	1.85	0.43	9.74
tetrahydrothiophene	110-01-0	88.174	HSCC	-0.2539	0.3829	1.5563	4.16	0.61	1.97	16.60	5.65	4.95
2-methylthiophene	554-14-3	98.169	HSCC	-0.2677	0.4603	1.2028	0.32	1.04	0.21	16.94	5.04	7.42
3-methylthiophene	616-44-4	98.169	HSCC	-0.2695	0.4651	1.1877	0.40	1.05	0.25	16.09	4.53	8.96
thiane	1613-51-0	102.200	HSCC	-0.2012	0.6109	0.8765	0.15	0.69	0.21	35.10	9.92	3.48
2-methyltetrahydrothiophene	1795-09-1	102.200	HSCC	-0.0012	1.7581	0.3450	2.92	3.21	0.36	52.24	9.98	9.63
benzothiophene	95-15-8	134.202	HSCC	-0.2913	0.4134	1.7713	1.81	3.47	0.78	17.59	7.87	3.52
acetone	67-64-1	58.080	Ketones	-0.2653	0.4619	1.4876	3.07	2.56	1.42	4.26	3.98	2.69

Component	CAS	MW, g/mol	Family	α_1	α_2	α_3	Twu AARD, %			Soave AARD, %		
							P^{sat}	ΔH_v	C_p^{sat}	P^{sat}	ΔH_v	C_p^{sat}
butanone	78-93-3	72.107	Ketones	-0.1268	0.5941	1.5404	3.32	2.20	34.83	1.92	2.65	48.99
cyclopentanone	120-92-3	84.118	Ketones	-0.2952	0.4284	1.4209	2.36	1.38	1.69	2.90	1.80	12.39
4-butanolide	96-48-0	86.090	Ketones	-0.2636	0.4483	1.8931	12.75	2.22	3.02	39.52	14.00	8.76
2-pentanone	107-87-9	86.134	Ketones	-0.3230	0.4285	1.6205	3.62	1.17	0.99	3.63	1.37	5.38
3-pentanone	96-22-0	86.134	Ketones	-0.3005	0.4444	1.6266	7.36	0.76	0.48	6.69	0.77	2.23
1,3-dioxolan-2-one	96-49-1	88.063	Ketones	-0.2656	0.5198	1.8978	4.58	6.46	1.44	28.76	13.47	10.40
cyclohexanone	108-94-1	98.145	Ketones	-0.0001	1.4977	0.5897	21.39	10.10	3.58	17.35	5.25	9.55
3-Penten-2-one, 4-methyl-	141-79-7	98.145	Ketones	-0.3212	0.3709	2.0281	9.52	3.37	0.49	51.89	17.75	11.70
methyl isobutyl ketone	108-10-1	100.161	Ketones	0.0000	1.4120	0.6624	6.15	1.18	0.39	5.73	0.55	4.82
3-hexanone	589-38-8	100.161	Ketones	-0.2678	0.5920	1.3031	4.03	1.37	0.08	4.43	1.15	4.30
2-hexanone	591-78-6	100.161	Ketones	-0.3296	0.4638	1.5887	5.71	0.48	0.29	6.40	0.31	3.21
4-heptanone	123-19-3	114.188	Ketones	-0.3534	0.5310	1.3151	4.10	2.24	0.06	47.86	18.67	1.35
2-octanone	111-13-7	128.214	Ketones	-0.3057	0.6028	1.3631	8.15	0.97	0.10	47.87	20.65	4.73
2,6-Dimethyl-4-heptanone	108-83-8	142.241	Ketones	0.0000	2.5777	0.2643	29.56	10.98	0.26	97.99	37.80	5.11
benzophenone	119-61-9	182.222	Ketones	-0.2740	0.7795	1.0138	1.70	3.68	1.80	84.63	38.10	5.20
cyanogen	460-19-5	52.036	Nitriles	-0.3664	0.3089	1.7447	0.11	2.55	0.28	1.55	2.28	3.76
acetonitrile	107-13-1	53.064	Nitriles	-0.2824	0.3691	1.9369	4.74	3.29	2.81	19.24	14.38	7.35
propionitrile	107-12-0	55.080	Nitriles	-0.2227	0.6068	1.6063	19.50	13.18	0.70	84.07	1.51	3.53
butyronitrile	109-74-0	69.107	Nitriles	-0.2265	0.4948	1.8022	1.60	2.36	1.72	9.05	6.54	13.32
trimethylacetonitrile	630-18-2	83.133	Nitriles	-0.4399	0.0357	0.5324	5.34	7.81	1.56	80.11	21.72	1.68
benzonitrile	100-47-0	103.124	Nitriles	-0.0879	0.9857	0.9030	5.53	3.19	1.18	9.65	4.12	0.98
pyridine	110-86-1	79.102	Pyridines	-0.1117	0.8792	0.7911	1.93	1.20	0.53	2.02	0.99	7.05
4-methylpyridine	108-89-4	93.129	Pyridines	-0.3374	0.3450	1.7980	1.53	0.56	0.98	3.39	1.50	3.37
3-methylpyridine	108-99-6	93.129	Pyridines	-0.2402	0.5503	1.1632	1.41	0.60	0.40	34.47	10.11	2.04
2-methylpyridine	109-06-8	93.129	Pyridines	-0.2719	0.4792	1.3688	0.89	0.82	0.59	1.82	1.06	5.74
2,4-dimethylpyridine	108-47-4	107.155	Pyridines	-0.2146	0.6527	1.1301	1.62	1.00	1.10	32.58	7.24	2.98
2,6-dimethylpyridine	108-48-5	107.155	Pyridines	-0.2455	0.5969	1.1413	4.79	2.30	0.22	33.33	6.69	1.49
3,4-dimethylpyridine	583-58-4	107.155	Pyridines	-0.2691	0.5405	1.2461	0.26	0.33	0.16	29.27	8.76	2.10

Component	CAS	MW, g/mol	Family	α_1	α_2	α_3	Twu AARD, %			Soave AARD, %		
							P^{sat}	ΔH_v	C_p^{sat}	P^{sat}	ΔH_v	C_p^{sat}
2,3-dimethylpyridine	583-61-9	107.155	Pyridines	-0.1830	0.7631	0.9532	0.86	0.50	0.88	31.43	8.45	1.95
2,5-dimethylpyridine	589-93-5	107.155	Pyridines	-0.2752	0.4891	1.3999	22.60	2.24	0.13	31.03	7.81	2.44
3,5-dimethylpyridine	591-22-0	107.155	Pyridines	-0.2382	0.5778	1.2972	1.15	0.85	0.67	32.45	7.34	3.17
isoquinoline	119-65-3	129.162	Pyridines	-0.0005	1.3834	0.5908	1.82	0.72	0.68	57.66	18.07	2.85
methanethiol	74-93-1	48.109	Thiols	-0.2615	0.2618	1.8879	1.12	14.51	4.25	3.21	12.52	5.47
propyl mercaptan	107-03-9	76.163	Thiols	-0.2242	0.5197	1.1178	1.17	1.13	0.38	1.24	0.43	8.27
2-propanethiol	75-33-2	76.163	Thiols	0.0000	1.6152	0.3381	4.07	6.10	1.13	41.23	8.13	7.72
1-butanethiol	109-79-5	90.189	Thiols	-0.2430	0.5160	1.2131	0.96	0.72	0.29	0.91	0.41	8.92
1-propanethiol, 2-methyl-	513-44-0	90.189	Thiols	-0.1389	0.8102	0.7504	1.30	0.82	0.82	18.76	4.05	7.65
2-butanethiol	513-53-1	90.189	Thiols	-0.1377	0.8104	0.6761	3.09	3.14	0.52	27.68	5.77	8.26
2-propanethiol, 2-methyl-	75-66-1	90.189	Thiols	-0.4116	0.0000	1.4688	7.12	9.79	0.76	66.26	17.09	3.53
cyclopentanethiol	1679-07-8	102.200	Thiols	-0.2965	0.4140	1.3554	0.77	1.58	0.56	11.51	4.83	13.25
1-pentanethiol	110-66-7	104.216	Thiols	-0.3447	0.3876	1.8445	1.60	1.93	0.99	20.91	3.25	9.90
2-butanethiol, 2-methyl-	1679-09-0	104.216	Thiols	0.0000	2.2167	0.2502	6.74	7.54	0.24	48.56	12.25	8.25
1-butanethiol, 3-methyl-	541-31-1	104.216	Thiols	-0.1845	0.7723	0.8765	0.65	0.52	1.20	5.83	1.11	14.92
benzenethiol	108-98-5	110.180	Thiols	-0.2806	0.5013	1.2055	8.45	3.07	0.22	12.75	4.02	8.28
1-hexanethiol	111-31-9	118.243	Thiols	-0.3332	0.4465	1.8218	1.42	1.26	1.40	31.72	6.15	7.00
1-heptanethiol	1639-09-4	132.270	Thiols	-0.3627	0.4362	2.0111	1.89	1.38	1.32	60.66	7.27	6.37

Table B2.5: Fitted Twu Parameter, and Absolute Average Relative Deviations (AARD) For the Twu and Soave α-Functions with the Peng-Robinson Cubic Equation of state, For Group 3 Hydrogen Bonding components.

Component	CAS	MW, g/mol	Family	α_1	α_2	α_3	Twu AARD, %			Soave AARD, %		
							P^{sat}	ΔH_v	C_p^{sat}	P^{sat}	ΔH_v	C_p^{sat}
methanol	67-56-1	32.042	Alcohols	-0.1261	0.7232	1.5380	1.16	3.67	2.34	6.12	7.76	46.73
ethanol	64-17-5	46.069	Alcohols	-0.0577	1.0449	1.1834	2.42	2.01	8.05	2.51	2.87	44.01
isopropyl alcohol	67-63-0	60.096	Alcohols	-0.0042	1.2319	1.0623	3.89	3.71	3.71	3.23	3.43	22.51
1-butanol	71-36-3	74.123	Alcohols	-0.0266	1.3726	0.8531	6.39	3.79	5.43	9.93	6.15	4.52
1-pentanol	71-41-0	88.150	Alcohols	0.0000	1.5451	0.7562	7.24	3.42	9.49	13.22	6.82	7.05
cyclohexanol	108-93-0	100.161	Alcohols	-0.0003	2.8390	0.3082	10.17	3.04	8.51	42.00	15.45	19.54
1-hexanol	111-27-3	102.177	Alcohols	-0.0986	1.4654	0.7200	8.35	2.28	11.00	38.86	10.10	9.69
1-heptanol	111-70-6	116.203	Alcohols	-0.0001	2.1976	0.5119	10.09	3.80	15.02	66.63	15.76	10.47
1-octanol	111-87-5	130.230	Alcohols	-0.0002	3.4832	0.3096	12.69	3.57	17.64	86.45	14.33	14.84
1-decanol	112-30-1	158.284	Alcohols	-0.0003	2.9513	0.3813	16.07	2.54	9.60	120.32	19.58	16.17
1-dodecanol	112-53-8	186.338	Alcohols	-0.0019	2.8921	0.3992	8.99	4.22	3.55	91.23	23.18	15.93
ammonia	7664-41-7	17.031	H2O/NH3	-0.3007	0.2424	1.9807	2.24	1.34	2.68	2.41	3.55	3.24
water	7732-18-5	18.015	H2O/NH3	-0.2296	0.3952	1.8104	3.19	1.56	5.77	10.18	4.42	10.75
methylamine	74-89-5	31.058	Amines	-0.3576	0.2271	1.9926	5.24	13.10	3.29	4.64	12.90	10.90
dimethylamine	124-40-3	45.085	Amines	-0.3321	0.4041	1.1844	3.32	8.43	4.35	58.28	17.92	23.61
propylamine	107-10-8	59.111	Amines	-0.3323	0.4435	0.9387	3.29	0.90	1.55	4.79	3.41	20.28
isopropylamine	75-31-0	59.111	Amines	-0.0023	2.0046	0.3545	1.14	1.45	2.10	7.63	3.86	22.44
trimethylamine	75-50-3	59.111	Amines	-0.2864	0.2415	1.6546	4.63	3.85	1.07	6.21	2.65	6.67
ethylenediamine	107-15-3	60.100	Amines	-0.0046	1.7057	0.5057	1.43	6.04	0.22	61.85	20.59	21.41
diethylamine	109-89-7	73.138	Amines	-0.4450	0.1594	2.3048	2.40	1.04	0.68	2.44	1.33	7.07
1,2-diaminopropane	78-90-0	74.126	Amines	-0.4162	0.3847	1.3285	2.09	4.41	1.70	111.72	10.64	22.12
amylamine	110-58-7	87.165	Amines	-0.4987	0.1865	2.4146	2.19	1.52	0.45	9.76	3.99	11.74
triethylamine	121-44-8	101.192	Amines	-0.2942	0.4689	1.0746	1.78	1.78	1.35	2.08	0.51	6.55
acetic acid	64-19-7	60.053	Acids	-0.3870	0.3578	2.1770	24.58	8.04	4.06	15.41	6.81	2.27
butyric acid	107-92-6	88.106	Acids	-0.0637	1.1241	1.1016	21.08	2.64	0.30	19.69	1.74	9.31

Component	CAS	MW, g/mol	Family	α_1	α_2	α_3	Twu AARD, %			Soave AARD, %		
							P^{sat}	ΔH_v	C_p^{sat}	P^{sat}	ΔH_v	C_p^{sat}
isobutyric acid	79-31-2	88.106	Acids	-0.0252	1.2543	0.9406	9.57	3.71	0.87	9.79	3.85	4.50
Pentanoic acid	109-52-4	102.133	Acids	-0.1651	0.9432	1.2346	22.13	11.00	0.29	16.41	10.60	6.51
3-methylbutanoic acid	503-74-2	102.133	Acids	0.0000	1.3346	0.9569	9.62	3.53	0.44	9.46	2.21	3.50
hexanoic acid	142-62-1	116.160	Acids	-0.0902	1.1567	1.1141	26.67	14.32	0.09	32.71	13.13	3.27
heptanoic acid	111-14-8	130.187	Acids	-0.1654	1.0075	1.1987	44.31	6.80	0.05	29.85	4.64	4.14
octanoic_acid	124-07-2	144.214	Acids	-0.1910	1.0025	1.1909	42.18	8.32	0.06	35.46	7.69	0.74
n-decanoic acid	334-48-5	172.268	Acids	-0.0500	1.4622	0.9203	94.13	4.65	0.25	97.29	6.42	1.50
undecanoic acid	112-37-8	186.294	Acids	0.0000	1.7628	0.6564	151.23	15.59	0.19	51.31	2.14	0.64
dodecanoic acid	143-07-7	200.321	Acids	-0.0658	1.5763	0.6966	157.26	16.61	0.31	60.30	1.79	0.39
pyrrole	109-97-7	67.091	HNCC	-0.0916	0.8859	0.8047	2.97	0.39	0.89	5.55	1.44	6.90
pyrrolidine	123-75-1	71.122	HNCC	-0.3573	0.3681	0.9626	1.08	1.87	1.32	2.69	2.94	23.34
piperidine	110-89-4	85.149	HNCC	-0.3316	0.2766	1.4702	2.68	0.62	3.32	6.42	2.89	7.51
2,4,6-trimethylpyridine	108-75-8	121.182	HNCC	-0.0480	2.5753	0.1938	41.51	9.90	0.74	67.50	11.85	6.22

Table B2.6: Fitted Twu Parameter, and Absolute Average Relative Deviations (AARD) For the Twu and Soave α-Functions with the Redlich-Kwong Cubic Equation of state, For Group 2 Polar Components.

Component	CAS	MW, g/mol	Family	α_1	α_2	α_3	Twu AARD, %			Soave AARD, %		
							P^{sat}	ΔH_v	C_p^{sat}	P^{sat}	ΔH_v	C_p^{sat}
methanol	67-56-1	32.042	Alcohols	-0.1221	0.8156	1.5268	1.84	4.56	5.56	7.41	9.15	55.05
ethanol	64-17-5	46.069	Alcohols	-0.0912	1.0180	1.3392	2.14	2.46	6.48	3.61	4.14	52.28
isopropyl alcohol	67-63-0	60.096	Alcohols	-0.0159	1.2639	1.1432	2.98	3.14	4.26	2.24	2.72	28.16
1-butanol	71-36-3	74.123	Alcohols	-0.0001	1.4500	0.9240	5.36	3.32	4.76	7.95	5.06	4.88
1-pentanol	71-41-0	88.150	Alcohols	0.0000	1.5507	0.8417	5.94	3.01	8.32	11.51	5.75	7.60
cyclohexanol	108-93-0	100.161	Alcohols	-0.0002	2.3178	0.4310	9.42	2.64	7.80	38.53	14.18	17.89
1-hexanol	111-27-3	102.177	Alcohols	0.0000	1.7542	0.7319	7.31	1.90	9.39	32.13	8.57	8.61
1-heptanol	111-70-6	116.203	Alcohols	-0.1122	1.6381	0.7039	9.31	3.55	13.68	55.56	14.19	8.10
1-octanol	111-87-5	130.230	Alcohols	-0.0001	2.8586	0.4232	11.94	3.48	16.03	71.98	12.67	12.89

Component	CAS	MW, g/mol	Family	α_1	α_2	α_3	Twu AARD, %			Soave AARD, %		
							P^{sat}	ΔH_v	C_p^{sat}	P^{sat}	ΔH_v	C_p^{sat}
1-decanol	112-30-1	158.284	Alcohols	-0.0002	2.5319	0.4985	15.87	2.40	8.08	94.45	17.50	14.48
1-dodecanol	112-53-8	186.338	Alcohols	-0.5258	0.7404	1.0788	9.06	4.22	3.82	71.34	21.02	14.63
ammonia	7664-41-7	17.031	H2O/NH3	-0.2493	0.3685	1.8584	1.83	2.11	6.16	2.97	4.45	7.98
water	7732-18-5	18.015	H2O/NH3	-0.2311	0.4846	1.6923	1.14	0.72	2.89	13.32	6.43	16.99
methylamine	74-89-5	31.058	Amines	-0.1970	0.6518	1.0768	1.55	11.34	0.61	3.52	12.19	6.50
dimethylamine	124-40-3	45.085	Amines	-0.0852	1.1791	0.6921	4.09	8.12	2.53	56.18	17.36	20.52
propylamine	107-10-8	59.111	Amines	-0.3882	0.3625	1.3845	3.43	1.24	1.89	4.98	2.23	17.48
isopropylamine	75-31-0	59.111	Amines	-0.2393	0.7892	0.7592	1.67	1.63	2.02	6.30	2.74	19.60
trimethylamine	75-50-3	59.111	Amines	-0.0014	1.1832	0.6496	8.54	2.57	3.25	6.46	2.37	3.48
ethylenediamine	107-15-3	60.100	Amines	-0.2387	0.8349	0.9197	1.31	5.96	0.13	60.37	19.13	18.85
diethylamine	109-89-7	73.138	Amines	-0.1286	0.9184	0.8408	0.91	1.40	0.20	1.59	0.75	4.67
1,2-diaminopropane	78-90-0	74.126	Amines	-0.4492	0.3806	1.6554	2.14	4.46	1.99	100.31	8.85	19.77
amylamine	110-58-7	87.165	Amines	-0.5065	0.2429	2.4349	2.15	1.63	0.50	9.75	2.47	9.55
triethylamine	121-44-8	101.192	Amines	-0.4044	0.3101	1.7795	1.81	1.86	1.58	1.53	0.93	4.69
acetic acid	64-19-7	60.053	Acids	-0.2732	0.6121	1.4552	11.64	6.20	2.20	17.30	8.66	2.34
butyric acid	107-92-6	88.106	Acids	-0.1438	0.9944	1.3359	20.26	2.11	0.21	19.99	2.65	13.30
isobutyric acid	79-31-2	88.106	Acids	-0.0335	1.2854	1.0361	6.73	1.78	1.05	7.51	2.22	8.30
Pentanoic acid	109-52-4	102.133	Acids	-0.0004	1.4724	1.0101	17.64	11.79	1.85	12.42	10.84	10.53
3-methylbutanoic acid	503-74-2	102.133	Acids	-0.2605	0.8094	1.4935	9.15	3.02	1.58	11.60	1.78	6.60
hexanoic acid	142-62-1	116.160	Acids	-0.1579	1.0574	1.3142	23.98	15.03	0.08	24.52	14.17	6.15
heptanoic acid	111-14-8	130.187	Acids	-0.1944	1.0053	1.3350	38.59	5.90	0.04	20.97	3.66	7.40
octanoic_acid	124-07-2	144.214	Acids	-0.2354	0.9622	1.3711	37.92	7.65	0.04	27.42	5.34	3.67
n-decanoic acid	334-48-5	172.268	Acids	-0.1256	1.3049	1.1019	85.45	4.17	0.25	82.55	4.31	0.85
undecanoic acid	112-37-8	186.294	Acids	-0.0352	1.6428	0.7721	125.59	14.18	0.12	56.61	2.52	1.88
dodecanoic acid	143-07-7	200.321	Acids	0.0000	1.8099	0.7191	131.09	15.04	0.22	64.47	2.81	1.95
pyrrole	109-97-7	67.091	HNCC	-0.1979	0.6358	1.1782	2.94	0.52	1.34	4.06	0.38	3.07
pyrrolidine	123-75-1	71.122	HNCC	-0.4483	0.2185	1.9967	0.97	1.29	2.19	2.18	1.70	20.42
piperidine	110-89-4	85.149	HNCC	-0.3553	0.2971	1.7624	2.53	0.58	3.15	5.06	1.60	6.19
2,4,6-trimethylpyridine	108-75-8	121.182	HNCC	-0.0001	2.1659	0.3014	37.61	8.78	0.59	68.89	14.23	3.58